



UNIVERSITÀ DEGLI STUDI DI PADOVA

Sede Amministrativa: Università degli Studi di Padova

Dipartimento di Fisica

SCUOLA DI DOTTORATO DI RICERCA IN:

SCIENZA ED INGEGNERIA DEI MATERIALI

CICLO XXI

Innovative solutions in organic photovoltaic devices

Direttore della scuola: Prof. Gaetano Granozzi

Supervisore: Prof. Alberto Carnera

Co-Supervisore: Dr. Massimo Tormen

Dottorando: Simone Dal Zilio



UNIVERSITÀ DEGLI STUDI DI PADOVA

Sede Amministrativa: Università degli Studi di Padova

Dipartimento di Fisica

SCUOLA DI DOTTORATO DI RICERCA IN:

SCIENZA ED INGEGNERIA DEI MATERIALI

CICLO XXI

Innovative solutions in organic photovoltaic devices

Direttore della scuola: Prof. Gaetano Granozzi

Supervisore: Prof. Alberto Carnera

Co-Supervisore: Dr. Massimo Tormen

Dottorando: Simone Dal Zilio

to my bear family

Abstract

New technologies for photovoltaic energy generation can contribute to environmentally friendly, renewable energy production and may lead to the reduction of carbon dioxide liberated by burning fossil fuels and biomasses. Besides the established silicon based solar cells new photovoltaic technology has gained a lot of interest during the last decade. Among them organic solar cells (OSC) based on conjugated molecules or polymers are promising candidates for the manufacturing of environmentally safe, flexible, lightweight, and inexpensive photovoltaic devices which can be used in low cost applications. Particularly attractive are in photovoltaic (PV) elements based on thin plastic films. The flexibility offered through the chemical tailoring of desired properties, as well as the cheap technology already well developed for all kinds of plastic thin film applications would make such an approach widely adopted. Unfortunately a main bottleneck is to be solved before industrial production could become economically viable, particularly represented by the still low conversion efficiency. In organic semiconductors the primary photo-excitations do not directly and quantitatively lead to free charge carriers but to coulombically bound electron-hole pairs, called excitons, that need strong electric fields to generate free charge carriers, present for example at the discontinuous potential drops at the interfaces between donors and acceptors as well as between semiconductors and metals. The exciton diffusion lengths in polymers and in organic semiconductors is usually around 10-20 nm: for efficient photovoltaic devices, the excitons have to split before recombining and the free electrons and holes must be transported towards the electrodes to produce the photocurrent. Major problem derives from loss mechanism, such as exciton decay, charge recombination and low mobility, resulting in reduced photocurrent extraction at the electrodes and low power conversion efficiency. The improvement of the efficiency is one of the most important aspect in which is concentrated the research in OSC, our too. Two different routes going towards this objective focalized in this aspect have been explored, in order to contribute to realize a novel and effective technology in the photovoltaic field. The first concerns the development of a novel light trapping system bases on microlenses, The second, on which we are still working, regards the fabrication of nanostructured solar cells by top-down techniques, particularly nanoimprinting (NIL).

Sommario

Il problema energetico sta destando negli ultimi anni sempre maggior interesse e preoccupazione, per il ridursi delle risorse fossili e dal conseguente acuirsi dei problemi d'inquinamento derivanti dal loro quasi esclusivo utilizzo per la produzione di energia elettrica. Non è sorprendente quindi che dal mondo della ricerca un grande sforzo sia dedicato allo sviluppo della tecnologia fotovoltaica. Attualmente, il silicio possiede una posizione centrale nel panorama delle celle fotovoltaiche: l'elevato costo di questo tipo di tecnologia, derivato dall'alto costo del materiale e dei processi fabbricativi, ha incoraggiato lo sviluppo di soluzioni alternative che si basino su materiali innovativi. Tra queste, grande risalto è stato dato negli ultimi anni alle cosiddette "organic solar cell", basate sull'impiego di semiconduttori organici. Il loro vantaggio risiede nel fatto che questi possono essere depositati, su larghe aree e a costi molto ridotti, in fase liquida, utilizzando quindi metodi tipici dell'industria della stampa nel campo del fotovoltaico ed eliminando così alti costi di materiale e di processo tipici dell'industria a semiconduttore inorganico. L'impiego di film sottili e conseguentemente di poco materiale, contribuisce a rendere il fotovoltaico organico uno dei più quotati candidati per lo sviluppo di una tecnologia solare a basso costo. Una tipologia di celle solari organiche utilizza come materiali foto attivi i polimeri coniugati; evidenti progressi sono stati compiuti, col raggiungimento di efficienze ragguardevoli, dell'ordine del 4-5%. Purtroppo però, questo non è ancora sufficiente perché la tecnologia possa essere trasferita su scala industriale. Molti sforzi si stanno facendo nell'ambito della ricerca per migliorare l'efficienza di queste celle. Sullo sviluppo e l'impiego di soluzioni alternative e innovative applicabili al campo del fotovoltaico organico, e in particolare polimerico, è concentrata la nostra attività di ricerca. Due percorsi in particolare sono stati investigati, basate sull'impiego di un nuovo sistema per l'intrappolamento in cavità della luce e sull'impiego delle nanotecnologie fabbricative.

Contents

1	The energy question	1
1.1	Photovoltaic technologies	3
1.1.1	Inorganic solar cells	3
1.1.2	Organic solar cells	8
2	Electronic Model for Organic Solar Cells	11
2.1	The two level system in thermal equilibrium	12
2.2	The Two-Level System under Illumination	13
2.3	Charge Carrier Extraction at the Contacts	14
2.4	Contact Models for the Two-Level System	16
3	Organic semiconductors	21
3.1	Absorption and exciton generation	23
3.2	Exciton diffusion	25
3.3	Free charge generation at A/D interfaces	27
3.4	Organic semiconductor structure	31
3.5	Conduction in organics	33
3.6	Charges recombination	34
3.7	semiconductor-electrodes interface	36
4	Photovoltaic Characterization of Organic Solar Cells	43
4.1	Equivalent Circuit Diagram	43
4.2	Short Circuit Current, Open Circuit Voltage and Fill Factor	45
4.3	Photoresponsivity, External Quantum Efficiency and Power Conversion Efficiency	46
4.4	I-V Characteristics of a 'real' solar cell	48
4.5	Origin of the Open Circuit Voltage	50
4.5.1	Optical Filter Effect in Organic Films	51
4.6	Experimental Setups	51
5	Trapping light with microlenses in organic photovoltaic devices	53
5.1	Methods of fabrication	56
5.2	Characterisation of devices	67
5.3	Modeling of LTS behaviour	77

5.4	Conclusions	79
6	Nanostructured solar cells	81
6.1	Some concepts in organic solar cells	81
6.2	Main idea: nanostructured solar cells	83
6.2.1	Block Copolymer Lithography	85
6.2.2	Self assembled tin nano-islands	86
6.3	Organic solar cell: experimental section	88
6.3.1	Cells fabrication	90
6.3.2	Materials and processing	92
6.4	Cells characterisation	95
6.5	Small molecules evaporated solar cells	101
6.5.1	Fabrication of evaporated solar cells	101
6.5.2	Characterisation of evaporated solar cells	103
6.6	Conclusions	105
	Bibliography	109

List of Figures

1.1	Total energy consumed annually in the most important country (source http://www.energy.eu).	1
1.2	The percentage share of electricity generated by different sources (source http://www.energy.eu).	2
1.3	The hubbert curve (from Strategic Significance of America's Oil Shale Resource Volume I Assessment of Strategic Issues)	3
1.4	Photovoltaic capacity installed in Europe (source http://www.energy.eu).	4
1.5	Reported timeline of solar cell energy conversion efficiencies.	4
1.6	How reducing the cost!	5
1.7	synergistic effect of thickness and efficiency on cost of silicon solar cells.	6
1.8	Fraction of incident light absorbed by P3HT film at different thickness.	9
2.1	A simple two-level system. For organic semiconductors the valence band corresponds to the HOMO and conduction band to the LOMO.	11
2.2	Ideal contacts at which no energy and no charge carriers are lost during the conversion of chemical potential energy to electrical energy.	15
2.3	Extractable current as function of QFL-splitting in an illuminated semiconductor.	16
2.4	Energy diagrams of solar cells under different bias conditions.	17
2.5	Energy diagrams for solar cells with semipermeable membranes under different bias conditions.	18
3.1	Orbital structure of conjugated sp^2 hybridized carbon atoms. (a) Ethene is composed of a pair of double bonded carbon atoms. The first bond is formed by overlapping σ -orbitals, while the second bond is formed by interacting π -orbitals. (b) Delocalisation of π -electrons. (c) The complete orbital structure of ethene (or ethylene).	21
3.2	Organic semiconductors can be divided into different categories according to their properties: soluble, insoluble and liquid crystalline.	22
3.3	The molecular structure of Benzene and of poly(p-phenylene)	23
3.4	Conversion steps in organic solar cell.	24
3.5	exciton density profiles	27
3.6	Facilitate charge transfer and exciton-scission.	28
3.7	Foerster energy transfer (no exciton splitting)	29

3.8	Dispersed heterojunction between a transparent ITO electrode and a metallic (Al, Au...) electrode. The exciton is separated in hole and electron at interface that are collected at respective electrodes.	30
3.9	Examples of organic semiconductors used in organic solar cells.	31
3.10	The <i>poly(3-hexylthiophene)</i> (P3HT) and the [6,6]-phenyl-C61-butyric acid methyl ester (PCBM).	32
3.11	Energy band diagrams of D/A devices with the electrode interfaces. a) the situation before contact. After contact the Fermi levels (dashed lines) and ψ_f equalize and band bending occurs. b) the formation of a blocking contact for holes (ITO/D) and electrons (A/Al). c) the formation of a non-blocking (ohmic) contact for holes (Au/D) and electrons (A/Ca).	37
3.12	The chemical structure of poly(3,4-ethylenedioxythiophene) (PEDOT) and poly(styrene-sulfonate) (PSS). In mixture, PSS oxidises PEDOT, making it a highly conducting polymer. Facilitating holes transport across the anode interface, it is used in organic electronics as anode.	39
3.13	The positive doping of PEDOT leaded by PSS: the PSS-acid donates a proton from its HO_3S group to a sulphur atom of PEDOT.	40
4.1	Equivalent circuit diagram for a typical solar cell.	43
4.2	Extended equivalent circuit diagram for a solar cell.	44
4.3	Current versus voltage characteristic of a solar cell under illumination.	45
4.4	Our sun simulator, the ABET 2000. On the right, the internal working scheme.	47
4.5	Efficiency limits for different solar cells.	48
4.6	Effect of the shunt resistor on the I-V characteristic. The graph shows I-V curves for high (black), medium (green), and low (red) values of R_{Sh}	49
4.7	Effect of the series resistor on the I-V characteristic. The graph shows I-V curves for a low (black), medium (green), and high (red) value of R_S	50
4.8	Effect of low short circuit currents on the I-V characteristic. The graph shows I-V curves for high (black), medium (green), and low (red) values of I_{SC}	50
4.9	The spectrographs Acton SpectraPro SP-2300i with monochromators and the Keithley 2400 source meter.	52
4.10	ABET 2000 SunSimulator and Agilent B1500A Semiconductor Device Analyzer.	52
5.1	Optical confinement for light path enhancement.	53
5.2	The proposed Winston-type collectors [1].	55
5.3	Operational principle of the light trap and its constituents.	55
5.4	Figure display configuration with relevant radius of curvature, hole openings and	56
5.5	Same device as before but with a 100% reflecting cell. All rays are accordingly reflected.	56
5.6	Scheme of fabrication of light trapping system.	57
5.7	Scheme of fabrication procedure of silica mold.	58
5.8	Scheme of fabrication of microlenses.	60
5.9	SEM picture of lenses fabricated without applying pressure during the exposure.	61

5.10 SEM picture of lenses fabricated from same the mold applying pressure during the exposure.	61
5.11 SEM picture of spherical microlenses.	62
5.12 Optical microscope of spherical microlenses.	62
5.13 SEM picture of cylindrical microlenes.	63
5.14 Fabrication scheme of light trapping system.	63
5.15 Optical micrograph of structures in negative resist produces from exposure through spherical (a) and cylindrical (b) microlenses. The quality of the edges and the control of feature size look insufficient.	64
5.16 The rotating stage with possibility of tilting. In the picture is set on the mask aligner used for the UV-exposure.	65
5.17 Optical micrograph of negative resist structures produced by exposure trough microlenses. a) Doughnut like structures were obtained. b) posts exposed at larger tilt angle of the rotation axis with respect the (a). The central region was not sufficiently exposed.	65
5.18 Optical micrograph of negative resist structures produced by (a) spherical and (b) cylindrical lenses. The size of the corresponding metal apertures would be too small in the final devices.	66
5.19 Negative resist dots with large size. To notice the very well difined edges. . . .	66
5.20 Optical micrograph of $200\mu m$ period lines. The width of lines is on average $40\mu m$	67
5.21 Optical micrograph of $400\mu m$ period lines. The width of lines is on average $50\mu m$	67
5.22 Optical micrograph of $80\mu m$ period dots. The diameter of circles is around $25\mu m$	68
5.23 Optical transmission microscope picture of the backside of the samples: the backside mirrors for spherical (a) and cylindrical (b) lenses are displayed. . . .	68
5.24 The integrating sphere setup. Blue beam is the sample beam and violet beam is reference beam.	69
5.25 Transmission of spherical lenses: it is clear that when illuminated through the lenses a smaller portion is transmitted compared to the cylinder case. A significantly lower backside transmission (illuminated through mirror side) is also confirmed. This is in agreement with the smaller area the holes occupy compared to the stripes. The transmission lies around 50% when illuminated through lenses and around 2 – 5% when illuminated through the holes. When the best sample is tilted slightly to optimize the transmission it is possible to reach a value as high as 69%. The influence of tilting the samples effectively demonstrates how sensitive this configuration is to non perpendicular light. . .	69

5.26	Cylindrical lenses transmission with period $400\mu m$ of period: it displays rather high transmission (75%) over a large spectral range when the lenses are illuminated. When the mirror side is instead illuminated we record a transmission of 20 – 25%. A minor angle dependence of transmission can be observed. As can be seen the transmission is limited below wavelengths of $450nm$ to reach a zero value at $350nm$. This significant limitation for photovoltaic applications is solely attributed to the absorption of the negative photoresist employed in the lenses.	70
5.27	Graphic shows the obtained transmission as a function of wavelength for $400\mu m$ cylindrical and $80\mu m$ spherical lenses. In the case of cylindrical lenses, as high as 90% transmission was measured in the forward direction whereas a transmission of < 15% is measured when the sample is illuminated from the side of the mirror first. The dip in transmission at shorter wavelength is attributed to absorption in the lens material and in the metal, which primarily consists of silver.	71
5.28	Device absorptance as measured from reflectance and blend material absorption as measured from transmission. Inset: chemical structures of the utilized donor (APFO Green 9) and acceptor (PCBM[70]) materials in the blend. . . .	72
5.29	Photocurrent (left) and EQE (right) of thick and thin samples without laminated lenses. A pronounced difference in the current response was obtained between the thicker film that generates more current than the thinner film. Also for the EQE the thicker cell performed better than thinner one except in the spectral range 350-470 nm with LTS.	73
5.30	Left) Photocurrent from two samples with laminated cylindrical lenses. The photocurrent depends rather strongly from the angle of incidence of the light on LTS. The effect of tilting is strong: the tilt angle was not evaluated. We tilted the sample until obtain the maximum of light transmission in foward direction. Right) EQE for device 3. The cells primarily lose efficiency upon lamination of lenses. Nowhere in the spectrum can an enhancement be seen.	74
5.31	Left) Photocurrent from two samples with laminated spherical lenses. A very small improvement can be identified for wavelengths above 620 nm in sample 4 (the area in the red circle). Right) EQE for device 4. The cells primarily lose efficiency upon lamination of lenses and the small photocurrent improvement can hardly be identified in the EQE curve.	74
5.32	Sample with 35 nm active layer and $400\mu m$ period lenses placed in front. The measured photocurrent is improved from 450 nm and above.	75
5.33	Photoresponsivity of same thin sample. Here we pay attention to the intensity of the lamp. Green inset displays solar illumination spectra.	75
5.34	External quantum efficiency of same thin sample. Electrons out per photons in.	76
5.35	An increase in short circuit current of 5% can be confirmed upon the addition of the light trap.	76
5.36	Photoresponsivity and solar irradiance graph.	77

5.37	JV characteristics from simulated AM 1.5 solar illuminated APFO Green 9/PCBM[70] solar cell with and without the light trapping element. An increase in short circuit current of 25% can be confirmed upon the addition of the light trap.	77
5.38	a. Schematic of the multiple bounces and the according Fresnel intensity coefficients. b. Calculated total cell absorptance for the APFO Green 9/PCBM[70] system with and without the trap system. For different number of absorption events included, a noticeable improvement above 400 nm can be found.	78
6.1	Lamellar structure of regio-regular P3HT.	82
6.2	Ideal nanostructure for organic solar cell.	83
6.3	Fabrication scheme of nanostructured solar cells: (1)Deposition by spin coating of PEDOT:PSS and P3HT on ITO coating. (2)Imprint of the nanostructured master in the P3HT film by nonoimprinting process at temperature $t > t_g$, with t_g the glass transition temperature of polymer. (3)Master release at $t < t_g$. (4)Transfer of sample in evaporation chamber. (5)Deposition by sublimation of C60 to fill the nanostructures. (6)The final structure of cell.	84
6.4	SEM micrograph of a partially etched, ozonated monolayer film of spherical microdomains. (B) An SEM micrograph of hexagonally ordered arrays of holes in silicon nitride on a thick silicon wafer. The pattern was transferred from a copolymer film such as that in (A). The darker regions are 20-nm-deep holes in silicon nitride, which has been etched out [2].	85
6.5	Novel patternable block copolymers to achieve spatially controlled nanostructures. (a) An asymmetric P MS-b-PHS copolymer/photoacid generator/crosslinker solution is spin-coated onto a Si substrate and forms vertical P MS cylinders as a result of rapid solvent evaporation. (b) 248 nm stepper exposure and subsequent development forms micropatterns. (c) Strong ultraviolet irradiation under high vacuum removes P MS, thus generating patterned nanochannels.	87
6.6	Schematic representation of the fabrication process with representation of the phenomenon of nano-droplet formation.	88
6.7	Representative SEM micrographs depicting biomimetic samples A, B, C and D realised by incremental tin deposition of thickness 1.5, 2.5, 5 and 7 nm, respectively.	89
6.8	Silicon nanostructures abricated by dry etching in ICP using the small tin island as mask. Increasing the etching time, we observe the decrise of the diameter of structure, the increase of their height and a change in the aspect: for prolonged etching, the structures look more sharpened, where, for brief processes, they remain a round tip, probably due to the presence of tin mask. A) Etching time: 3 sec. B) Etching time: 6 sec. C) Etching time: 9 sec. D) Etching time: 12 sec.	90
6.9	The scheme of the fabrication process of solar cells investigated in this thesis.	91
6.10	Schematic representation of polymeric solar cells.	92
6.11	A P3HT:PCBM cell after the deposition of Al electrode and the annealing carried in glove box.	93
6.12	Different PEDOT:PSS solution from H.C.Starck.	95

6.13	On the left, the current/wavelength response of one of solar cell: maximum value 0.827 nA at 490 nm . On the right the Spectral Irradiance measurement.	96
6.14	The calculated EQE vs wavelength: the maximum EQE at small wavelengths probably derives from an incorrect Spectral Irradiance measurement.	97
6.15	I-V curve of a cell realized using regiorandom P3HT, high resistant PEDOT:PSS and PCBM 99, 5%. The I-V curve shows a V_{OC} of 427 mV , a lower value with respect the V_{OC} founded in literature ($\approx 700 \text{ mV}$).	97
6.16	On the left, the current/wavelength response: on the right the calculated EQE: not effect of the diode calibration are noticed. The wavelength range correspondent to the maximum values of EQE according to that found in literature.	98
6.17	I-V curve of a cell realized using regiorandom improved annealing process and thicker active film. The V_{OC} was 637 mV , much higher than before; also the J_{SC} has been increased (20 nA), that is still a low value. The effect of poor electric properties of P3HT is evident.	99
6.18	On the left, the current/wavelength response of one of our best P3HT/PCBM cells. On the right the Spectral Irradiance measurement.	99
6.19	The calculated EQE in function of wavelength.	100
6.20	The I-V curve under AM 1.5 illumination.	100
6.21	The general scheme of a cell fabricated by evaporation.	102
6.22	Two cells fabricated at CRP of Amaro.	102
6.23	The CuPC and BA1q molecules.	103
6.24	left) scheme of cell: the layer and the respective thickness are highlighted. right) the current vs wavelength curve of the cell in function of the baking temperature: the generated current decrease with the increasing of temperature annealing.	104
6.25	left) scheme of cell: the layer and the respective thickness. right) the current vs wavelength curve of the cell in function of the baking temperature: the generated current increase with the increasing of temperature annealing.	104
6.26	I-V curve of the best evaporated cell.	105
6.27	I-V curve of a cell with lower PCE.	105

Introduction

New photovoltaic technologies can contribute to environmentally friendly, renewable production of energy and lead to a reduction of the amount of carbon dioxide liberated in the atmosphere from the combustion of fossil fuels. Besides the established silicon based solar cells thin film photovoltaics has gained momentum during the last decade. Among them organic solar cells based on conjugated molecules or polymers are promising candidates for the manufacturing of environmentally safe, flexible, lightweight, and inexpensive photovoltaic devices which can be used in low cost, mass produced applications. Strong light absorption and easy processability from solution, are among the main advantages of organic solar cells, which would make production potentially very cost effective. Particularly attractive from the market point of view, are photovoltaic (PV) elements based on thin plastic substrates. The flexibility obtainable by chemical tailoring of the properties, as well as the cheap technology already well developed for all kinds of plastic thin film applications would make such an approach a sure hit. The mechanical flexibility of plastic materials is welcome for all PV applications onto curved surfaces for architectural integration. By casting semi-transparent plastic PV thin films between insulating window glass, large unused areas (the windows) can be employed for power generation in addition to the limited roof areas of crowded cities. Even the colour of such PV elements can be varied by sacrificing some parts of the visible solar spectrum. Because of the large band gap in organic materials, only a small portion of the incident solar light is absorbed. A band gap of 1.1 eV (1100 nm) is capable of absorbing 77% of the solar irradiation on earth.³⁰ However, the majority of semiconducting polymers have band gaps higher than 2 eV (620 nm), which limits the possible harvesting of solar photons to about 30%. On the other hand, because the absorption coefficients of organic materials are high, only 100 nm thicknesses is enough to absorb most of the photons when a reflective back contact is used. The thicknesses of the films are not the bottleneck. Major problems have to be solved before industrial production could become economically viable: they are represented by the still low conversion efficiency and stability. A shelf lifetime of several years as well as an operational lifetime of tens of thousands of hours are requested for all durable applications. Conjugated polymers have to be protected from air and humidity to achieve such lifetimes. These protection methods are being developed for light emitting diodes (LEDs) as well as PV elements. Recent reports from LED research indicate that the stability problem has been sufficiently overcome in order to enter into large scale applications, which in turn is a good sign for plastic solar cells. The improvement of the efficiency is still the most important aspect in which is concentrating the research in OSC. It is now important to explain the physical processes taking place in this kind of devices. An important difference between inorganic and organic solar cells lies in the nature

of the primary photoexcited state. In the former, the absorption of photons leads directly to the creation of free electrons and holes at room temperature. The charge carriers can then diffuse and/or drift to their respective collective electrodes. In organic semiconductors the situation is somewhat different; it's not completely clear the physical aspects that occur after sunlight absorption and, for this reason, they are still the object of debate within the scientific community. It is generally accepted that the primary photo-excitations in organic materials do not directly and quantitatively lead to free charge carriers but to coulombically bound electron-hole pairs, called excitons. It is estimated that only 10% of the photoexcitations lead to free charge carriers in conjugated polymers. For efficient dissociation of excitons, strong electric fields are necessary, and it can be achieved by several different ways: dissociation by trap sites in the bulk of material (ex: oxygen traps) or at the discontinuous potential drops at the interfaces between donors and acceptors as well as between semiconductors and metals. In the case of conjugated polymers, when an exciton reaches the interface between the polymeric donor and the acceptor (generally a C60-based material PCBM for example), an ultrafast electron transfer occurs from the lowest unoccupied molecular orbital (LUMO) of the donor to the lower lying LUMO of the acceptor, leaving a hole on the highest occupied molecular orbital (HOMO) of the donor. For efficient photovoltaic devices, the free electrons and holes must be transported towards the respective electrodes within their lifetime to produce the photocurrent. This occurs via percolative pathways in the case of devices made with disordered blend of the p and type organic semiconductors. A gradient in the chemical potentials of electrons and holes is built up in a donor-acceptor junction. This gradient is determined by the difference between HOMO level of the donor (quasi Fermi level of the holes) and the LUMO level of the acceptor (quasi Fermi level of the electrons). This internal electrical field determines the maximum open circuit voltage and contributes to a field-induced drift of charge carriers. However, loss mechanism such as exciton decay, charge recombination and low mobility result in reduced photocurrent extraction at the electrodes and low power conversion efficiency. It's just this last aspect the most important reason of the actual low efficiency. Exciton diffusion lengths in polymers and in organic semiconductors are usually around 10-20 nm. If we have a bilayer device, the thickness has to be in the order of exciton diffusion length, value too small to have the complete absorption of light. An encouraging breakthrough in realizing higher efficiencies has been achieved by mixing electron-donor-type polymers with electron-acceptor-type. A fine separation in random nanophase domains is more beneficial for exciton dissociation. A successful system for these solar cells is a blend of *poly(3-hexylthiophene)* (P3HT) and [6, 6]-*phenylC61-butyracacidmethylester* (PCBM), a soluble Buckminster fullerene C60-derivative. With this solution the best performances have been measured, up to 5% of efficiency. We have developed two new solutions to achieve the increase of performances of solar cells, in particular to obtain the improvement of efficiency; the first one is based on the employment of top-down nanofabrication methods to modify the structure of solar cells realizing of an ordinate interdigitated system of nanostructures with feature size in the order of the exciton diffusion length (5-10 nm). The second one, is related to the realization of a novel light trapping device based on a micro-optic system, suitable to solve efficiently the problem of incomplete absorbing of light for cells with reduced active layer thickness, by making use of a new type of light trapping elements.

We can schematically summarize the arguments presented in this thesis as follow:

- in the first chapter, a brief introduction to the energy question and the current state of the photovoltaic technology.
- in the second chapter, we will present the Electronic Model for Organic Solar Cells
- in the third chapter, we will give a general introduction to the organic semiconductors , highlighting the main principles of conjugated polymer solar cells.
- In the fourth, the project in light trapping system will be illustrated: the experimental detail of fabrication and the characterization will be the central themes .
- In the fifth chapter, we will present the project in nanostructures solar cells, showing the main concept on which is based the idea: then, we will discuss about the preliminary results in nanofabrication and, at last, about the work realized on polymeric solar cells.

*”L’intelligenza è pertanto circolare:
i molto stupidi e i molto intelligenti sono quasi uguali!”*

Dominique Canton.

Chapter 1

The energy question

The energy question has become one of most major and worrying problem of the modern society. The worldwide demand for energy has grown dramatically over the last century as consequence of the increase in the industrialization of the world. The need for energy is likely to grow even more in the 21st century with the improvements in living standards across the planet; moreover, the economic develop of Asiatic nation, like China and India, has emphasized the problem of energy demand 1.1. This high demand of energy, the pollution generated by energy sources currently used and the depletion of natural resources bring into question.

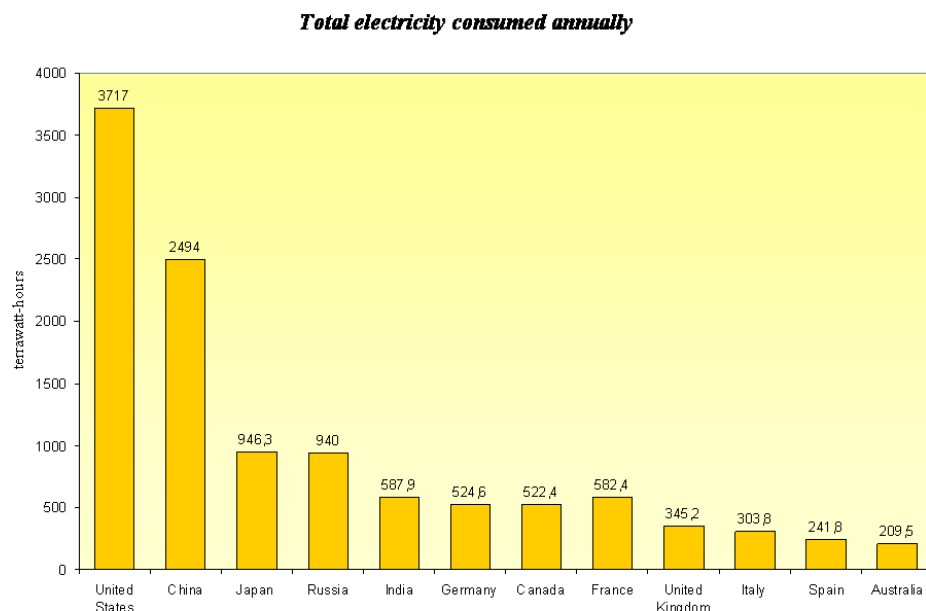


Figure 1.1: Total energy consumed annually in the most important country (source <http://www.energy.eu>).

Oil gas and coal are usually referred to as fossil fuels. The percentage of energy production that is from fossil fuels (oil, coal, and natural gas) was actually still high, more than 70% in the

US in 2006 and nearly 80% in Italy (see figure 1.2). The production of electric power and heat is achieved by the combustion of fossil fuels. Carbon dioxide (CO_2) and sulfur compounds like SO_2 are the product of this process. While the former is related to the greenhouse effect leading to global warming and the rise in sea level, the latter is a cause of acid rain harming the environment.

Moreover, everybody knows that the earth's resources of oil, coal, and natural gas are limited and will deplete sooner or later. Was M. King Hubbert the first to predict in 1956 the Peak oil, the point in time when the maximum rate of global petroleum extraction is reached. After this peak, the rate of production enters terminal decline, as shown in his famous Hubbert curve 1.3.

Most of analyses indicate that the worldwide Hubbert peak would reach in the second decade of 21st century, between 2010 and 2020. This suggests that within 15 years oil and natural gas production rates will start to decrease. With these prospects, new sources of energy must be implemented that do not rely on depleting resources.

The energy sources that use natural resources without depleting them and with no harmful side effects for the environment are called Renewable Sources. Wind energy, energy from water (hydroelectricity), biomass, geothermal and solar energy are the most renowned examples. The most interesting source for its availability, is the sun. The sun has produced energy for billions of years. Solar energy is the sun's rays (solar radiation) that reach the earth. The amount of

The percent share of electricity generated by fossil fuel

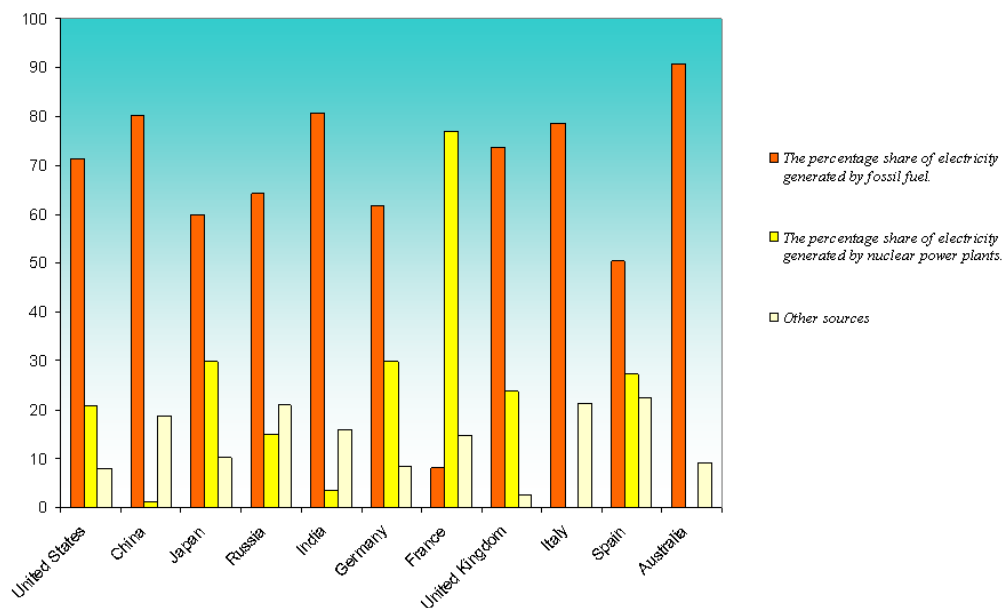


Figure 1.2: The percentage share of electricity generated by different sources (source <http://www.energy.eu>).

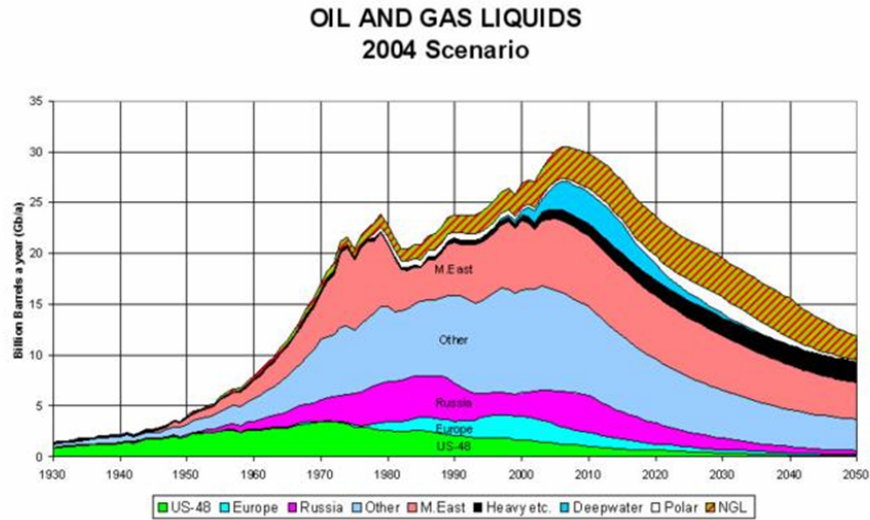


Figure 1.3: The hubbert curve (from *Strategic Significance of America's Oil Shale Resource Volume I Assessment of Strategic Issues*)

energy available from the sun outside the Earth's atmosphere is approximately 1367 W/m^2 ; obviously, some of the solar energy is absorbed as it passes through the Earth's atmosphere. As a result, on a clear day the amount of solar energy available at the Earth's surface in the direction of the sun is typically 1000 W/m^2 . The high power reaching every day all regions of our planet makes this primary source the most interesting between the renewable energy sources. Two are the most important way to exploit sun energy: the solar collector systems, which permit to heat water, or the direct conversion into electric energy in photovoltaic devices. The first technology is quite mature, and already finds a large use also in domestic employment. Unfortunately, at the moment, the second one cannot produce energy at the low cost that conventional fossil fuel power plants can. The R&D focalizes its attention to improve the efficiencies of the PV devices making this technology more convenient (also in term of cost) in respect of those based on fossil fuel. The governs are fortunately investing in this technology, as demonstrate the high photovoltaic capacity installed in some European country, Germany in the lead (fig.1.4).

1.1 Photovoltaic technologies

In the follow, we will present a brief description of most important technologies actually present in PV field, drawing pro and cons of each one. The best research-cells efficiencies are displayed in fig.1.5

1.1.1 Inorganic solar cells

Single-crystal and polycrystalline silicon solar cells

The silicon based PV devices are the most diffused system to convert sun energy in electricity: they dominate the photovoltaic market by 80%. The first silicon solar cell was developed by Chapin, Fuller and Pearson at the Bell Telephone Laboratories in the mid 1950's, and it had

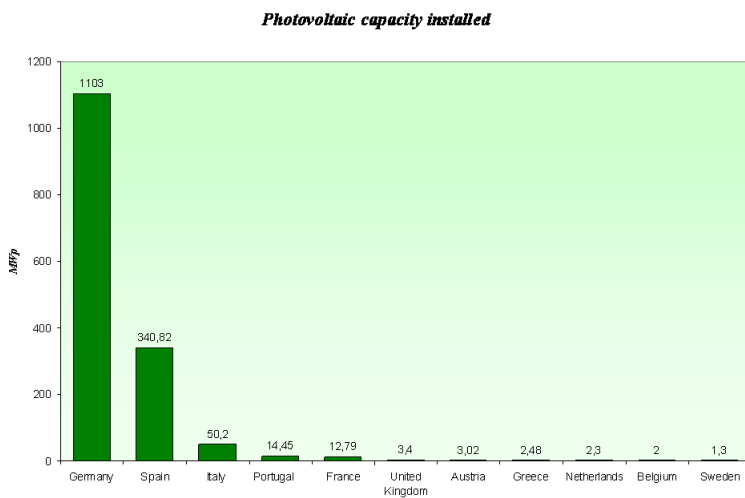


Figure 1.4: Photovoltaic capacity installed in Europe (source <http://www.energy.eu>).

already about 6% efficiency which was rapidly increased to 10%. Solar cell technology benefited greatly from the high standard of silicon technology developed originally for transistors and later for integrated circuits. This applied also to the quality and availability of single crystal silicon of high perfection. In the first years only Czochralski (Cz) grown single crystals were used for solar cells. This material still plays an important role. Polycrystalline material in the form of fragments obtained from highly purified polysilicon is placed in a quartz crucible which itself is located in a graphite crucible and melted under inert gases by induction heating. A seed crystal is immersed and slowly withdrawn under rotation. At each dipping of the seed crystal into the melt, dislocations are generated in the seed crystal even if it was dislocation free before. To obtain a dislocation free state, a slim crystal neck of about 3 mm diameter must be grown with a growth velocity of several millimetres per minute. The dislocation free state is rather stable and large crystal diameters can be grown despite the high cooling strains

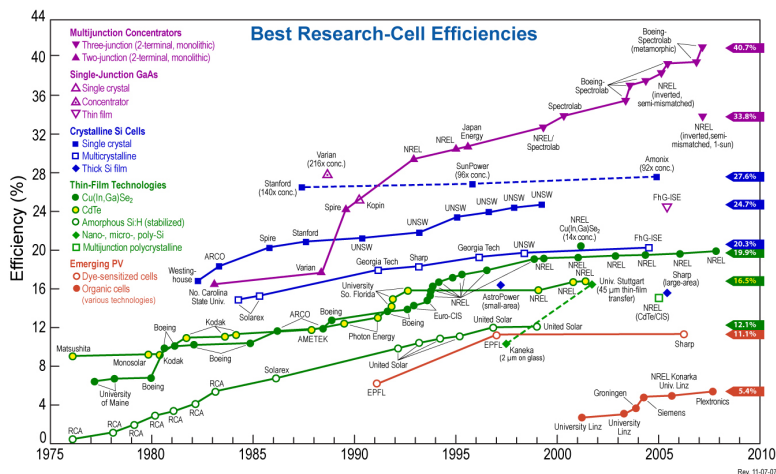


Figure 1.5: Reported timeline of solar cell energy conversion efficiencies.

in large crystals. Actually, the efficiency of the commercial crystalline silicon solar panels is in the best case about 15% (Sharp modules for example REF SHARP), while for a laboratory cell efficiencies over 24% has been measured by Professors Martin Green and Stuart Wenham of University of New South Wales (Highest Silicon Solar Cell Efficiency Ever Reached. ScienceDaily. Retrieved January 21). The high quality of the silicon produced today by the semiconductor industries and the well known technology are the reasons why Si has dominated the PV market. The processing of crystalline silicon wafers is high-level semiconductor technology, and as such expensive and very capital intensive. This also adds directly to the cost of the photovoltaic modules, so that the cost of processed silicon wafers contribute to fifty per cent of the total manufacturing cost of the module.

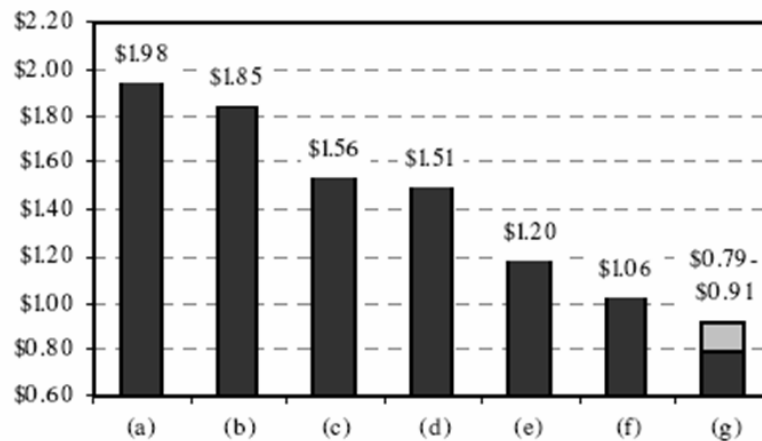


Figure 1.6: How reducing the cost!

The present technology is relatively mature but several studies have shown that it still has a large cost reduction potential. In particular, It has been calculated [3] that the module manufacturing cost is $1.98/W$ for $325 \mu\text{m}$ thick wafers, 13.5% efficient cells, $25/kg$ polysilicon and 25 MW annual production capacity (data of 2003 but approximately already valid today). Several cost sensitive factors have been identified and implemented to determine how reduce the manufacturing cost below $1/W$, limit that can make polysilicon cells cost less with respect standard fossil sources. In Figure 1.6 is shown that: a) slurry recycling during wafer slicing will reduce the cost to $1.85/W$; b) reduction of the cell thickness to $200 \mu\text{m}$ will then bring the cost down to $1.56/W$; d) increasing the cell efficiency to 17% will lower the cost to $1.20/W$. Fig. 1.7 shows a contour plot for the synergistic effect of thickness and efficiency on cost for a 25 MW production line. The $1/W$ line in this figure indicates that either 200- m thick, 18% cell or 160- m thick, 17% cell can produce $1/W$ modules for a 25 MW production line. The scale up of production lines from 25 MW to 100-500 MW will reduce the manufacturing cost appreciably below $1/W$. The reduction of thickness of silicon modules could become a real solution to reduce cost of PV silicon cells. The problem is the low absorption of this material: Light trapping and light recycling systems may be the solution.

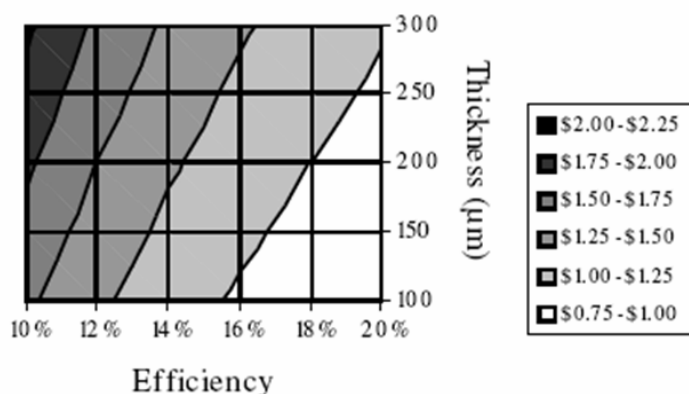


Figure 1.7: synergistic effect of thickness and efficiency on cost of silicon solar cells.

Thin film Si

Also from similar considerations, has been developed the thin crystalline silicon film technology. The first thinner silicon wafers for solar cells were made by Wolf and Lofersky while simulating the ideal parameters for record high efficiencies [4], [5]. They pointed out that with decreasing cell thickness, the open circuit voltage increases due to the reduced saturation current which again is a result of a decreasing geometry factor. In these papers, the benefits of a thickness in the order of 30 nm were quantified, also demonstrating the importance of low surface recombination velocities and a good optical confinement to make use of these advantages. There is a large variety of silicon deposition technologies which can roughly be allocated to the main groups liquid phase and gaseous phase deposition. In the liquid phase deposition, the respective substrate is brought into contact with a metal melt (Cu, Al, Sn, In) saturated with silicon. By lowering the temperature of the melt supersaturation occurs and silicon is deposited on the substrate. The term liquid phase epitaxy (LPE) process is also used when the growth is not epitaxial. In the chemical vapour deposition (CVD) method, which is a well-established method in microelectronics, a mixture of H₂ and the precursors SiH_4 , SiH_2Cl_2 , or $SiHCl_3$ is decomposed thermally at the hot surface of the substrate. The most common techniques are low pressure and atmospheric pressure CVD (LP-CVD, AP-CVD), but also plasma enhanced, ion-assisted or hot-wire CVD (PE-CVD, IA-CVD, or HW-CVD) are used. There is little known about the economical aspects of the different deposition methods when used in large scale production of solar cells, but there is a trend towards APCVD due to the potential for continuous inline processing and realized deposition rates of more than 5 mm/min. The efficiency potential of thin crystalline silicon can reach conversion efficiencies of up to 21% under ideal conditions. Generally, it must be noted, that most realized cells were still made on Si-wafers as substrates. Such test structures were made under ideal conditions using the best understood materials available aiming to prove the respective concept and to study the influence of the different boundary conditions on the cell performance.

Amorphous silicon

The first publications on amorphous silicon (a-Si) relevant for solar cell fabrication appeared after the late 1960s [6]. The first paper at a photovoltaic conference was presented in the 12th IEEE PVSC (1976). Only 5 years later, the first consumer products appeared on the market. Amorphous silicon begins to enter the power market with stabilized cell efficiencies reaching 13%. Module efficiencies are in the 6-8% range. Amorphous silicon is an alloy of silicon with hydrogen. The distribution of bond length and bond angles disturbs the long range of the crystalline silicon lattice order and consequently changes the optical and electronic properties. The optical gap increases from 1.12 to about 1.7 eV. Basis for all deposition processes is silane as precursor gas in a chemical vapor deposition (CVD) process. Sputtering is not the method of choice for active semiconductor layers also in the case of amorphous silicon. Typical deposition temperatures are below 500°C, otherwise no hydrogen is incorporated in the film. The most commonly used method is plasma enhanced chemical vapour deposition (PECVD). Besides a variety of designs of the plasma reactor (diode, triode configurations) a range of frequencies from radio frequency (RF) to ultra high frequencies (UHF) is applied.

Non silicon based thin film solar cells

Thin film solar cells are referred to as the second generation photovoltaic technology (the crystalline silicon is the first). The materials used in this technology are: amorphous silicon (a-Si), cadmium telluride (CdTe), copper indium gallium diselenide (CIGS), and thin film crystalline silicon. The driving force for the development of thin film solar cells has been their potential for the reduction of manufacturing costs: thin film semiconductor materials can be deposited onto large surfaces, while silicon solar panels are assembled from individual cells processed from about 100 cm² silicon wafers, that is a problem for the industrial processes. An interesting property of these materials (CdTe, CIGS, CIS) is that they are direct band gap semiconductors: they have a higher absorption coefficient than silicon. This means that it's possible to employ a reduced amount of material (typically 100-1000 times less than for Si) to absorb the same solar radiation and reduce the cost of modules.

Cadmium telluride

With a direct optical energy bandgap of 1.5 eV and high optical absorption coefficient for photons with energies greater than 1.5 eV, only a few microns of CdTe are needed to absorb most of the incident light. Because only thin layers are needed, material costs are minimized, and because a short minority diffusion length (a few microns) is adequate, expensive materials processing can be avoided. Moreover, its optimal band gap permits to have efficiencies up to 16% in laboratory [7]. The CdTe p-type absorber layer, 3–10 μm thick, can be deposited using a variety of techniques including physical vapour deposition (PVD), CSS, electrodeposition, and spray pyrolysis. The problem is on materials: the Cadmium present in these cells creates some problem that could be solved by recycling. The efficiencies of commercial modules reach efficiencies in the range of 8-9%.

Copper indium diselenide

The first chalcopyrite solar cells developed were based on the use of CuInSe_2 (CIS). It was, however, rapidly realized that incorporating Ga to produce the solid solution $\text{Cu}(\text{In,Ga})\text{Se}_2$ (CIGS), results in a widening of the energy bandgap to 1.3 eV and an improvement in material quality, resulting in solar cells with enhanced efficiencies. CIGS has a direct energy bandgap and high optical absorption coefficient for photons with energies greater than the bandgap, such that only a few microns of material are needed to absorb most of the incident light, with consequent reductions in material and production costs. CIGS solar cells have been produced with efficiencies of 19.5% [8] and modules with efficiencies of 13.4%. The CIGS absorber layer is formed mainly by (i) the coevaporation of the elements either uniformly deposited or using the so-called three-stage process, or (ii) the deposition of the metallic precursor layers followed by selenization and/or sulfidization.

III-V Semiconductor

s GaAs, GaAlAs, GaInAsP, InAs, InSb, and InP are materials with very good properties for solar cell technology: they have near-optimal band gaps. Their defect is in the cost: they are too expensive to be employed on commercial solar cells. In fact they have found applications only in the space vehicle power supplies, where performances are more important criteria than cost. An other possibility is to use these materials coupled with concentrating systems where the active surface area of the cells can be reduced significantly: this point is could be very important for our PhD thesis, as we will show in the follow.

1.1.2 Organic solar cells

In our daily life synthetic organic materials such as plastics are used everywhere: as coatings and packing materials and in form of plastic consumer products. It isn't a big surprise, the discovery of possibility replacing of the inorganic semiconductors with new semiconducting polymers. One of the possible future applications of these materials is an organic solar cell. Organic materials used presently in solar cells include for example conducting polymers, dyes, pigments, and liquid crystals. The potential of organic solar cells is related to low-cost of polymer technology, and the easily large area films fabrication, cut from rolls and installed onto permanent structures. Inspired by the significant progress in solar cell efficiencies with some organic materials such as dyes in the case of dye-sensitized solar cells and the discovery of efficient charge transfer between certain organic electron donor and acceptor molecules, the research on organic photovoltaic materials has grown rapidly during the last decade and is very active at the moment.

In a crystalline inorganic semiconductor with a 3D crystal lattice the individual LUMOs and HOMOs form a Conduction Band (CB) and a Valence Band (VB) throughout the material. This is fundamentally different from most organic dye semiconductors where the intermolecular forces are too weak to form 3D crystal lattices. Consequently the molecular LUMOs and HOMOs do not interact strongly enough to form a CB and VB. Thus charge transport proceeds by hopping between localised states, rather than transport within a band. This means that

charge carrier mobility in organic and polymeric semiconductors are generally low compared to inorganic semiconductors. Also, charge separation is more difficult in organic semiconductors due to the low dielectric constant. In many inorganic semiconductors photon absorption produces a free electron and a hole (sometimes called charge carriers), whereas the excited electron is bound to the hole (at room temperature) in organic semiconductors (the so called Exciton).

Dye solar cells

Photoconductivity was first observed on anthracene in the beginning of the 20th century. But the first real PV investigations were done on porphyrins and phtalocyanines, and this class of compounds has remained among. The easiness to prepare these compounds, their highly colouration and tendency to form crystalline films by vacuum sublimation with good semiconducting properties make this class of compounds the most investigated dyes. Also, they readily form complexes with a number of metal ions.

Plastic Solar Cells

A promising approach towards low cost photovoltaic devices is fabrication of solar cells based on semiconducting polymer materials. Two are the most important characteristic of these materials: the high absorption coefficient and the solubility in common organic solvents. The combination of these two properties makes the polymer PV technology one of most interesting and promising in the PV panorama. For the high absorption coefficient, 100 nm thick film can absorb up to 70% of incident light the becomes 90% when we use a metallic electrode. (In figure 1.8 the fraction of absorbed incident light with the P3HT film thickness). Small quantities of material are used to produce a large surface of solar cells.

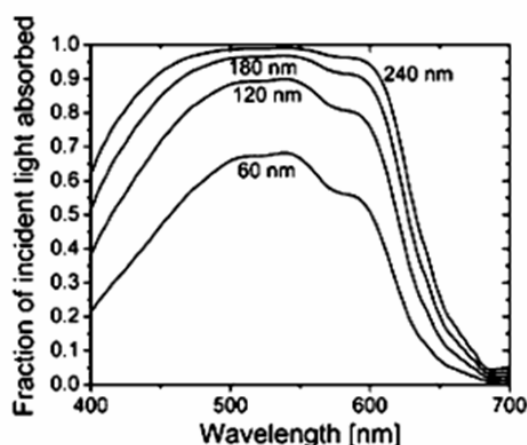


Figure 1.8: Fraction of incident light absorbed by P3HT film at different thickness.

The solubility makes thin film device production relatively easy by spin cast or doctor bladed or some other similar technique. Moreover, the thinnest of film could be exploited to

realize flexible devices on plastic substrates. The chemical and physical details of the plastic solar cell technology will be presented in the chapter 2.

Hybrid solar cells

Hybrid solar cells are a mix of nanostructures of both organic and inorganic materials. Therefore, they combine the unique properties of inorganic semiconductor nanoparticles with properties of organic/polymeric materials. Their attractive drives from low cost synthesis, processability and versatile manufacturing of thin film devices. Also, the size of inorganic semiconductor nanoparticles may tune the optical band-gap. Thus, the organic/inorganic hybrid concept for photovoltaic solar cells is getting interesting and attractive in recent years. In the literature, hybrid solar cells are manufactured using different concepts such as solid state dye-sensitized solar cells and hybrid solar cells using the bulk heterojunction concept with different nanoparticles such as TiO_x, ZnO, PbS and others. A dye-sensitized solar cell of Graetzel type comprises of several different materials such as nanoporous TiO₂ electrodes, organic or inorganic dyes, inorganic salts and metallic catalysts. After absorption of a photon, the excited electron within the sensitizer molecule is transferred to the conduction band of TiO₂, and diffuses through the porous TiO_x network to the contact. The oxidized sensitizer molecule is reduced to the original state by supply of electrons through a liquid electrolyte redox couple thin the pores. This photovoltaic conversion system is based on light harvesting by a molecular absorber attached to a wide band-gap semiconductor surface. It's useful to enlarge the interface between the semiconductor oxide and the dye to promote the increase of absorbed incident light by introducing a nanoparticle based electrode. Many different compounds have been investigated for semiconductor sensitization, such as porphyrins, phthalocyanines and others. Cells based on this concept show energy conversion efficiencies up to 11% [9] on small-area cells and module efficiencies between 5% and 7%.

Chapter 2

Electronic Model for Organic Solar Cells

Inorganic semiconductor physics can not be completely applied in organic solar cells: their specific physics is still under investigation. However, special feature of both semiconductors are two quasi-continua of charge carrier transport levels: the energetically lower quasi-continuum is nearly completely filled with electrons, whereas the upper one is nearly empty. They are separated by an energy exceeding by far $k_B T$ at moderate temperatures T (at room temperatures $k_B T \approx 0.26 meV$): for this reason, thermal excitation of an electron from the lower into the higher level is unlikely at room temperature. The energetic distance between the discrete levels is much smaller than $k_B T$: for this reason the name quasi-continua. The region between the quasi-continua has no available electronic levels and is the forbidden region or energy gap E_G . In figure is shown the simple electronic model system of a semiconductor with two levels.

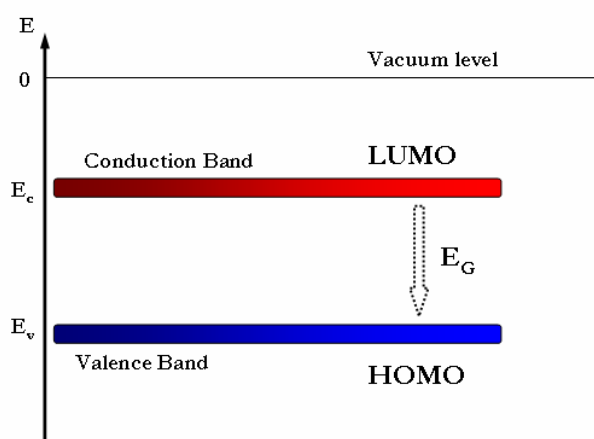


Figure 2.1: A simple two-level system. For organic semiconductors the valence band corresponds to the HOMO and conduction band to the LOMO.

In inorganic semiconductor the lower level, the so-called valence band is delocalised over the whole material in the ideal case of perfect crystallinity, while in organic semiconductors the basic entities are molecules and the delocalisation of the levels is much less pronounced due to

the weak Van-der-Waals binding. Here the bands are formed by the occupied binding orbitals of the single molecules, the so-called Molecular Orbitals (MO). The *HOMO* (Highest Occupied Molecular Orbital) in molecular semiconductors corresponds to the edge of the valence band in inorganic semiconductors. The energetically higher lying quasi-continuum, called conduction band, corresponds to the *LUMO* (Lowest Unoccupied Molecular Orbital). A large number of molecules, each-one characterised by these two distinct energy levels, forms the molecular semiconductor which consequently consists of an ensemble of two energy levels called a two-level system. Organic solar cells consist of a donor-acceptor system of two semiconducting components with their respective energy levels: here the HOMO is represented by the lower energy level of the donor component whereas the LUMO is represented by the upper energy level of the acceptor component.

2.1 The two level system in thermal equilibrium

Under equilibrium conditions, whereby the system is kept in the dark and the occupation of the states is in equilibrium with the background radiation (300 K), the occupation of the upper energy level is very small. The probability of electron occupation $f_F(E)$ of one-electron states with energy E is described by the Fermi-Dirac distribution:

$$f_F(E) = \frac{1}{\exp\left(\frac{E-E_F}{k_B T}\right) + 1} \quad (2.1)$$

where E_F is the so-called Fermi energy. In order to calculate the number n of electrons per unit volume in the energy interval $[E, E + dE]$, the states occupation probability $f_F(E)$ has to be multiplied by the density of states $D_e(E)$ in this energy interval. Hence the density of electrons between E and $E + dE$ is then given by:

$$dn(E) = D_e(E)f_F(E)dE \quad (2.2)$$

$D_e(E)$ represents the number of charge carriers which can occupy the distinct energy level in a certain volume of the semiconductor. For small electron and hole densities relative to the density of states, Fermi-statistics can be approximated by Boltzmann statistics. This precondition is fulfilled for energies exceeding the Fermi energy on the order of $k_B T$.

$$f_{B,e}(E) = \exp\left(-\frac{E-E_F}{k_B T}\right) \quad (2.3)$$

The density of electrons n in the conduction band can then be calculated according equation (2.2):

$$n = \int_{E_C}^{\infty} D_e(E)f_B(E)dE \approx N_C \exp\left(-\frac{E_C-E_F}{k_B T}\right) \quad (2.4)$$

E_C is the energy of the conduction band edge and N_C is the effective density of states of the conduction band, containing the constant factors of integration. The equation is valid as

long as n is small compared to N_C . Similar calculations can be made for the density of holes p , that are unoccupied electron states of the valence band; thus they have the same density of states as the electrons:

$$p = \int_{-\infty}^{E_V} D_e(E)(1 - f_B(E))dE \approx N_V \exp\left(-\frac{E_F - E_V}{k_B T}\right) \quad (2.5)$$

with E_V the energy of the valence band edge and N_V the effective density of states of the valence band. The intrinsic carrier density n_i is a constant property of the material; thermal excitation of electrons into the upper energy level of an intrinsic (undoped) semiconductor leads to equal densities of electrons and holes in their respective energy levels ($n = p = n_i$). Consequently we have that

$$n_i^2 = np = N_C N_V \exp\left(-\frac{E_C - E_V}{k_B T}\right) = N_C N_V \exp\left(-\frac{E_G}{k_B T}\right) \quad (2.6)$$

For an intrinsic semiconductor, electrons in the conduction band originate from the valence band and hence $p = n$. From equations (2.4) and (2.5), the position of the Fermi energy can be calculated as:

$$E_F = \frac{1}{2}(E_V + E_C) + \frac{1}{2}k_B T \ln \frac{N_V}{N_C} \quad (2.7)$$

At low temperature or when $N_V \approx N_C$ the Fermi level of a intrinsic semiconductor is in the middle of the gap.

2.2 The Two-Level System under Illumination

In the following section the thermal equilibrium of our system will be disturbed by illumination. Upon illumination of the two-level system with a photon energy which exceeds the energy gap E_G , an electron in valence bond can absorb it and be excited to the conduction band. This leaves a hole in the valence band: thus, the density of electrons and holes increases with equal quantities, as determined by the charge carrier generation rate G . As a consequence, the description of the system according to equation (2.6) is no longer valid: this new situation can be described applying Boltzmann statistics by introducing two separate quasi-Fermi energies for electrons and holes. The corresponding charge carrier densities can be calculated as:

$$n = N_C \exp\left(-\frac{E_C - E_{F,C}}{k_B T}\right) \quad (2.8)$$

$$p = N_V \exp\left(-\frac{E_{F,V} - E_V}{k_B T}\right) \quad (2.9)$$

Here $E_{F,C}$ and $E_{F,V}$ are the quasi-Fermi energy levels (QFL) for electrons and holes respectively. The product of the electron and hole density is:

$$np = N_V N_C \exp\left(-\frac{E_C - E_V}{k_B T}\right) \exp\left(-\frac{E_{F,C} - E_{F,V}}{k_B T}\right) = n_i^2 \exp\left(-\frac{E_{F,C} - E_{F,V}}{k_B T}\right) \quad (2.10)$$

The average energy, which can be extracted from an electron-hole pair is equal to the difference of the Fermi energies of valence and conduction band, and respectively

$$E_{F,C} - E_{F,V} = E_G + k_B T \ln \frac{np}{N_V N_C} \quad (2.11)$$

The difference of the QFL energies increases with increasing density of charge carriers in their respective energy levels by illumination, but it is always below the energy gap E_G because the excitation of electrons into the upper energy level competes with the process of stimulated emission and radiative recombination. Stimulated emission is mediated by a photon under emission of a photon of the same wave function. The predominant mechanism in organic solar cells, recombination over trap states, will be discussed in following chapter. Without external influence, an electron decays directly from the conduction band to the valence band and recombines with a hole emitting a photon of energy $\hbar\omega = E_G$. The probability of recombination increases with the increasing occupation of the upper level. The recombination rate R per unit volume is given by

$$R = r (np - n_i^2) \quad (2.12)$$

where R is the number of recombinations in a certain volume and time interval and r the recombination rate that has the dimension s^{-1} . Only the charge carriers exceeding the intrinsic charge carriers have to be taken into account. The system is described under illumination and with consideration to recombination, corresponding to the situation of the open-circuit condition of an illuminated solar cell where no charges are extracted. Now, we consider the case with ideal contacts and an external load, calculating the current-voltage behaviour will be calculated.

2.3 Charge Carrier Extraction at the Contacts

Extra charges generated in semiconductor under illumination, require suitable contacts to be extracted converting the chemical potential energy into electrical energy. Ideal contacts at which no charges and no energy are lost during charge carrier extraction have to be semipermeable, i.e. only permeable for the respective type of charge carriers, to guarantee that no current is lost at the contacts and have the Fermi levels matching the QFL of their respective charge carriers, to not losing chemical potential energy. In the case of ideal contacts, shown in 2.2, both have semipermeable membranes and hence allow only the selective passage of the respective charge carriers. The workfunctions Φ_m , i.e. the Fermi levels of the contacting metal, match the QFLs of the allowed charge carrier at the membranes; the difference, $\Phi_{m1} - \Phi_{m2}$

defines the built-in potential V_{bi} .

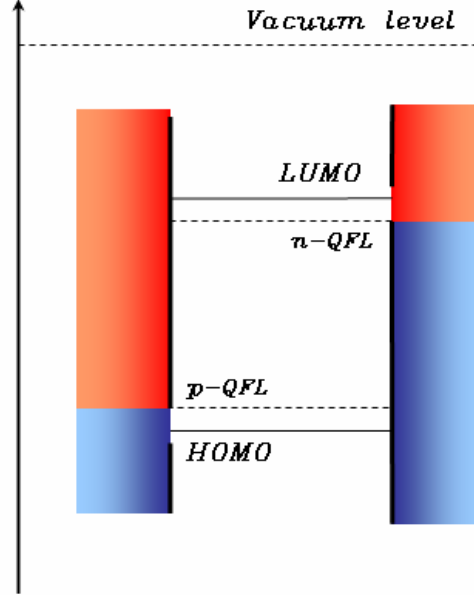


Figure 2.2: Ideal contacts at which no energy and no charge carriers are lost during the conversion of chemical potential energy to electrical energy.

Extractable current can be calculated using the continuity equation for holes and electron; it describes the relation between the charges generation rate G , the recombination rate R and the current flow of charge carriers J through the external load. For the stationary case the continuity equation becomes:

$$G - R - \nabla \cdot J = 0 \quad (2.13)$$

Using equation (2.12) and (2.11), the external current can be calculated as:

$$\nabla \cdot J = G - r \left[n_i^2 \exp\left(\frac{E_{F,2} - E_{F,1}}{k_B T}\right) - 1 \right] \quad (2.14)$$

Equation describes a fundamental relation in photovoltaics, in ideal case consisting of a two-levels system with ideal contacts attached to an external load. The difference in the quasi-Fermi energies corresponds to the voltage of the solar cell under distinct working conditions. In figure 2.3 it's shown that the extractable power reaches a maximum at a determinate value of QFLs splitting: this splitting is influenced by the G and by the bias voltage applied to the contacts.

In the ideal case J increases linearly with the generation rate when $E_{F,C} - E_{F,V} = 0$, or in short circuit conditions; in this case all charges are extracted. At open circuit, i.e. when $j = 0$, all generated charge carriers recombine: the splitting of the QFLs increases logarithmically with G .

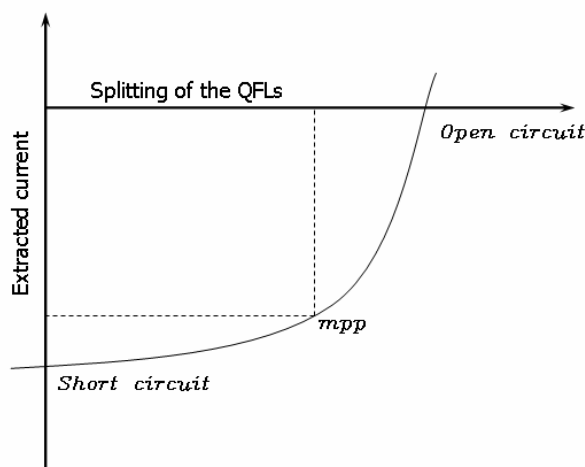


Figure 2.3: Extractable current as function of QFL-splitting in an illuminated semiconductor.

2.4 Contact Models for the Two-Level System

The conditions of ideal contacts cannot be assumed for most of the organic solar cells: the analogy with semi-permeable membranes can be regarded valid for bilayer type organic solar cells with the donor-type and an acceptor-type layer sandwiched between electrodes that are attached to the respective semiconductor, resulting in the specific selectivity. The bulk hetero-junction solar cell, the most diffused polymeric solar cells system consist of a donor-acceptor interface which is distributed over the entire volume of the absorber. For this reason, both transport levels will be in contact with both electrodes: thus, selective electrodes are not likely but we can assume a partial selectivity. Two possible models under different working conditions are presented: the electric field driven cell with asymmetric and not semi-permeable contacts and the solar cell with semi-permeable and symmetric contacts. A superposition of these two models is better picture of the behaviour of real organic solar cells.

Electric Field driven Solar Cell

When electrodes with different workfunction are contacted to the semiconductor, the built-in potential V_{bi} is generated, and its amplitude is given by the difference of workfunctions of metals:

$$V_{bi} = \Phi_{m1} - \Phi_{m2} \quad (2.15)$$

Different working conditions are shown in figure 2.4: the work function of the electrode forming the hole contact matches the HOMO-level of the donor component, whereas, for electrons, the LUMO-level of the acceptor component matches the work function of the cathode.

Six different conditions are presented:

1. Short-circuit conditions in the dark. After contact the Fermi-level is aligned between the

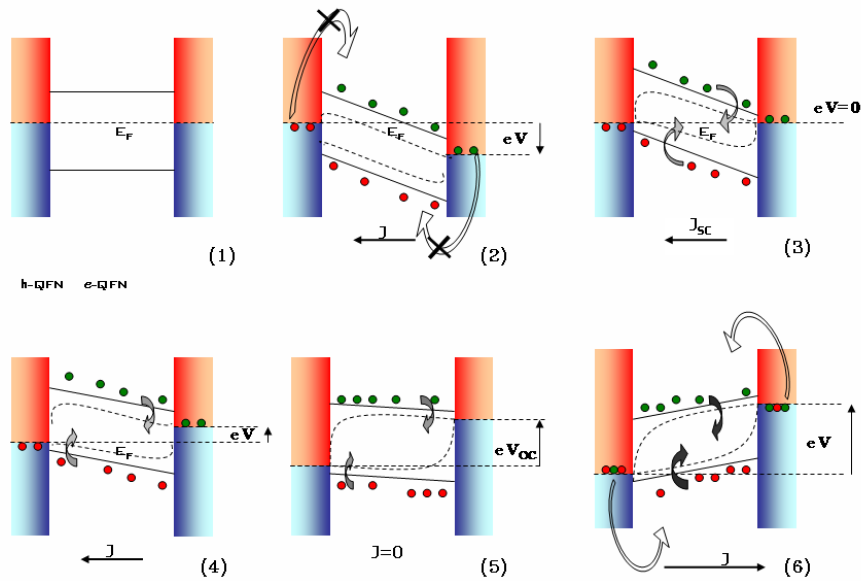


Figure 2.4: Energy diagrams of solar cells under different bias conditions.

two electrodes: electrons are injected from the low work function electrode (anode) into the LUMO-level and holes are injected from the high work function electrode (cathode) into the HOMO level until the created built-in potential V_{bi} opposes further current flow and chemical equilibrium is reached. The diffusion through the thin semiconductor into the counter electrode is compensated by the resulting electric field.

2. Reverse bias under illumination. Two Fermi-levels for electrons and holes are generated by the splitting of Fermi level. Only the photogenerated charge carriers can be extracted at the respective electrodes: the injection of holes from the anode into the HOMO-level as well as the injection of electrons from the cathode into the LUMO-level are energetically unfavourable.
3. Short-circuit conditions. The difference between the potentials of the two contacts is zero, but a gradient in the chemical potential energy drives the charges to their respective contacts. Without series resistance and no charge recombination, all generated electron-hole pairs will be extracted.
4. Working conditions. When an external load is inserted in the circuit, the potential difference reduces the electric field inside the solar cell. Recombination increases and some charges are lost at the wrong contact because interfaces are not semipermeable.
5. Open circuit conditions. No current is extracted from the solar cell, because all charges recombine inside.

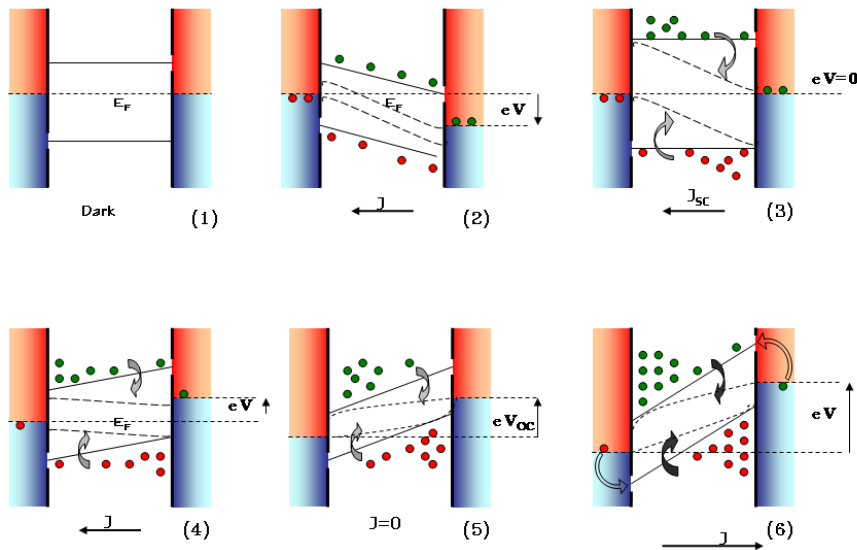


Figure 2.5: Energy diagrams for solar cells with semipermeable membranes under different bias conditions.

6. Forward bias conditions. Electrons are injected from the anode into the LUMO-level and holes are injected from the cathode into the HOMO-level and they either recombine in the bulk or at the opposite electrode. Which are the working conditions for the OLED.

Solar Cells with Semipermeable Membranes

The case of semipermeable contact with same workfunction which does not match either QFL in the semiconductor is the extreme opposite case. The work functions of the electrodes are symmetric and are located in the middle of the semiconductor gap. The resulting built-in field V_{bi} is zero. Again, in figure 2.5 are shown characteristic situation like for the previous case.

1. Short-circuit conditions in the dark. The Fermi level is constant throughout the semiconductor and equals the work functions of the contacts. The resulting built-in potential $V_{bi} = 0$. The system is in thermal equilibrium with the ambient at temperature T .
2. Reverse bias under illumination. A splitting of the QFLs is generated by the photogenerated charge carriers. Applying a reverse bias leads to a quick extraction of nearly all photogenerated charge carriers. Recombination can largely be neglected.
3. Short circuit conditions. The internal electrical field is zero, but a concentration gradient builds up for the accumulation of charges at their non-permeable contact and drives the charge carrier to their respective permeable contact. The recombination is increased due to the population of the states. Not all generated charges are extracted.

4. Working conditions. When a small external load is attached, the superimposed electric field opposing the current flow inside the solar cell is further increased by the potential drop at the external load. The diffusion gradient of the QFLs however still drives the charge carriers to their respective electrode, but recombination rises further.
5. Open circuit condition. No current can be extracted from the cell: all charges recombine and the open circuit voltage can be measured by the contacts. It results from the splitting of the QFLs.
6. Forward bias conditions. Charges are injected from the contacts and are accumulated at the opposite electrode. They recombine in the bulk, but not at the surface of interfaces.

Chapter 3

Organic semiconductors

Organic semiconductors have essential differences from inorganics and it's importante to highlights these differences before discussing in detail the organic solar cell architecture. The conducting and semiconducting properties of polymers were discovered with the accidentally iodine doping of poly-acetylene: it turned out that with high doping levels, PA changed from being an insulator to being a good conductor which had not been observed in polymers before. Subsequently other polymers showed this conducting and semiconducting behaviour and it was possible to create new materials with these properties.

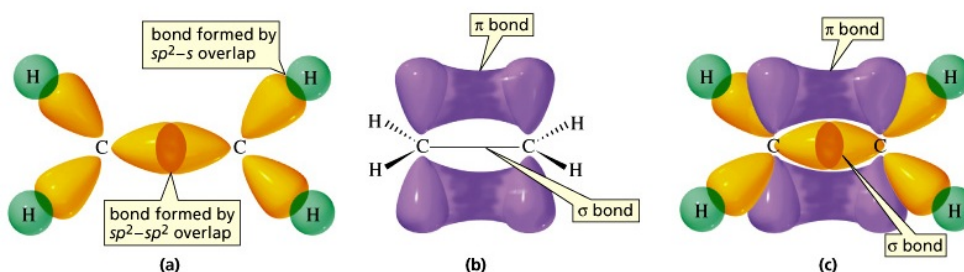


Figure 3.1: Orbital structure of conjugated sp^2 hybridized carbon atoms. (a) Ethene is composed a pair of double bonded carbon atoms. The first bond is formed by overlapping σ -orbitals, while the second bond is formed by interacting π -orbitals. (b) Delocalisation of π -electrons. (c) The complete orbital structure of ethene (or ethylene).

Polymers, oligomers, dendrimers, dyes, pigments, liquid crystals, organo-mineral hybrid materials, all organic semiconductors share in common part of their electronic structure, based on conjugated π -electrons. By definition, a conjugated system is made of an alternation between single and double bonds. Ethene, butadiene and benzene are basic representative elements of conjugated systems; in fig.3.1 the orbital structure of ethene, the simplest example of a conjugated π -electron structure, is illustrated. Non-carbon substituents may also be introduced into conducting organic molecules, and as long as they also contain a π -orbital, π -conjugation within the system can be preserved. The essential property which comes out from conjugation is that the π electrons are much more mobile than the σ electrons; they can jump from site to site between carbon atoms with a low potential energy barrier as compared to the ionisation potential. The π electron system gives all the essential electronic features of organic materials:

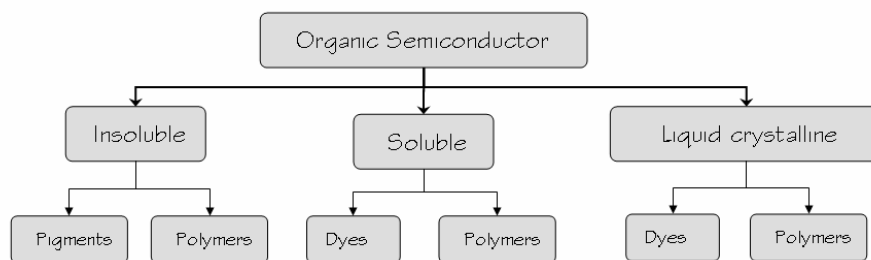


Figure 3.2: Organic semiconductors can be divided into different categories according to their properties: soluble, insoluble and liquid crystalline.

light absorption and emission, charge generation and transport. Each carbon atom in a conjugated system has 3 nearest neighbours with which it forms 3 equivalent σ bonds made from the trigonal sp^2 hybridisation of 3 valence atomic orbitals of the carbon atom: $2s$, $2p_x$ and $2p_y$ for instance. For such a hybridisation state, the fourth orbital $2p_z$ lies perpendicular to the σ bond plane. It is the lateral overlap of these out of plane $2p_z$ atomic orbitals which gives the π bonds. In most molecules double bonds are localised and the two extreme positions are usually not equivalent. A more general definition of a conjugated system would be an ensemble of atoms whose p -orbitals overlap.

In 3.2 shows how organic semiconductors can be divided into different categories due to their processing and mechanical properties. We also distinguish between molecules that have only a few (oligomers) or no (monomer) repeat unit and molecules (polymers) which have more than about 10 repeat units. Oligomers and monomers that absorb visible light are often called chromophores and are referred to as dyes if they are clearly soluble or pigments if they are not. Liquid crystalline materials have only recently been investigated for the use in LEDs and organic solar cells [10]-[11]-[12]-[13]. For a certain temperature range these material exhibit a phase where the molecules move like in a liquid but are still able to sustain or attain a certain structural order among the molecules as in crystalline materials. Such molecules have to have a strong asymmetry to show structural order and are therefore either rod-like (calamitic) or disc-like (discotic) molecules. "Mechanical" properties depend mainly on the position and number of side chains. Side chains are usually attached to molecules to introduce or improve solubility. They are more successful in solubilising the molecule the better they can prevent aggregation between molecules. Flat molecules in particular have a strong tendency to stick together due to π - π interaction and form clusters of solids in many solvents. Bulky side chains can separate these molecules and make it easier for solvent molecules to surround the individual molecules i.e. dissolve them. Typically, smaller molecules are better soluble and/or have lower sublimation temperatures but larger molecules give better films upon spincoating. When the carbon chain length is increased, the molecule becomes a polymer. It has been proved experimentally, in the case of thiophene [14], for instance, and theoretically in the case of phenyl-vinylene oligomers for instance [15], that oligomers with more than 5 to 8 repeat units bear all the essential electronic properties of the infinite polymer chains as concerns absorption and emission of light.

Polymers are bonded by strong covalent bonds. As π -orbitals overlap is weaker than σ -

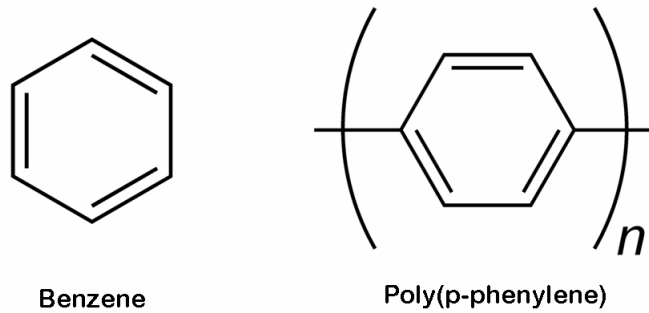


Figure 3.3: The molecular structure of Benzene and of poly(p-phenylene)

orbitals overlap, the energy spacing (band gap) between bonding and antibonding molecular orbitals is larger for the π - π^* difference than for the σ - σ^* one. One can thus, in a first approach, limit the band study to the π - π^* molecular orbitals. Those are respectively the HOMO and LUMO, in terms of molecular physics. σ -bonds only contribute to the stability of the molecular structure. As an example, the case of the infinite polyparaphenylene (PPP) chain is treated by Moliton within the Hückel theory [16]. PPP (with molecular formula $-(C_6H_4)_n-$) is a chain of benzene rings attached in the para position. In the case of benzene, the HOMO-LUMO band-gap is $E_g = 5.5eV$, as determined experimentally. In the case of the PPP polymer chain, the π and π^* orbitals split into two bands: the valance VB and conduction CB bands, with a band gap $E_g = 3eV$. When the chain length is reduced, the maximum absorption of PPP shifts continuously to the blue, according to an experimental law $E_{max} = (3.36 + 3.16/n)eV$ [17], where n is the number of repeat units (benzene rings) of the oligomer. The same type of law applies to all the so-called alternated conjugated polymers (polymers in which double bonds are localized). This implies that in a 'real' conjugated polymer with random length, corresponding to what most chemical synthetic routes deliver, the bands are broadened and the band gap is apparently reduced.

The diagram (3.4) shows the conversion steps of photons into separated charges as it takes place in an organic solar cell and the associated loss mechanism. In the following single conversion steps are explained, with regard to the special situation in organic solar cells.

3.1 Absorption and exciton generation

In most organic device not all incident light is absorbed; the majority of semiconducting polymers have bandgaps too high, more than 2.0eV (600nm), limiting the possible absorption to about 30%, whereas a bandgap of 1.1eV (1100nm) is required to absorb 77% of the solar radiation on earth. Upon absorption of an incoming photon, an electron is promoted into the LUMO level, leaving behind a hole in the HOMO level. Due to the low dielectric constant ($\epsilon_r \approx 3 - 4$) compared to most inorganic semiconductors (>10) and to energy gap, the strong electron-phonon interaction in organic materials the photo-physics in this class of materials is often different compared to the inorganic semiconductors and not yet fully understood. One of the main differences is that photo-excitation in these materials does not automatically lead to

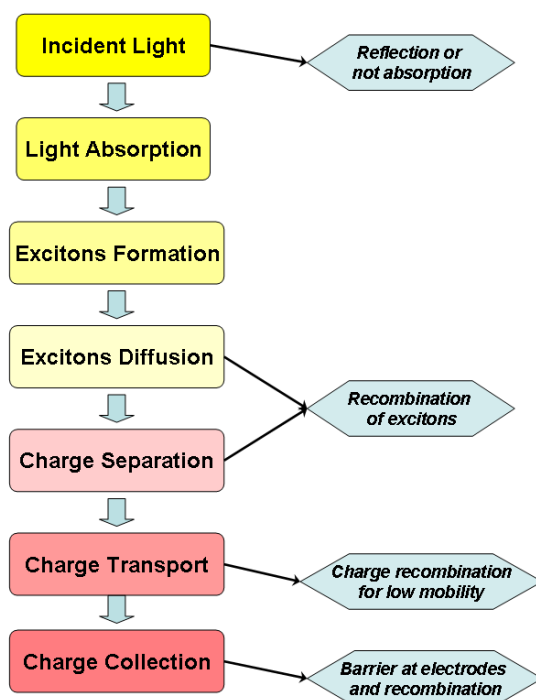


Figure 3.4: Conversion steps in organic solar cell.

the generation of free charge carriers, but to bound electron-hole pairs (excitons). This means that the electron and hole remain localised on a few polymer repetition units or a molecule and are bound to each other by their electrostatic attraction. Excitons have Coulombic binding energies ranging from about 100meV to 1eV, but they are electrical neutral (thus to first order unaffected by external electric fields); they carry energy but no net charge and need to be split up (or dissociate) before the charges can be transported through the film and collected at the electrodes. For example, exciton dissociation can occur at a rectifying interface (Schottky contact) in single layer devices or at the interface between an electron-donor and an electron-acceptor semiconductor material. The separated charges then need to travel to the respective device electrodes, holes to the anode and electrons to the cathode to provide voltage and be available for injection into an external circuit. For inorganic semiconductors typical binding energies of photogenerated electron-hole pairs are typically far below $k_B T$ (ca. 26meV at room temperatures) such that free charge carriers are generated upon photoexcitation due to thermal dissociation. The categorisation into conventional semiconductors, i.e. most inorganic, and excitonic semiconductors, which includes organic semiconductors, has been done by the ratio of the width r_C of the Coulombic potential well at $k_B T$ and the Bohr radius of the relevant

charge carrier r_B [18]:

$$\gamma = \left(\frac{r_C}{r_B} \right) \approx \left(\frac{e^2}{4\pi\epsilon_0\kappa_B r_0 m_e} \right) \left(\frac{m_{eff}}{\epsilon_r^2 T} \right) \quad (3.1)$$

where e is the electronic charge, ϵ_0 the permittivity of free space, r_0 the first Bohr radius of an electron of the hydrogen atom, m_e the mass of the electron and m_{eff} the effective electron mass in the semiconductor. If $\gamma > 1$ an excitonic behaviour is observed. The binding energy E_b of singlet excitons has been a subject of great debate over the last decade. Evidence seems to indicate that E_b 0.3 – 0.4eV gives a correct picture of most conjugated polymer [19],[20],[21]. Some different types of excitons can be distinguished:

1. Frenkel exciton: The electron-hole pair is confined to not more than one molecular unit[22].
2. Mott-Wannier exciton: The distance between electron and hole is much greater than the spacing between unit cell (here molecular units) [23].
3. Charge transfer exciton: The exciton extends over only a few adjacent molecular units.
4. Inter-chain excitons: This term is used for polymeric semiconductors to indicate that the constituent charges are located on different polymer chains. It can be regarded as a charge transfer exciton.
5. Intrachain excitons: This term also refers to polymeric semiconductors to indicate that the constituent charges are located on the same polymer chain. It is believed that intrachain excitons represent the main species that is formed after photoexcitation in conjugated polymers [24]-[25].

Polarons

Upon adding a charge to a polymer chain, the chain will deform to lower the energy of the carrier. This charge and deformation together constitute a polaron, hereafter denoted as P^+ or P^- depending on the sign of the charge. The energy levels of a polaron are within the HOMO-LUMO gap. Polarons can drift along the conjugated chain. Once they reach the end of a conjugated segment, a hopping process to another conjugated chain can occur. Thus, in an applied electric field, a combination of drifting and hopping of polarons leads to charge transport through the film. It should be noted here that for creation of a P^+ / P^- polaron pair upon photon absorption, the electron and hole must be separated sufficiently in space, so that there is no Coulomb attraction binding them together. This can be achieved by removing the electron or hole within femtoseconds after photon absorption from the chain or by trapping one of the charges at an impurity or defect.

3.2 Exciton diffusion

The typical lifetime of singlet excitons in organic semiconductors is in the hundreds of picoseconds [26] after which they can recombine radiatively or nonradiatively. The diffusion length

is typically of the order of 5-10 nm [27]-[28]. A theoretic model to describe the diffusion of generated excitons in the bulk of the absorbing material is reported in [29]. Authors start from the continuity equation for neutral excitons, adding terms for exciton generation and exciton recombination; the time-dependent exciton diffusion equation becomes:

$$\frac{\partial n_{exc}(x,t)}{\partial t} = g\alpha N_0(t) (1 - R) e^{-\alpha x} - \frac{n_{exc}(x,t)}{\tau_{exc}} + D_{exc} \frac{\partial^2 n_{exc}(x,t)}{\partial x^2} - F(x - x_{int}) n_{exc}(x,t) \quad (3.2)$$

Time-dependent exciton density n_{exc} is described by four different terms all dependent on the distance x from the illuminated ITO electrode into the bulk of the absorbing material. These terms are:

- the exciton generation with the number of incident photons $N_0(t)$ and the internal photon-to-exciton efficiency g , with an additional term $(1 - R)$ due to the reflectivity losses at the glass substrate. The exciton generation term is mainly determined by the exponential decay of the light intensity in the absorbing layer, characterised by the absorption coefficient α ,
- the exciton recombination with a recombination lifetime τ_{exc} ,
- the exciton diffusion expressed by the exciton diffusion constant D_{exc} ,
- a term for exciton dissociation at the donor-acceptor interface (x_{int}) with the dissociation rate $F(x - x_{int})$

For stationary illumination ($\partial n_{exc}/\partial t = 0$), with the boundary conditions $n_{exc}(x = 0) = 0$, i.e. drain of excitons at the illuminated ITO electrode and $n_{exc}(x \rightarrow \infty) = 0$, i.e. no exciton creation far away in the bulk, because all light is absorbed before, the differential equation for the exciton density n_{exc} is solved by

$$n_{exc}(x) = \frac{gN_0(1-R)}{D_{exc}} \frac{\alpha L^2}{1 - (\alpha L)^2} \left(e^{-\alpha x} - e^{-(\alpha L)} \right) \quad (3.3)$$

Therein L is the exciton diffusion length defined as

$$L = \sqrt{D_{exc}\tau_{exc}} \quad (3.4)$$

This expression gives the exciton density in the bulk of the absorbing material without taking in consideration the exciton dissociation at the donor-acceptor interface. In figure 3.5 are shown exciton density profiles, according to (3.3), for different parameter values of L and α . The maximum exciton density always occurs at a distance x_{max} from the illuminated ITO electrode given by

$$x_{max} = \frac{L \ln(\alpha L)}{\alpha L - 1} \quad (3.5)$$

The position of x_{max} is only dependent on the exciton diffusion length L and the absorption coefficient α of the absorbing material. When $\alpha L = 1$, the maximum exciton density is obtained at $x_{max} = L$.

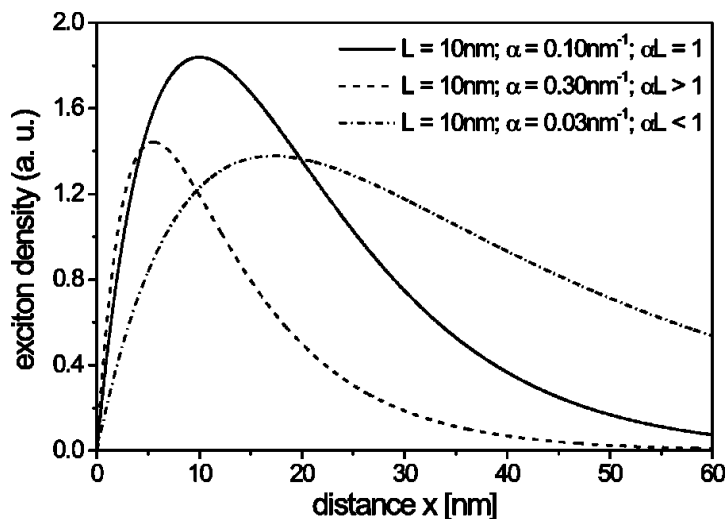


Figure 3.5: exciton density profiles

3.3 Free charge generation at A/D interfaces

Excitons generated upon illumination in organic semiconductors need to be separated creating free electrons and holes; therefore, they decay within less than $1\mu s$ with emission of a photon (photoluminescence, PL). Generally the spontaneous separation into free charge carriers is highly unlikely at room temperatures, when a single compound forms the organic layer. This is because in conjugated materials the binding energy of the lowest singlet exciton (i.e., the strength of the Coulombic attraction between the electron and hole) is significant (it is considered to be around 0.3-0.4 eV in conjugated polymers and even larger in small molecules); this makes excitons rather stable species. An efficient way to generate free charge carriers is the formation of an electron donor (D) / electron acceptor (A) interface, a so called heterojunction between two materials. The concept may be similar to $p - n$ junction in inorganics, but the physical process is quite different. The transfer of charges can be realised at the interface between two materials if one material has a higher electron affinity (χ) whereas the other has a lower ionisation potential (I_P). In figure 3.6 is shown the process of free charges generation for a donor-acceptor system: in close proximity of interface, the differences in electron affinity (χ) and ionisation potential I_P between the two materials permits the dissociation of strongly bound exciton on the donor material into free charge carriers by transferring the electron to the acceptor material. The difference in the electron affinity of donor and acceptor, i.e. the difference between the two LUMOs, needs to be large enough so that the resulting field (potential gradient at the junction), can overcome the coulomb field of one charge on the other. Otherwise charge transfers from the material with the higher bandgap occur without excitons splitting into their constituent charges and, eventually, they can recombine at the D/A interface. This is possible also in the case which both the hole and the electron decrease their energy thereby. This process, shown in fig.3.7 is known as Foerster transfer and is used in OLEDs technology to shift the emission band of the exciton towards lower energies.

Thus, the photoinduced electron-transfer process has converted light into charges. Note that the same final charge separated state can be reached when the acceptor is initially photoexcited,

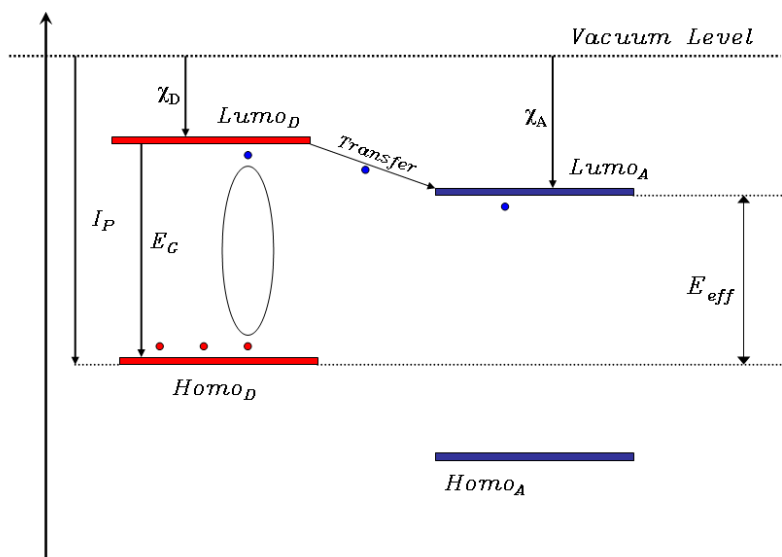


Figure 3.6: Facilitate charge transfer and exciton-scission.

following a photoinduced hole-transfer from the HOMO level of the acceptor to the HOMO level of the donor. To produce a current, the charges have to escape from their mutual Coulombic attraction and migrate toward the electrodes, usually via a polaron-hopping mechanism, under the influence of the built-in electric potential created by connecting the two electrodes. C60 (buckminsterfullerene) is a well-known acceptor material for its ultrafast charge transfer from conjugated polymers [30], [31], [32]. The charge transfer typically occurs within the femtosecond time regime: an upper time limit was found to be 300 fs [33], [34] which is three orders of magnitude faster than any electron-hole recombination process within the polymer. In the kind of OSCs treated in this work fullerene derivative PCBM as electron acceptor is used and P3HT semiconducting polymer as electron donor. The transfer of the excited electron to the PCBM takes place in some picoseconds leading to a conversion of nearly 100% of the excitons into free charge carriers. The achieved charge separation is meta-stable because the back reaction is much slower with life times in the milliseconds [18]. There is an analogous process for generation of excitons on the PCBM: the electron of the exciton remains on the PCBM whereas the hole is transferred to the polymer. However, due to the higher band gap of PCBM, this process can be neglected in the solar spectrum. From figure 3.6 we can see that the fundamental limitation of the donor-acceptor system obvious is the losing of a substantial amount of energy, typically more than $0.5eV$, during the dissociation of the exciton and the transfer of the electron from the donor to the acceptor. Due to the fast transfer the maximum attainable splitting of the electron and hole QFLs is limited by the HOMO of the donor and the LUMO of the acceptor. This implies that the effective electrical gap E_{eff} of the combined materials is much smaller (about 1.2-1.7eV for the combination of P3HT and PCBM as electron donor and electron acceptor respectively) than the optical gap E_G of either

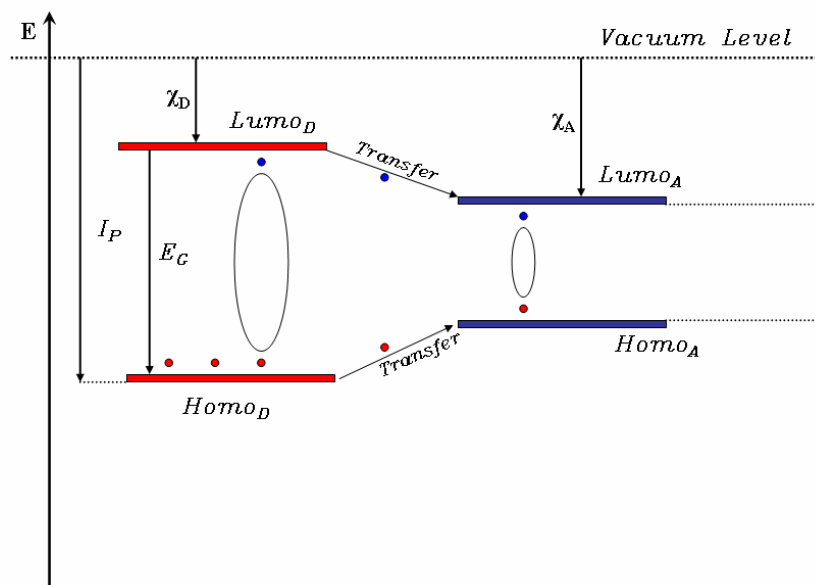


Figure 3.7: Förster energy transfer (no exciton splitting)

P3HT or PCBM. The limit of the maximum attainable V_{oc} is thus given by E_{eff} rather than by the difference in work-functions of the contacts [r 13]. First organic solar cells were realised as bilayer devices consisting of a donor and an acceptor component which can be either two conjugated polymers or a conjugated polymer and a fullerene. A heterojunction is formed between the p-conducting conjugated polymer and the n-type organic semiconductor. These devices show rectifying current-voltage characteristics due to their favourable charge injection at the specific contact. Despite the high quantum efficiency of photo-induced charge separation near unity close to the interface, the overall photo current of such devices is very little. This can be explained by the small diffusion lengths of the excited states to the dissociating interface. Since typically diffusion lengths are in the range of 10 nm, this limits the effective light-harvesting layer. However, for most organic semiconductors the film thickness should be more than 100nm in order to absorb most of the light. It follows that thicker film layers increase light absorption but only a small fraction of the excitons will reach the interface and dissociate. This problem can be overcome by blending donor and acceptor, a concept called dispersed (or bulk) heterojunction as in Fig. 3.8.

One of the inherent problems with dispersed heterojunction is that of solid-state miscibility. Large extended conjugated systems are normally not miscible; this goes for dyes and particularly for conjugated polymers. Thus cell fabrication should be carried out so equilibrium is never reached, e.g. by spincoating where solvent evaporation is fast. Hiramoto [35] reported the first dye/dye-dispersed heterojunction in 1991. Hiramoto investigated the effect of introducing a third organic layer in the middle of a two-layer heterojunction PV. This middle layer was a mixture of the two dyes made by co-sublimation from different thermal sources. In 2001 Schmidt-Mende et al. [36] fabricated PV cells of self-organized discotic liquid crystals of hexaphenyl-substituted hexabenzocoronene (HBC) and perylene. In 1994 Yu [37] made the first

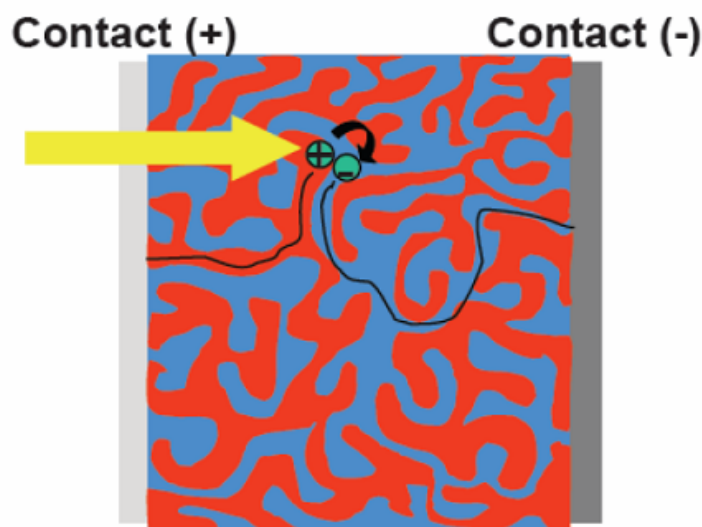


Figure 3.8: Dispersed heterojunction between a transparent ITO electrode and a metallic (Al, Au...) electrode. The exciton is separated in hole and electron at interface that are collected at respective electrodes.

dispersed polymer heterojunction PV cell by spincoating on ITO covered glass from a solution of MEH-PPV and C60 in a 10:1 wt ratio. The cell showed a photosensitivity of 5.5 mA/W , an order of magnitude larger than the photosensitivity of the pure polymer. In 2003 Brabec et al [38] showed that very high QE (76%) in poly(3-hexylthiophene)/methanofullerenes bulk heterojunctions are attainable. The limitation seems to be optical loss in the cell, thus QE approaching 100% should be within reach. Geens et al. [39] have shown that sandblasting of the glass substrate can effectively reduce optical loss due to reflection in organic PV cells. The first reports of polymer/polymer bulk heterojunction PV came independently from Yu et al. [40] and Halls et al. [41] in 1995. Both worked with the same PPV based derivatives: CN-PPV as acceptor and MEH-PPV as the donor polymer. Halls made a PV cell from a blend of the two polymers in equal amounts by spincoating. This type of composite cell was found to be three orders of magnitude more efficient than pure cyano-PPV (CN-PPV) and two orders of magnitude more effective than pure MEH-PPV. The effectiveness of this type of polymer-blend is strongly dependent on the morphology. Ideally the microphase domains should be no larger than the exciton diffusion length, which for PPV-type polymers is around 7 nm according to Halls. In addition the network should be bi-continuous, leaving a free path for both holes and electrons so that they can reach the respective electrodes without the necessity for tunnelling through domains. The aim of research is to realise the optimal morphology in which the phase separation is small enough to have efficient charge carrier separation while still to ensure that there are continuous pathways, i.e. percolation paths, to the corresponding contact.

3.4 Organic semiconductor structure

Materials having a delocalized π -electron system can absorb sunlight, create photogenerated charge carriers, and transport these charge carriers. In general, organic semiconductors can be regarded as "intrinsic wide band gap semiconductors" (band gaps above 1.4 eV) down to "insulators" (band gaps above 3 eV) with a negligibly low intrinsic charge carrier density at room temperature in the dark. Chemical, photochemical or electrochemical doping is used to introduce extrinsic charge carriers into organic semiconductors. For example, photoinduced electron transfer from a donor to an acceptor-type organic semiconductor film introduces free charge carriers (positive charge carriers on the donor layer, i.e., p-type, and negative charge carriers on the acceptor layer, i.e., n-type). Donor-acceptor-type bilayer devices can thus work like classical p-n junctions.

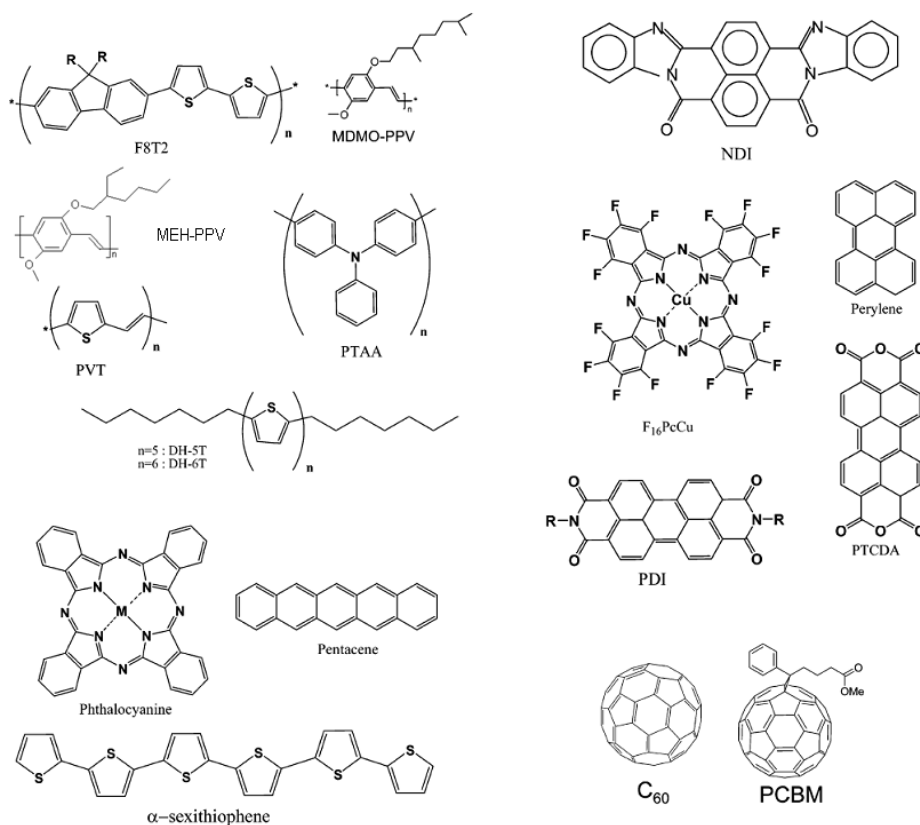


Figure 3.9: Examples of organic semiconductors used in organic solar cells.

In figure 3.9 are shown some examples of most common organic semiconductors used in organic solar cells. Phthalocyanine and perylene are pigments that have commonly found applications in thin film organic solar cells. Phthalocyanine is a p-type, hole conducting material that works as electron donor, whereas perylene and its derivatives show an n-type, electron conducting behavior and serve as electron-acceptor material. The optical and electronic properties of organic semiconductors can be tailored by attaching certain functionalities to the conjugated system. These properties are crucial for the operation of devices such as solar cells or LEDs. Also the "mechanical" properties can be influenced by the presence of

side chains; usually they are attached to molecules to introduce or improve solubility, as in the case of PCBM, because C_{60} has not good solubility in commune organic solvent (chloroform, toluene...). Typically, smaller molecules are better soluble and/or have lower sublimation temperatures but larger molecules give better films upon spin-coating. In the polymeric field, the three most common organic semiconductors used for organic solar cells are *poly*(2-methoxy-5-(3,7-dimethyloctyloxy)-1,4-phenylenevinylene) (MDMO-PPV), *poly*[2-methoxy-5-(2'-ethyl-hexyloxy)-1,4-phenylenevinylene] (MEH-PPV) and *poly*(3-hexylthiophene) (P3HT) shown in fig. 3.10. Usually, as we show previously, they are combined with fullerene derivative 1-(3-methoxycarbonyl)-propyl-1-phenyl-(6,6) C_{61} (PCBM) that belongs to the group of semiconducting molecules.

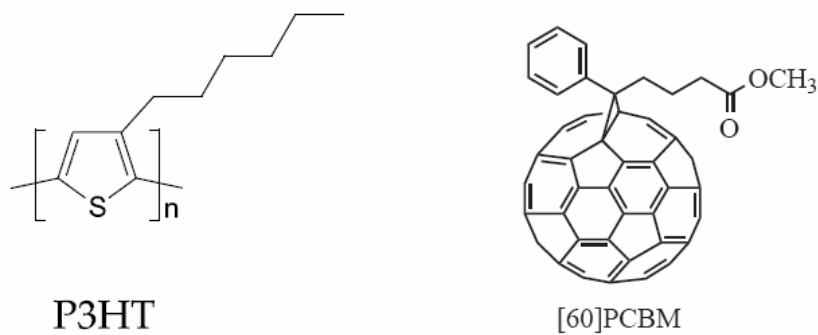


Figure 3.10: The *poly*(3-hexylthiophene) (P3HT) and the [6,6]-phenyl-C₆₁-butyric acid methyl ester (PCBM).

The structure of the polymers is complex, but they share the same structural feature of alternating single and double carbon bonds. PPV and Polythiophene are the actual conjugated polymer backbones, and the additions label the side chains. The primary use of the side chains is to make the materials soluble in organic solvents. Without side chains the polymer would hardly or not at all be soluble and therefore very difficult to process from solution. Additionally, the side chains can change the electro-optical properties of the materials and thus be used to tune the materials. The morphology in the solid is crucially influenced by the regioregularity of the side chains; this means that the alkyl side chains of the P3HT are aligned in a periodic structure as opposed to the regiorandom case. The buckminsterfullerene C_{60} is an electron acceptor, which can be electrochemically reduced up to 6 electrons. For photoinduced electron-transfer reactions (i.e., photodoping), it is blended into electron-donating matrices with hole conducting properties. Within the field of molecular electronics and the role of fullerenes therein, PCBM plays a special role. In the search for a soluble fullerene for anti HIV treatment, PCBM was developed in the labs of Wudl by Hummelen. Although its use as an intermediate in the preparation of a medicine for anti HIV treatment never fully materialized, PCBM would later become the most widely used fullerene compound in molecular electronics. In 1992 the groups of Heeger and Wudl showed, for the first time, ultrafast electron transfer from a polymer to buckminsterfullerene [42]. The application of C_{60} in, for example, solar cells, was however severely hampered by its poor solubility. The development of PCBM, as a highly soluble C_{61} derivative, offered the solution to this problem. In the same paper, where PCBM

was introduced as the electron acceptor in solar cells, the concept of mixing the donor and the acceptor, thus concept was also shown for mixing two polymers by the groups of Friend and Holmes in the same year [41]. Derivatization of higher fullerenes C_{70} and C_{84} with the same addend as in PCBM, thus creating [70]PCBM and [84]PCBM (as mixtures of isomers), has also led to successful applications in solar cells.

3.5 Conduction in organics

In contrast to crystalline semiconductors, the amorphous structure of organic bulk heterojunctions is kept together by weak Van der Waal's interaction with small electronic transfer integrals and a strong electron phonon coupling [13] which supports efficient scattering of charges. The free charge carriers in organic materials are also localised to within a few polymer repetition units or a molecular unit and strongly couple to the lattice, which locally changes both optical and electronic properties of the material. The charges, i.e. electrons and holes in the π and π^* orbitals respectively, can move along the delocalised π bands of the $1-D$ polymer backbone. However, due to defects caused by twisting and bending of the polymer backbone the delocalisation of both π and π^* orbitals is in reality limited to about 10-20 polymer repetition units, the so-called conjugation length. The transport over these defects, which can be considered to be equivalent to the transport between different molecules, is much slower than band transport and is best described as thermally assisted hopping process. This hopping of charge carriers between localised sites is the dominant charge carrier transport mechanism in disordered organic materials at ambient temperatures. Whereas band transport in crystalline semiconductors is characterised by decreasing charge carrier mobility with increasing temperature, the charge transport in organic materials improves due to activated hopping. From the perspective of inorganic semiconductors, organic materials have small mobilities μ and short lifetimes t of charge carriers. As a consequence, diffusion coefficients D and diffusion lengths L are small. Higher charge carrier mobility in semiconducting polymers would be achieved by aligning and ordering the polymer, but is limited by the high gain of entropy for the unordered structure. An important consequence of this behaviour is that band diagrams used for representing semiconducting polymers, are only an approximation of the available energies. They do not imply that there is band transport or that the energy levels remain the same in presence of charge carriers. There are two principals models describing the hopping transport between two localised orbitals between different molecules: the Miller-Abrahams model [43] and the diabatic model based on the electron transfer theory of Marcus [44]. In the Miller-Abrahams model the transfer rate ω_{ij} from hopping site i to j with energy E_i and E_j respectively are given by:

$$\omega_{ij} = \omega_0 |V_{ij}|^2 \begin{cases} \exp\left(\frac{-(E_i - E_j)}{k_B T}\right) & E_i < E_j \\ 1 & \text{otherwise} \end{cases} \quad (3.6)$$

If sites i and j have the same energy, the transfer rate is simply given by the product of proportion ω_0 and the square of the overlap integral of the electronic wave functions $|V_{ij}|^2$. If the final state is higher in energy than the starting state, the transfer rate is reduced by the Boltzmann factor. Since organic molecules are only bound by Van-der-Waals forces, the

distance dependence of the overlap integral can be approximated by

$$|V_{ij}|^2 \propto \exp(-2\zeta |R_{ij}|) \quad (3.7)$$

where R_{ij} is the distance between both electron orbital centres of site i and j and ζ is proportional to the inverse of the localisation radius of the orbitals. The diabatic model is a result of first order perturbation theory [r 16]. The hopping rate from site i to j is given by:

$$\omega_{ij} = |V_{ij}|^2 \sqrt{\frac{\pi}{\hbar k_B T E_\lambda}} \exp\left(\frac{-(E_i - E_j - E_\lambda)^2}{4k_B T E_\lambda}\right) \quad (3.8)$$

The reorganisation energy, E_λ , is a parameter of the material which is determined by the vibrational modes of the molecules in the mixed phase. Contrary to the Miller-Abrahams model hopping events between states with lower energy and states of higher energy can be thermally activated and get faster with increasing temperature.

3.6 Charges recombination

Oxygen traps

Another possibility for a singlet exciton to dissociate is at an oxygen trap in the polymer chain. When the polymer is exposed simultaneously to oxygen and light for the process of photo-oxidation traps are introduced for electrons in the CB of organic materials and thereby lead to a higher number of free holes in the VB.. In this sense oxygen can act as a dopant that favours p-type conductivity as discussed above. Oxygen traps can also act as exciton dissociation sites and therefore generate free charge carriers in the presence of excitons. For example we report the case of PPV: the oxygen reacts with a vinylene group forming a carbonyl group. This carbonyl group has a strong electron affinity which makes it favorable for the electron of an exciton to transfer onto the carbonyl group thereby dissociating the exciton [45]. The hole is now free to move along the polymer as a free charge carrier while the electron is trapped at the site of the carbonyl group. This charge separation process is similar to the dissociation of an exciton at a donor-acceptor interface. The main difference is that the electron remains on the polymer chain at the location of the trap. While the hole can be transported to the collecting anode, the electron is not free to move and will eventually recombine with a hole in the valence band of the polymer. Thus, photo-oxidation can be interpreted as p-doping the polymer by increasing the number of free holes and enhancing the photoconductivity. In general, photo-oxidation is not sought to be used as a charge separation mechanism since it can decrease the transport properties of electrons and holes in the device by building up space charges. To prevent oxidation, devices should be produced and handled in an oxygen-free environment or they should be encapsulated immediately after production.

Recombination

The previous discussion in 3.3 suggests that an offset of the frontier electronic levels of the donor and acceptor units is just what it takes to induce exciton dissociation. However, the situation is far from being that simple: exciton dissociation into a polaron pair can take place only if the energy stabilization of the electron when it transfers from the LUMO L_D of the donor to the LUMO L_A of the acceptor or that of hole for the transferring from the HOMO H_A of the acceptor to the HOMO H_D of the donor is more than compensation for the binding energy of the intrachain exciton. In other words, the charge separated state has to be lower in energy than any intramolecular excited state. This can be assessed by estimating to first approximation the ordering of three key excited states:

- the lowest intramolecular excited state of the donor with an energy $E_D = L_D - H_D - \Delta_D$ (with Δ_D being the binding energy of the donor intrachain exciton),
- the lowest intramolecular excited state of the acceptor with an energy $E_A = L_A - H_A - \Delta_A$,
- the lowest charge-transfer (CT) excited state with an energy $E_{CT} = H_D - L_A - \Delta_{CT}$ (with Δ_{CT} being the binding energy of the photoinduced polaron pair).

Indeed, the exciton dissociation process competes with charge recombination, the mechanism by which the charge separated state decays back to the ground state of the blend (i.e., the electron in the LUMO level of the acceptor transfers to the HOMO level of the donor. Charge recombination must be prevented to the highest possible extent to ensure efficient generation of charge carriers in the device. These processes can occur right at the photoexcitation site before the electron and hole are sufficiently separated or during charge transport through the film or at the interface of the organic film and the metal electrodes. We will show the most important loss mechanisms due to recombination and charge in the following. The singlet exciton created by photon absorption typically has a lifetime in the hundreds of picoseconds, after which electron and hole recombine radiatively yielding photoluminescence. With a charge separation of the exciton faster than picoseconds in the bulk heterojunction, the direct radiative recombination of the exciton is unlikely; thus, in cases of high photoluminescence, it means that most of the excitons are created far away from a donor-acceptor interface and that they have no chance of being dissociated. In good bulk-heterojunction devices, the presence of an exciton-dissociating interface between donor and acceptor throughout the bulk of the device, comport the quenching of the photoluminescence. In this case mobile charge carriers can be transported to the contacts either by carrier diffusion or electric field induced drift. In order to have unity quantum efficiency for charge extraction, one needs to fulfil the condition that the charge carrier transit time t_{tr} is much smaller than the carrier lifetime τ ($t_{tr} \ll \tau$). The carrier transit time $t_{tr} = d/\mu E$ is determined by the charge carrier mobility μ , sample thickness d , and the electric field E inside the film. If the photocurrent is governed by the carrier drift in the applied electric field, then the drift distance $l_{drift} = \mu\tau E$. If the photocurrent is governed by the carrier diffusion, then the diffusion distance $\sqrt{D\tau} = \sqrt{\mu\tau kT/e}$, where D is the diffusion coefficient, k the Boltzmann

constant, and e is the electron charge. As it can be seen from above in both cases the $\mu\tau$ product will determine the average distance the charge carrier can travel before recombination. The mobility lifetime product $\mu\tau$ is therefore an important parameter determining whether or not the power conversion efficiency of the photovoltaic devices is limited by the charge transport and recombination. In recombination, a very important role is played by traps, spatially localized states that are energetically favourable for the charge carrier. They are usually divided into two groups: shallow and deep traps. Shallow traps are states where the charge carrier is trapped for a certain time, after which it can be thermally released and can continue drift or diffusion. Therefore, the effective total flight time τ_{eff} through a distance L is the sum of the flight time τ_0 through a trap-free material and the average reside time τ_{re} in a trap multiplied by the number of traps N in the path

$$\tau_{eff} = \tau_0 + N\tau_{re} \quad (3.9)$$

This increase in effective flight time with trap density has a direct influence on the mobility of the charge carriers

$$\mu_{eff} = \frac{L}{\tau_{eff}E} = \frac{L}{(\tau_0 + N\tau_{re})E} \quad (3.10)$$

The equation shows that the mobility of the charge carriers decreases with increasing trap density. Since the mobility is inversely proportional to the resistance, the resistance for the charge carriers increases with higher trap densities. Deep traps are states where, charge carriers, once trapped, are not released any more. This does not only reduce the number of free charge carriers that can reach the electrodes, but it also leads to the build-up of space charges. These space charges can create an electric field that significantly hinders the transport of free charge carriers. Traps can be introduced to the polymer by foreign atoms, impurities, or defects in the chain. A common example is oxidation of the polymer.

A separate loss mechanism in the OSC is the optical loss: reflections at the interfaces and absorption of photons in layers, which are not photovoltaic active, reduce the number of photons available for absorption in the absorber layer. The main reflections occur at the air-glass interface and at the metal electrode. The latter reflection leads to the creation of an optical interference pattern, because the thickness of the layer structures is in the same order at the wavelength of the incident light. Thus interference effects have a crucial effect on the absorption and any optical treatment has to be carried out coherently. The interesting region for the current materials (P3HT:PCBM) is between 300nm and 800nm. Optical simulations have shown that below 350nm most of the light is absorbed in the glass. At higher wavelengths, the absorption of the photovoltaic active materials decreases and more photons are absorbed in PEDOT:PSS layer and the cathode.

3.7 semiconductor-electrodes interface

As shown in first chapter, in the case of ideal contacts the chemical potential energy in the semiconductor can be converted without loss into electrical energy in the external circuit. However,

real contacts doesn't show the same behaviours and the choice of materials influences significantly the performances of solar cells. After the contact between a metal and a semiconductor, charge carriers are transferred across the interface until the Fermi level of the metal and semiconductor align at the interface and throughout the combined system. A Schottky contact is formed: between each metal electrode and his respective semiconductor.

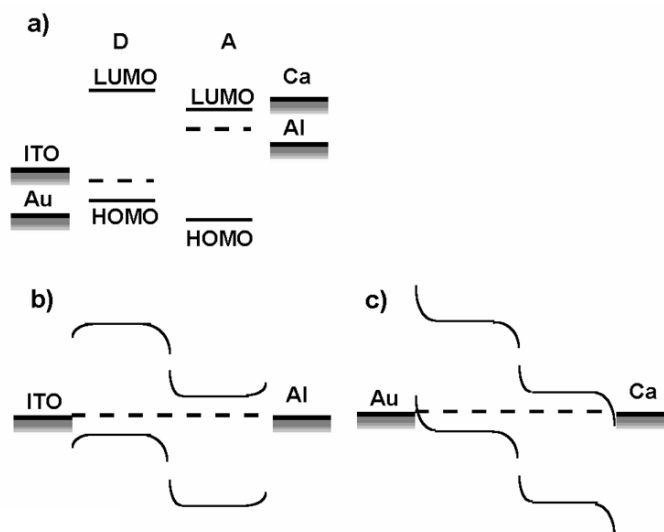


Figure 3.11: Energy band diagrams of D/A devices with the electrode interfaces. a) the situation before contact. After contact the Fermi levels (dashed lines) and W_f equalize and band bending occurs. b) the formation of a blocking contact for holes (ITO/D) and electrons (A/Al). c) the formation of a non-blocking (ohmic) contact for holes (Au/D) and electrons (A/Ca).

In figure 3.11 we present the band energy diagram as it is expected for the situation before contact and after contact in short circuit conditions: the redistribution of charges due to equilibration of the Fermi levels creates a potential difference leading to a bending of the bands inside the semiconductor. The band bending can be qualitatively predicted by assuming that the edges of the LUMOs and HOMOs are pinned to their absolute energy values as they were before contact. The bulk of the semiconductor sustains the same distance to the equalising Fermi-level. The region of band bending is called the depletion region and for organic semiconductors it can extend, depending on the material, through the whole absorber layer [46]. The W_f of the electrode control the direction in the band bending, in particular if it is above or below the Fermi-level of the semiconductor. In case the work-functions of both electrodes are deeper inside the bandgap than the Fermi-levels of the materials they are contacting, band bending occurs as depicted in figure. Note that band bending at the D/A interface would be the other way round (blocking) if both Fermi-levels are assumed to be close to the middle. Photoexcited electrons from the CB of the electron acceptor (A) encounter a barrier before they can reach the Al electrode. The same is true for holes from the VB near the ITO contact. These types of contacts are referred to as blocking contacts or rectifying because they can become non-blocking upon changing the potential of the electrodes. Al forms a blocking contact only

with the CB of the n-type semiconductor and an ohmic contact with the VB. The analog situation is for the semiconductor/ITO interface. Since charge separation at the D/A interface leads to an excess of electrons in the CB of A (n-type) and holes in the VB of D (p-type), both charge carriers find barriers if they want to get out of the semiconductor. Thus currents through this device are decreased by the contact barriers. If Au and Ca are used as contact materials the situation is improved: the W_f of both electrodes is further away from the middle of the bandgap than the semiconductors Fermi-levels. Thus, after contact, band bending occurs the other way round so that electrons in the excited state can reach the Ca electrode and holes the Au electrode without encountering a barrier. Devices made using Au and Ca instead of ITO and Al show indeed considerably higher open circuit voltages and often also higher photocurrents and EQE values [47]. However Ca is more prone to oxidation than Al and gold electrodes are expensive and have to be very thin to become transparent: for these reasons, Al and ITO electrodes are actually more suitable for research devices. A detailed description of the physical processes involved at the interfaces between metals and organic semiconductors is referred to the reviews in references [45] and [48]. In the follow we will describe the most commune electrodes used in OSC.

ANODE

In organic devices the workfunction of the electrode materials is very important since it determines together with the LUMO/HOMO and Fermi-level of the semiconductor whether the electrode forms an ohmic or a blocking contact for the respective charge carrier. Moreover a large difference in workfunction of the electrode materials can increase the V_{oc} considerably. For the anode, where holes are collected, high workfunction materials like Au are preferred. Generally the anode is also the transparent contact. Semi transparency can be obtained if the sublimed metal e.g. Au is not much thicker than about 15-20nm (non transparent contact are in the order of 50-100nm). The small thickness of electrodes can behave that sheet resistance can be considerably increased and possibly add to the series resistor. For these reasons so called conducting glasses are often used.

Indium Tin Oxide (ITO)

Indium tin oxide (ITO) films have been widely employed as a pixel electrode in flat panel display devices, such as liquid crystal displays (LCD) and organic light emitting diodes (OLED), due to its excellent optical transparency and good electrical conductivity. Additionally, with the rapid development of photovoltaic industry, ITO films are also an important material for fabricating solar cells. Particularly Indium Tin Oxide which is a degenerated semiconductor comprising a mixture of In_2O_3 (90%) and SnO_2 (10%) with a bandgap of 3.7eV and a Fermi-level between 4.5 and 4.9eV. The large bandgap allows no absorption of wavelengths longer than about 350nm. A strong excess of In, working like an n-type dopant and giving a lack of oxygen, can highly increase the conduction leading low sheet resistances for already only 100nm thick layers of ITO. Films of this material deposited by sputtering on quartz substrates are commercially available. Values smaller than $5 \Omega/cm^2$ are available. The transmission properties of the thicker ITO substrates do not change much since the material does not absorb

in the visible but interference effects cause significant spectral dependence of the transmission. Very thick ITO layers are problematic because of the increased absolute surface roughness which can cause shorts in the thin organic films.

Pedot:PSS

The most commonly used anode is the organic conductor PEDOT:PSS, supported by the metal oxide ITO, leading to two interfaces for the charge carrier: ITO|PEDOT:PSS and PEDOT:PSS|Absorber. Its chemical structure is shown in figure 3.12.

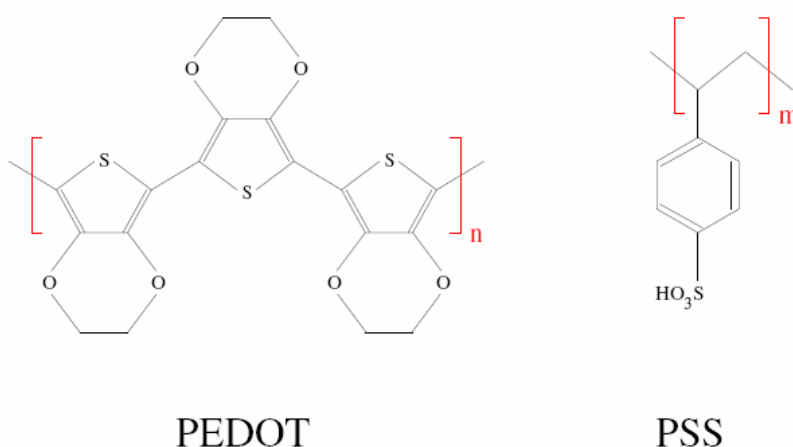


Figure 3.12: The chemical structure of poly(3,4-ethylenedioxythiophene) (PEDOT) and poly(styrene-sulfonate) (PSS). In mixture, PSS oxidises PEDOT, making it a highly conducting polymer. Facilitating holes transport across the anode interface, it is used in organic electronics as anode.

The work function of PEDOT:PSS is independent from the W_f of substrate, and for this reason the use of this material is promising for reproducible electrodes fabrication in OLED or OSC. In OSC Pedot:PSS ensure improved interfaces between active layer and electrode, in particular ITO and also change the shape of EQE curve, behaviour probably due to the doping of active layer by PSS. The role of PEDOT:PSS on OSC have been studied by UV photoemission spectroscopy (UPS): it has been demonstrated that the vacuum levels of a semiconducting polymer spin-coated onto a PEDOT:PSS layer and of the PEDOT:PSS itself align and the barrier for holes injection is determined by the workfunction of PEDOT:PSS instead of ITO [49]. PEDOT:PSS typically has a higher work function than ITO, matching more closely the HOMO (VB) of the semiconducting polymers, hence reducing the barrier for holes transport over the interface. Additional improvement is the reduction of topological variation from ITO: a film of optimized thickness cover the possible pin holes generally present on ITO films. Thicker layers can cause large increase in the series resistance, also influenced by the annealing treatment after the deposition. Especially a heat treatment after spincoating increases the conductivity of the PEDOT:PSS layer up to two orders of magnitude by changing the morphology of the film. PEDOT itself is an insoluble polymer: however, simple processability, e.g. from solution, is of high importance for many applications. The low solubility can be circumvented by either

polymerising and doping EDOT, the monomer, in situ or by stabilising it with poly(styrene sulfonic acid) (PSS), a soluble poly-electrolyte, while polymerising it in a solvent. In mixture, the PSS-acid donates a proton from its HO_3S group to a sulphur atom of PEDOT. This leads to a positive doping of PEDOT, while the PSS guarantees charge neutrality, leading to the oxidised state of PEDOT with its advantageous properties. There are different kinds of PEDOT:PSS commercially available and their conductivity, work function and chemical properties can be further modified to suit the particular application.

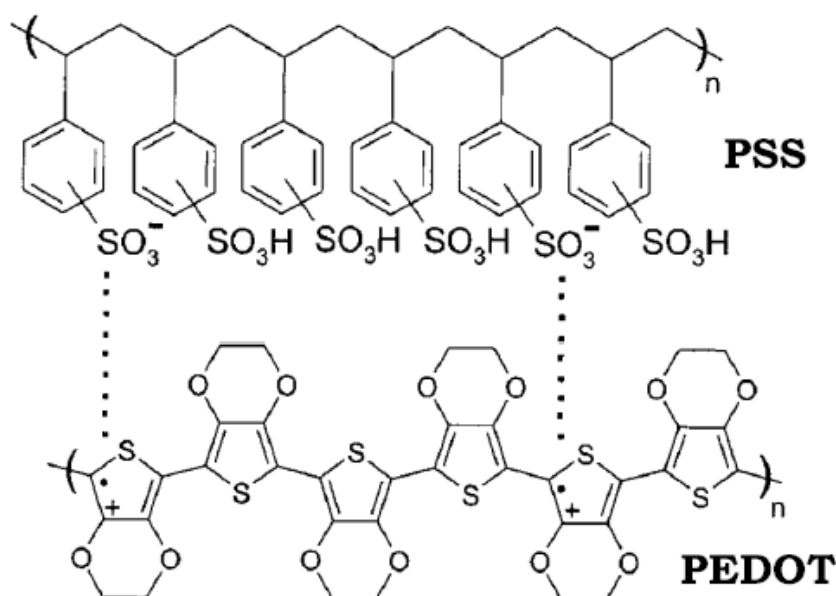


Figure 3.13: The positive doping of PEDOT led by PSS: the PSS-acid donates a proton from its HO_3S group to a sulphur atom of PEDOT.

CATHODE

The cathode is typically realised by evaporation of a low workfunction metal. The most common material is Al, but other materials have been tested, e.g. Ca or Ag. Brabec et al. have investigated the dependence of V_{OC} on the metal workfunction for the MDMO-PPV:PCBM combination. Whereas the V_{OC} exhibited only a weak dependence on the change in workfunction is was directly proportional to the acceptor strength of the fullerene, suggesting that the difference in energy levels (HOMO donor to LUMO acceptor) is more relevant to V_{oc} than the metal workfunctions. Differences in bonds nature (strong bonds in the metal and weak van-der-Waals bonds in the organic semiconductor) and the charge transport (mechanism dominated by thermally assisted hopping for organic semiconductor, band-like transport for metals) lead direct transfer of charges between metals and organic materials not possible. Many studies have been done to improve the extraction efficiency and understand the physic of charge transfer. Brabec et al. [50] have shown that the efficiency of conjugated polymer/fullerene bulk heterojunction solar cells can be significantly enhanced efficiency when using LiF/Al electrodes

instead of Al electrodes alone. A similar enhancement was observed for LiF/Au electrodes. The formation of a dipole moment across the junction, due to either orientation of the LiF or chemical reactions leading to charge transfer across the interface, is suggested as the mechanism for the enhancement.

Chapter 4

Photovoltaic Characterization of Organic Solar Cells

It is important describe the main properties characterizing the photovoltaic behaviour of organic solar cells, to detect the problems of the devices and deduce possible changes and improvements. A basic understanding of organic photovoltaic devices is given: a full description of all details can be founded in [51]. Here inorganic and organic solar cells are compared to point out the difference between these two classes of devices. Even though it deals with inorganic thin film solar cells, helps to interpret the I-V characteristics of photovoltaic devices and draw conclusions about the detrimental mechanisms.

4.1 Equivalent Circuit Diagram

The description of the electric behaviour of complex devices in terms of basic ideal components such as current or voltage sources, resistors, diodes and capacitors can be done using the *equivalent circuit diagram (ECD)*. Figure 4.1 shows the ECD typically used for inorganic solar cells.

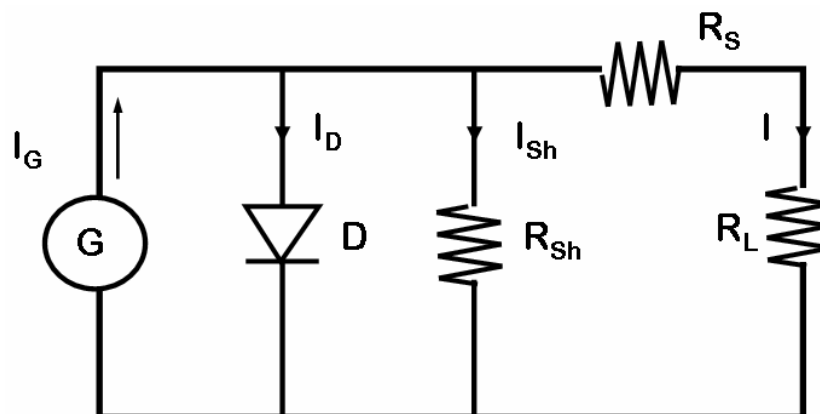


Figure 4.1: Equivalent circuit diagram for a typical solar cell.

Since the loss mechanisms are basically the same for organic and inorganic solar cells,

the ECD can be applied to organic devices, even though the specific physical processes are significantly different. The components shown can be described as follows:

- The current source G generates a current I_G , resulting from dissociation of excitons into electrons and holes after photon absorption. I_G does not take into account any recombination but only depends on the charge carrier creation efficiency.
- The shunt resistor R_{Sh} : it represents the recombination of electrons and holes near the exciton dissociation site before significant charge transport through the bulk has occurred.
- The series resistor R_S : it is influenced by the mobility of charge carriers in the bulk of the solar cell, mobility dependent of defects and barriers as well as space charges in the device. R_S will also increase with thickness of the device since the distance that the charges have to travel to the collecting electrodes increases.
- The diode D : it describes the asymmetric conductivity in the solar cell. For inorganics, it is due to the pn-junction and its blocking behavior in one current direction. For organics, it can be due to a blocking contact at the semiconductor/electrode interface or a built-in field resulting from a donor-acceptor interface.
- The resistor R_L : it results when the solar cell is contacted to an external load. Alternatively, a source-measure unit can be connected to measure the I-V characteristics of the solar cell.

In the ideal case, R_{Sh} would be infinitely large and R_S would be zero. Typically, the values for inorganic cells are R_{Sh} larger than 1000 Ω and a few Ω for R_S . In organic devices, since the mobility is usually lower (increasing R_S) and charge recombination can be an issue (lowering R_{Sh}), the values generally increase significantly.

The *extended ECD* is often used for the organic solar cells to take into account additional loss mechanisms, as shown in Figure 4.2.

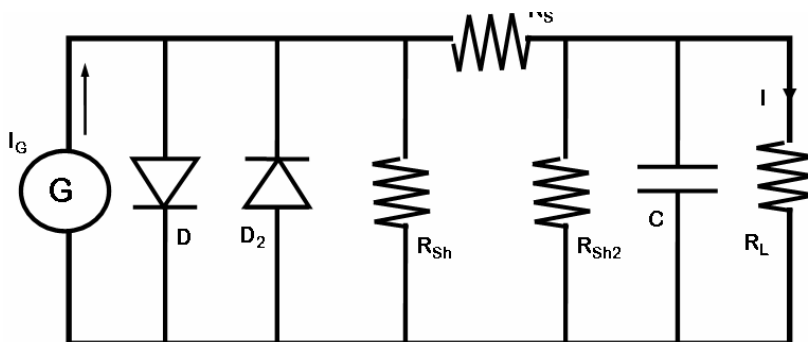


Figure 4.2: Extended equivalent circuit diagram for a solar cell.

The additional components are:

- A diode D_2 that takes into account a possible blocking contact at the electrode. This blocking contact can, for example, influence the extraction of holes at the ITO interface.

- A second shunt resistor R_{Sh2} that directly connects the electrodes. This shunt resistor accounts for possible recombination of charges at the extracting electrodes. In addition, this shunt resistor can result from direct conducting pathways between the electrodes, for example due to shorts in the film. When R_S is much smaller than either of the two shunt resistors, a splitting of the shunt resistance into R_{Sh} and R_{Sh2} is not necessary and both loss mechanisms can be represented by R_{Sh} .
- A capacitor C that accounts for charging and discharging effects in the device. Since the device area is usually much larger than the device thickness, the capacitance can become an important part of the device.

This ECD can be used to interpret I-V curves measured for a photovoltaic device. The observed shape can be related to certain components of the ECD, and from that conclusions can be drawn about the physical properties of the solar cell.

4.2 Short Circuit Current, Open Circuit Voltage and Fill Factor

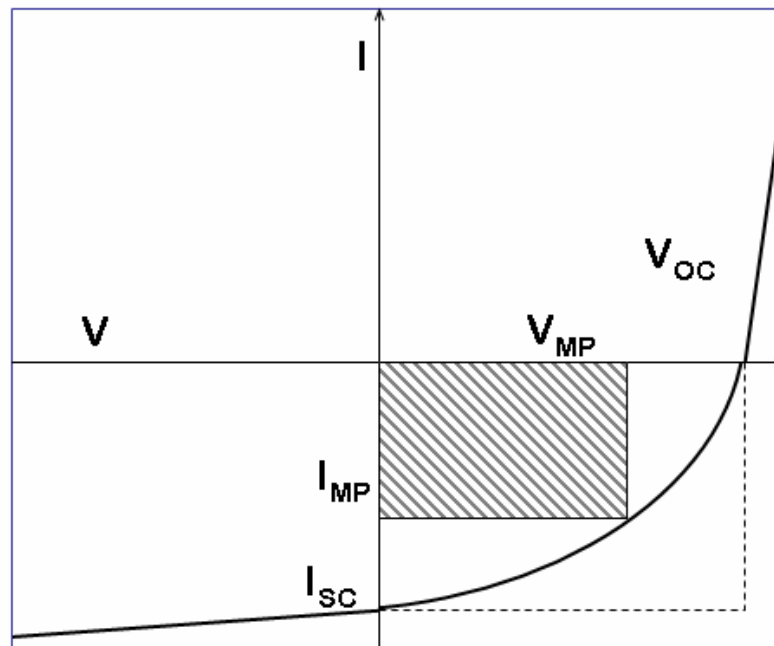


Figure 4.3: Current versus voltage characteristic of a solar cell under illumination.

As shown in 2.3 the current-voltage curve of a solar cell can give the specific characteristic of the behaviour of the device: to determine the efficiency of solar cells, and to compare different cells. In particular, a few important points on the curve are used 4.3:

- The intersection of the curve with the y-axis (current) is referred to as the short circuit current I_{SC} , the maximum current the solar cell can put out under a given illumination power without an external voltage source connected. It is measured by connecting both electrodes to an ammeter.

- The intersection with the x -axis (voltage): this is the open circuit voltage (V_{OC}), that is the maximum voltage a solar cell can put out. It is measured by connecting the illuminated solar cell to a voltmeter.
- The current and voltage at the point of maximum power output of the solar cell are called I_{MP} (maximum power current) and V_{MP} (maximum power voltage) are. They can be determined by calculating the power output P of the solar cell ($P = I * V$) at each point between I_{SC} and V_{OC} and finding the maximum of P .

The ratio of the rectangles given by the maximum power point and I_{SC} and V_{OC} gives the fill factor FF . It can be calculated by 4.1

$$FF = \frac{P_{\max}}{I_{SC} \cdot V_{OC}} = \frac{I_{MP} \cdot V_{MP}}{I_{SC} \cdot V_{OC}} \quad (4.1)$$

The Fill Factor therefore gives a measure of the quality of the I - V characteristic of the solar cell. Its theoretical limits are between 0.25 (ohmic nonrectifying behaviour of the solar cell) and 1, but in real case, FF can even drop below 0.25 when a blocking contact is formed at one of the electrodes. Generally, the overall efficiency of a solar cell is larger for larger FF . In the idea limit of FF approaching 1 the solar cell puts out a constant maximum current at any voltage between 0 and V_{OC} .

4.3 Photoresponsivity, External Quantum Efficiency and Power Conversion Efficiency

The dependency of the light absorption and produced photocurrent to the wavelength spectrum is one of most important property of a solar cell. In fact, this aspect of cell behaviour can help to determine whether a solar cell is capable of converting the available light illuminating into electric energy. There are two most commune ways to valuate this particular property:

- Characterising the *Photoresponsivity* PR ;
- Measuring the *External Quantum Efficiency* EQE .

The PR is defined as the photocurrent extracted from the solar cell divided by the incident power of the light at a certain wavelength

$$PR(\lambda) = \frac{I_{SC}(\lambda)}{P_{Source}(\lambda)} \quad (4.2)$$

PR of a solar cell can be determined by scanning through the wavelength range available from the light source; normalizing to the incident power of the light source, the PR spectrum is independent of the light source used and therefore the obtained data can be compared to other solar cells measured on different setups. EQE instead is defined as the number of charges N_e extracted at the electrodes divided by the number of photons N_{ph} of a certain wavelength incident on the solar cell:

$$EQE(\lambda) = \frac{N_e(\lambda)}{N_{ph}(\lambda)} \quad (4.3)$$

EQE can be calculated from PR

$$PR(\lambda) = \frac{I_{SC}(\lambda)}{P(\lambda)} = \frac{eN_e/\Delta t}{h\nu N_{ph}/\Delta t} = \frac{N_e}{N_{ph}} \frac{e}{hc/\lambda} \quad (4.4)$$

therefore

$$EQE(\lambda) = \frac{hc}{e} \frac{PR(\lambda)}{\lambda} \quad (4.5)$$

The most important difference between EQE and PR is that the first just considers the conversion efficiency from incident photons to extracted electrons, whereas the second also takes into account the energy of the incident photons. Since the number of photons per given power decreases with shorter wavelengths, the PR will be lower than the EQE for shorter wavelengths. The final parameter to evaluate the efficiency of solar cell to transform the sunlight into electric current is the *Power Conversion Efficiency* PCE , η defined as the ratio of the electric power output of the cell at the maximum power point to the incident optical power. It can also be expressed in terms of I_{SC} , V_{OC} and FF :

$$\eta = \frac{P_{electric}}{P_{light}} = \frac{FF \cdot V_{OC} \cdot I_{SC}}{P_{light}} \quad (4.6)$$

η can be calculated for monochromatic light illumination or for polychromatic illumination. Typically, it is calculated for sunlight illumination; to carry out this kind of measure in laboratory, a light source that simulates solar illumination is needed, the so-called solar or sun simulator 4.4, consisting of a white light source and a set of filters that simulate the solar irradiance.

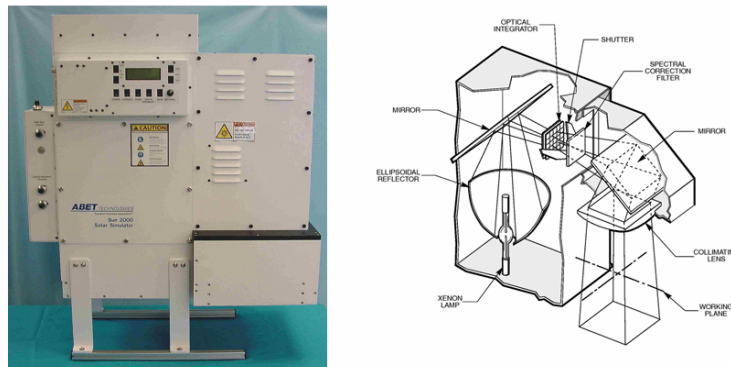


Figure 4.4: Our sun simulator, the ABET 2000. On the right, the internal working scheme.

The band gap of a solar cell influences the maximum theoretical power conversion efficiency. As previously discussed, the energy of the band gap determines the minimum energy of the absorbed photons. The lower the energy of the band gap, the more photons from the solar spectrum can be absorbed. On the other hand, electrons excited by photons with energies

larger than the gap will initially be in states higher than the LUMO, but will lower their energy by emitting phonons (and therefore heating the device) until they reach the LUMO level. This process is called thermalization. In solar cells with lower band gap, the losses due to thermalization of the excited charges increase. An example of how the power conversion efficiency depends on the band gap of a semiconductor for an ideal p-n junction device is shown in figure 4.5. The graph shows that there is a maximum in efficiency between 1.3 and 1.6 eV band gap energy. To achieve maximum efficiency of a solar cell, it is therefore important to utilize materials with an appropriate band gap. One of the attractions of organic solar cells is the ability to tune the band gap by derivatization. It should be noted that if the power conversion efficiency is calculated for monochromatic illumination, these values can be significantly higher than the efficiency for solar illumination since losses due to limited absorption and thermalization are neglected.

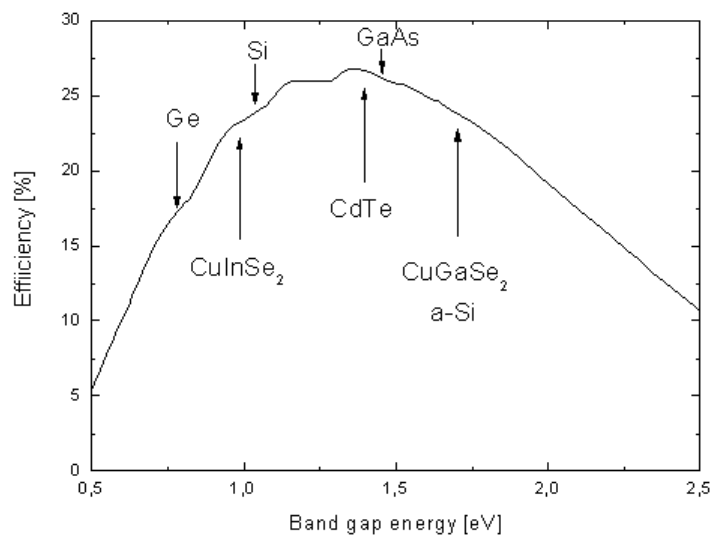


Figure 4.5: Efficiency limits for different solar cells.

4.4 I-V Characteristics of a 'real' solar cell

The shape of I-V curves can reveal various undesirable mechanisms present in the solar cell. Often, different mechanisms can lead to similar shapes in the 4th quadrant of the I-V graph. In the follow, we will show some different examples of detrimental mechanisms, including a sketch of an I-V curve characteristic for each detrimental mechanism, in order to explicate the possible situation that can occur.

Shunt Resistance

The effect of R_{Sh} on the I-V curve is shown in Figure 4.6. The value of R_{Sh} can be found from the inverse slope in the 4th quadrant. Three different curves are presented: the red-one has the smallest R_{Sh} whereas the dark line corresponds to the highest RSh condition. As we can see in figure, a lower R_{Sh} implies a reduction of the open circuit voltage VOC and the fill factor FF of the device. In addition, the slope in the 3rd quadrant increases with lower R_{Sh} . The short circuit current ISC is not influenced by the value of R_{Sh} because, generally, the R_{Sh} is still much larger than R_S and therefore the current through R_{Sh} can be neglected. In the limit of very small R_{Sh} , in other words when we are in short circuit condition, the V_{OC} will approach 0 and the FF will go to 0.25, that is its theoretical limit.

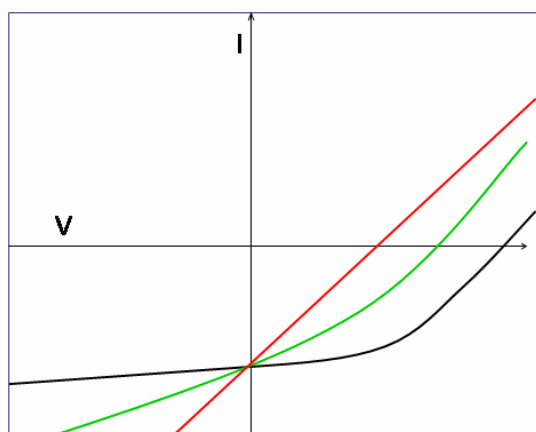


Figure 4.6: Effect of the shunt resistor on the I-V characteristic. The graph shows I-V curves for high (black), medium (green), and low (red) values of R_{Sh} .

Series Resistance

Variations in series resistance R_S on the I-V characteristic influence the I_{SC} and the FF . As in figure 4.7, for high R_S , FF and I_s are reduced. Also, the slope in the 1st quadrant is reduced for higher R_S values. The V_{OC} remains unchanged for higher R_S since at V_{OC} the current flow is zero through R_S . The slope in the 3rd quadrant is still dominated by the R_{Sh} and therefore, assuming R_{Sh} is constant, does not change with increasing R_S .

Short Circuit Currents

Also the current generated I_G by illumination of the solar cell can influence the I-V characteristic, as in Figure 4.8. Low I_G values can reduce V_{OC} and FF : in this way, I_G is influenced by the illumination intensity and V_{OC} and FF also have dependency on the light intensity shining on the solar cell. It is for this reason that is very important to quote light intensities when publishing data about the efficiency of solar cells, using, for example, standard conditions for solar simulator.

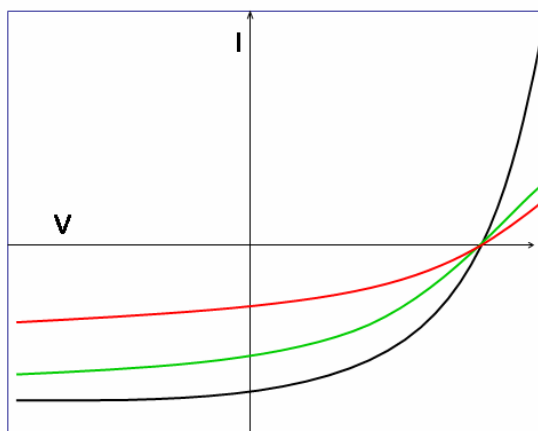


Figure 4.7: Effect of the series resistor on the I-V characteristic. The graph shows I-V curves for a low (black), medium (green), and high (red) value of R_S .

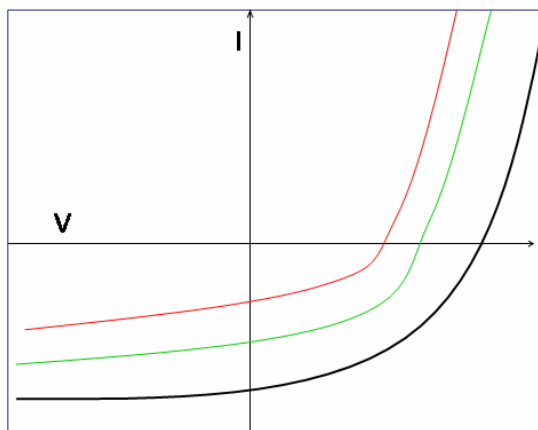


Figure 4.8: Effect of low short circuit currents on the I-V characteristic. The graph shows I-V curves for high (black), medium (green), and low (red) values of I_{SC} .

4.5 Origin of the Open Circuit Voltage

It is generally accepted that V_{OC} is related to the built-in potential of the photovoltaic device. The built-in potential is a parameter that influences charge dissociation, charge transport, and charge collection. The nature of the built-in field depends on the morphology of the active layer and is therefore different for various device structures. In devices with the active layer consisting only of a pristine polymer, the built-in potential is created by the difference in work-function W between the negative (low W) and the positive (high W) electrode. The upper limit for V_{OC} is given by the HOMO-LUMO gap of the polymer. Even in cases where the difference in W of the electrodes is larger than the HOMO-LUMO gap, no further increase in V_{OC} would be observed. Recent studies [50] [52] have shown a different origin of the V_{OC} in bulk-heterojunction devices made out of donor polymers and acceptor fullerenes: the main concept is that the Fermi level of the negative electrode is "pinned" to the reduction poten-

tial of the fullerene. Fermi level pinning describes a situation where the workfunction of the metal electrode is pinned to the workfunction of the semiconductor. This occurs independent of whether the metal workfunction is higher or lower than the semiconductor Fermi level. This results in a V_{OC} that is directly related to the energy difference between the HOMO level of the donor and the LUMO level of the acceptor material. Varying the difference in workfunction between positive and negative electrode in these devices has only minor effects on the V_{OC} . It should be noted here that the V_{OC} can be significantly reduced due to shorts between the positive and negative electrode and other recombination processes near the electrodes (represented by R_{Sh2} in Figure 4.2). Therefore, the V_{OC} can be used in addition to the shape of the I-V characteristic to evaluate the quality of the photovoltaic device.

4.5.1 Optical Filter Effect in Organic Films

The absorption in organic semiconducting materials is strongly wavelength dependent. This means that light that is subject to weak absorption can propagate through the whole film and is absorbed throughout the bulk of the material. In others words, wavelength with strong absorption in the active layer will be absorbed entirely in the surface layer, maybe not penetrating the bulk. The film acts as an optical filter. This effect has consequences for the performance of organic photovoltaic devices: since the photoexcitation has to occur in close vicinity of a donor acceptor interface, the device structure and morphology have to be well conceived. Early photovoltaic devices, for example, built in a bilayer structure where there is a single interface between donor and acceptor materials, will have low efficiencies because a large fraction of the light was absorbed in areas far away from the donor acceptor interface.

4.6 Experimental Setups

The laboratory for the devices characterisation has been improved during the period of PhD. When it started there was any characterisation setup: a part of experimental work of thesis has been spent for this purpose. This part of job has been led principally by Enrico Sovrnigo, PhD on Nanotechnology at University of Trieste. In particular, two independent equipments have been accomplished: the first to the measure of the light intensity at each wavelength and the produced current in (nearly) short circuit conditions in function of wavelength, useful for the EQE calculation. The second one for the measurements of current-voltage curves (I-V), from which deduce FF and PCE. The first equipment is constituted of a spectrographs Acton SpectraPro SP-2300i with monochromators for EQE measures coupled to a Keithley 2400 source meter (fig. 4.9).

A NIST traceable calibrated photodiode is used to measure the light intensity at each wavelength. The Acton SpectraPro SP-2300i permits to have 0.2 nm max resolution in the range of 300-1100 nm. The resolution in collected current is 10fA. An ABET 2000 SunSimulator providing the calibrated light in the second measurement system: the I-V characteristics under illumination and in dark are recorded with an Agilent B1500A Semiconductor Device Analyzer (fig. 4.10). The sun simulator is required to have a known standard spectrum (AM1.5G corresponding to $100 \text{ mW}/\text{cm}^2$) in order to match as close as possible the conditions of a clear

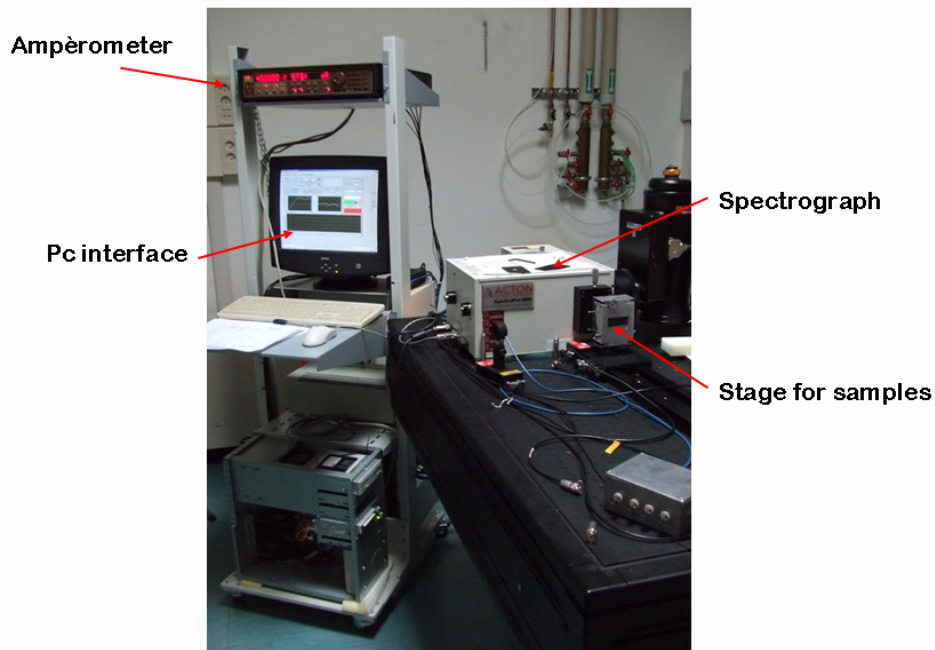


Figure 4.9: The spectrographs Acton SpectraPro SP-2300i with monochromators and the Keithley 2400 source meter.

sunny day at the sea level and at a medium latitude (42°N).

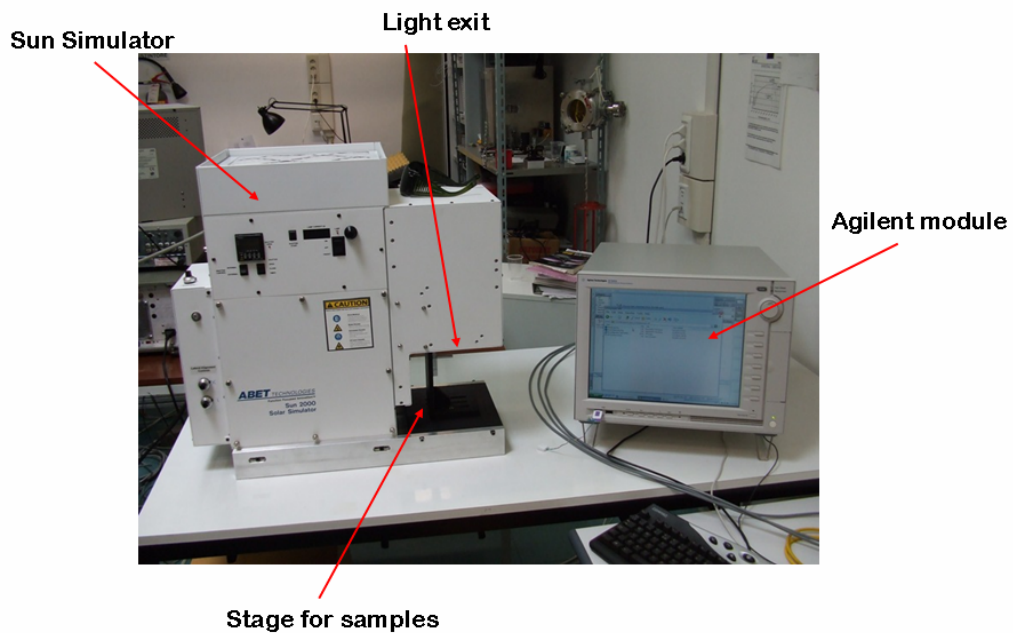


Figure 4.10: ABET 2000 SunSimulator and Agilent B1500A Semiconductor Device Analyzer.

Chapter 5

Trapping light with microlenses in organic photovoltaic devices

As shown in the introduction, the research on PV focuses its attention on thin film technology. The motivations are immediately clear: less material is used, with consequent reduction in the cost. Also the fabrication process could become quicker and cheaper when thin film is employed, as in the case of polymeric solar cell: the use of well known and not expensive processes of deposition of polymeric film from solution made this technology potentially low-cost. Problems can start when the thickness of active film is not enough to permit the complete absorption of incident sun light. The absorption of only a part of light implies the reduction of the efficiency of the cell or, in other words, a reduction of generated electric current. Without increasing the thickness of the film, a partial solution could be that of coupling to the cell for a system confining the light in the region comprising the active film: this is generally referred as Light Trapping System LTS. The concept is to induce sunlight to travel a longer distance in the active layer by multi-pass path in order to exploit most of the radiation. In the past, a large number of LTSs have been proposed and many paper have been written on the topic; often, different PV technology requires different LTSs solutions. One of the first systems has been realized by Goetzberger for silicon based PV devices, like a-Si or thin crystalline silicon film [53]: he suggested a Lambertian back reflector as a simple but efficient structure. Different possibilities of light trapping are shown in Fig. 5.1.

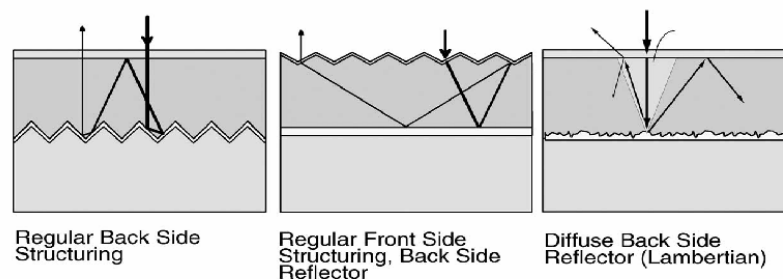


Figure 5.1: Optical confinement for light path enhancement.

Many other works have been presented since the demonstration of Goetzberger concept:

Zhao et al. ([54]) have demonstrate the improvement of multicrystalline cell performance by enshrouding cell surfaces in thermally grown oxide to reduce their detrimental electronic activity and from isotropic etching to form an hexagonally symmetric "honeycomb" surface texture. This texture reduces reflection loss as well as substantially increasing the cell's effective optical thickness by causing light to be trapped within the cell by total internal reflection. Springer et al. ([55]) investigated the influence of front textured transparent conductive oxide and different back reflectors on short circuit current density and fill factor of thin film silicon solar cells.

As regards to the sector of organic solar cells, the application of LTS to thin film has further advantages. As previously shown, the low mobility of excitons result in reduced photocurrent extraction at the electrodes and low power conversion efficiency. The diffusion length of an exciton, is typically around 5-10 nm, much less than the optical absorption length of 50-100 nm. This property requires a trade off between using a thick, resistive cell or a thin cell with low optical absorption efficiency. The alternative partial solution to these conflicting needs could be represented by the introduction of a LTS coupled with a very thin active layer: this would allow complete absorption of impinging light by multiple passing trough the film preserving the advantages of low sheet resistance and reduced recombination of excitons. In the past, light trapping systems have been actively investigated as means for increasing the total path length of light into the active material without the need of increasing its physical thickness. Many different light trapping schemes have been proposed to enhance the quantity of light absorbed in OPV cells such as metal gratings [56], buried nanoelectrodes [1] and scattering [57] and multireflection structures [58]-[59] are the most proposed solutions. However, the requirement that the feature sizes of the scattering structures be comparable to the film thickness of the OPV cells, i.e. 50-200 nm, and at the same time larger than the wavelength of light to effectively alter the photon propagation direction is intrinsically contradictory. Furthermore, electrical properties can be negatively affected by the introduction of light scattering elements in direct contact with such thin active layers: defects and shorts may easily occur.

Therefore, different engineering solutions may be required, where the light trapping element is separated from the thin active layer. Light trapping techniques compatible with thin film polymer cells have been suggested: Niggemann et al. [56] and Roman et al. [60] demonstrated small improvement in efficiency using this solution. The Niggemann approach consist of a novel cell architecture for organic solar cells has been presented by Niggemann et al. [57] which is based on a functional micropism substrate. In contrast to the most widely used planar cell architecture, the microstructure results in a folded solar cell. Optical simulations were performed and revealed a gain in absorption in the photoactive layer due to the inclined incidence of radiation and due to the second reflection. In particular, an interesting article about the utilization of small arrays of compound parabolic Winston collectors has been suggested but not realized: Peumans et al. [1] proposed that, in the case of very thin organic layers, with consequent low series resistance, an efficient power conversion is obtained under intense (≈ 15 suns!) illumination. These conditions can be obtained by placing multiple Winston-type collectors in front of the solar cell. In the article it was demonstrated that the external power conversion efficiency of a device based on *CuPc*/60, plotted versus the illumination intensity, reaches a maximum under intense ≈ 10 suns illumination.

A similar concept is at the origin of the work: the realization of a light trapping system

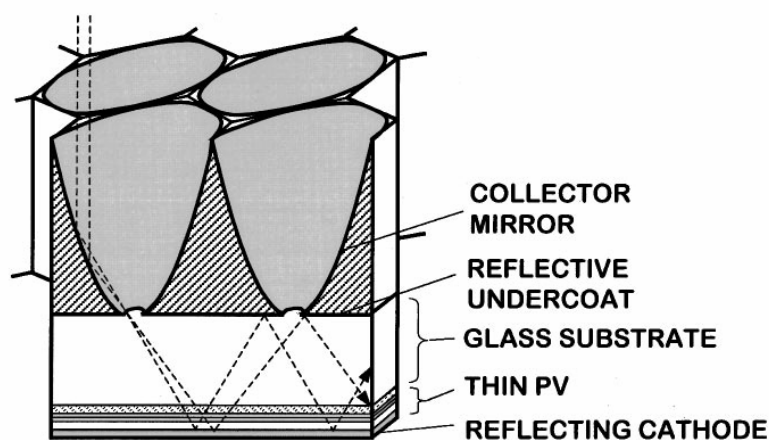


Figure 5.2: The proposed Winston-type collectors [1].

separated from the active layer in order to prevent possible electrical defects (shorts between the electrodes). It consists of a trap element that is transparent to collimated light in one direction and highly reflective in the opposite direction to both collimated and directionally randomized light that is placed in front of a solar cell with limited absorption. As light bounces back and forth between the reflective metal surface of the cell electrode and the back surface of the trap element, multiple transits through the active layer will occur, thus increasing the probability of photon absorption. In detail, the concept of the proposed and realized LTS consists of an array of microlenses focusing the sunlight that, passing through small apertures, is introduced into a cavity delimited by the reflective back-electrode of the cell and the mirror of the trapping system.

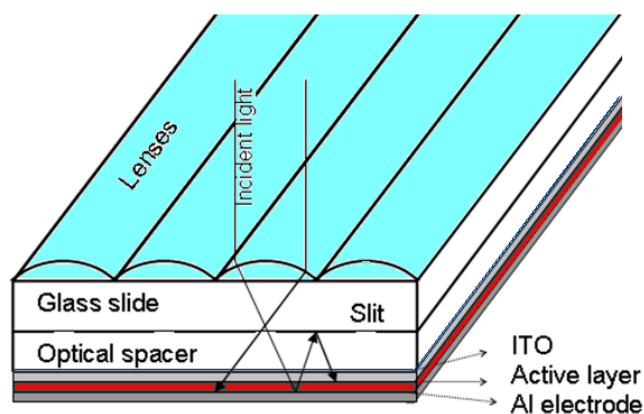


Figure 5.3: Operational principle of the light trap and its constituents.

Ray tracing for a trap with realistic features on top of a 100% absorbing solar cell is displayed in Fig.5.4 and for a 0% absorbing "solar cell" in fig. 5.5. Real photovoltaic devices display a wavelength dependent absorption ranging in between these two extremes. For wavelengths where absorption is limited, photons will be recycled and get additional chances for

absorption. As thin active organic films often are desired due to electrical limitations, the light trap can be a tool to remedy the mismatch of photon absorption length and free carrier diffusion length.

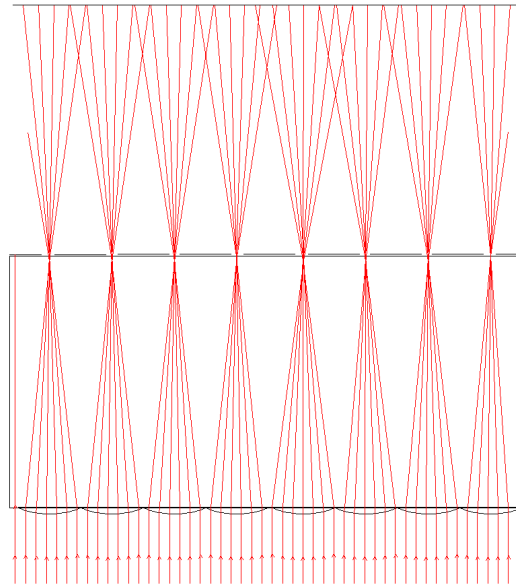


Figure 5.4: Figure display configuration with relevant radius of curvature, hole openings and

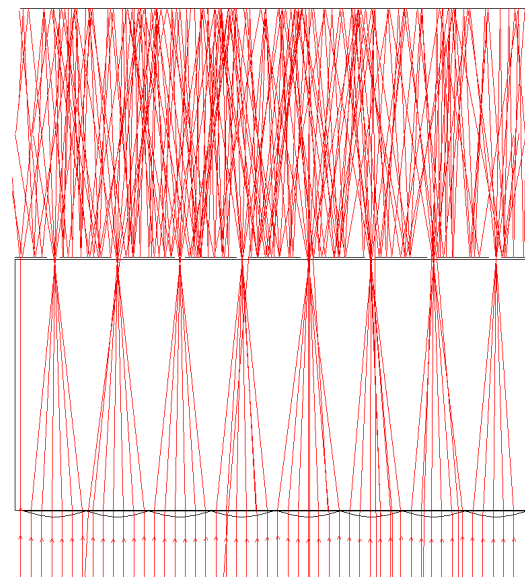


Figure 5.5: Same device as before but with a 100% reflecting cell. All rays are accordingly reflected.

5.1 Methods of fabrication

The fabrication scheme exploits an innovative self-aligned UV exposure to create the pattern of openings aligned to the focus of the micro-lenses: the choice of a similar scheme of fabrication

can be motivated as follow: first, setting up a process that would be suitable for up-scaling to large areas at high throughput as needed for photovoltaic applications and second, minimizing problems related to defects in the array of microlenses. This last concept will be more clear in the follow, after describing every step of the process. The fabrication process could be schematically represented as in fig.5.6: for each step is reported the technique or techniques employed.

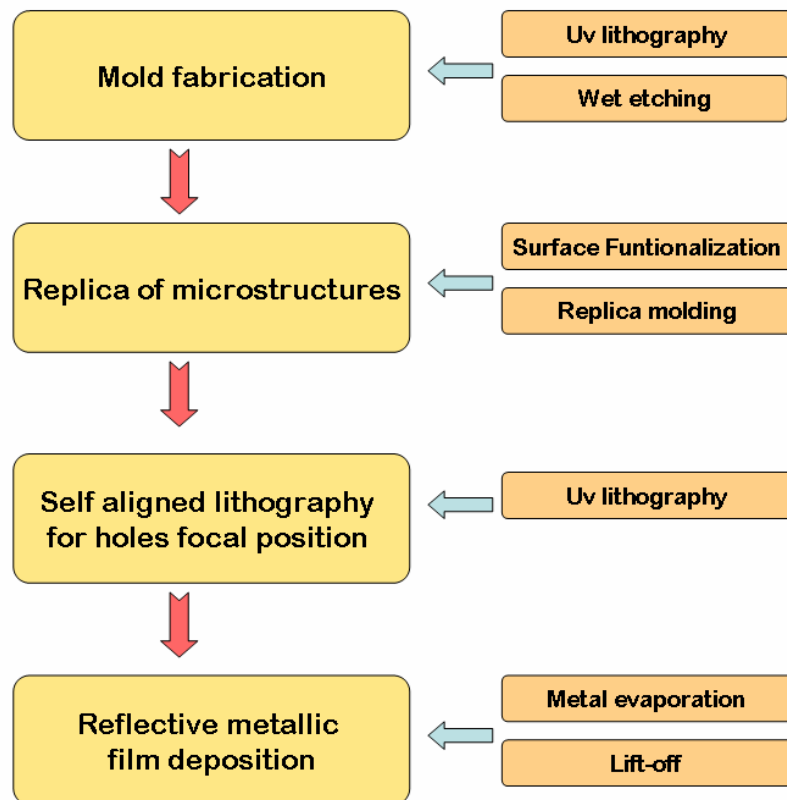


Figure 5.6: Scheme of fabrication of light trapping system.

The first step consists of fabricating the mould with an array of inverted (concave) microlenses. The fabrication follows concepts and procedures described in a previous publication [61]. Conventional proximity UV-lithography was employed to produce an array of circular holes or straight trenches in a chromium coating on the surface of a fused silica substrate (thickness 3 mm), by patterning a sacrificial positive photoresist, Shipley Microposit S1813, of $1.5\mu\text{m}$ thickness and MF-319 development. A bath in a solution of CH_3COOH (35 ml), H_2O (600 ml) and $(\text{NH}_4)_2\text{Ce}(\text{NO}_3)_6$ (200 g), has been used to wet etch the exposed Chromium. The result is a patterned film of metal where, replica of initial optical mask, that present an homogeneous chromium coating with well defined areas of exposed silica. Spherical or cylindrical concavities were realized by isotropic wet etching of the fused silica substrates in HF aqueous solution (48% w.), with the openings in chromium acting as the origins of etch (fig.5.7).

This has been one of most delicate steps: the radius of curvature of spherical or cylindrical

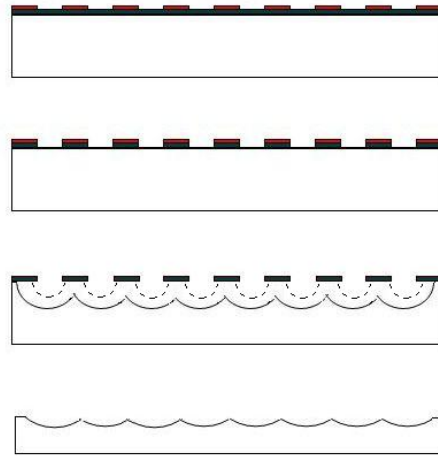


Figure 5.7: Scheme of fabrication procedure of silica mold.

concave elements on the mould determine the focal length (f) of the polymer microlenses that are obtained in the subsequent process of moulding through the following equation

$$f = R \frac{n_2}{n_2 - n_1}$$

where R is the radius of curvature of the lens, n_2 the refraction index of the material of the lenses (that we will assume equal to that of the substrate) and n_1 the refraction index of the external medium (for air, $n_1 = 1$). The realisation of structures with correct value of R satisfying the condition that the focus of microlenses molded onto a microscope glass slide falls onto the opposite surface of the glass, is realized by modulating the etching time of silica substrate. An accurate calibration of the etching rate of HF solution is needed to determine the time of immersion of sample; the experimentally measured etching rate of the reaction, resulted $1.1 \mu\text{m}/\text{min}$ for $\text{HF}48\%$, $0.9 \mu\text{m}/\text{min}$ in the case of 39% concentration. Unfortunately, the rate of dissolution of SiO_2 in HF is strictly dependent to the concentration of acid: the more diluted is the solution, the lower is the etching rate. Due to the large size of needed structures in the stamps, the estimated duration of the etching for $100 \mu\text{m}$ of silica was more than 1,5 hours. However, as the reaction progresses, we observed in general a slowing down of the etching rate from an initial value of $1.1 \mu\text{m}/\text{min}$, which we have attributed to the consumption of HF in the etching solution. The found solutions are principally three:

- Extending the time of immersion of sample. This is an easy way, but the control of the progress of etching is imprecise due to the approximate knowledge of the etching rate at any time
- Using a sizeable excess of solution, to make irrelevant the changes in concentration or frequently changing the solution.
- Using a buffered solution, like BOE (Buffered Oxide Etchant): this kind of solution contains particular reagents permitting to maintain constant (in a limited range) the con-

centration of a specific component of solution. In fact BOE is a solution of H_2O , HF and ammonium fluoride (NH_4F), where the latter is the buffering component that establishes an equilibrium in the reversible reaction $NH_4F \rightleftharpoons NH_3 + HF$: in presence of high concentration of F^- , the ammonium fluoride is not dissociated. As etching of SiO_2 proceeds, with consequent reduction of the concentration of F^- ions, the equilibrium of the reaction move to the right providing more HF and consequently F^- ions from the dissociation of NH_4F ; in this way the concentration of F^- ions remains constant. Unfortunately, the etching rate of similar buffered solution is quite low ($\approx 60 \text{ nm}/\text{min}$), and would require a very long time to complete the reaction ($\approx 30 \text{ h}$).

Therefore, in general the procedure for obtaining concavities with the requested radii of curvature consisted in a first etching step for the duration estimated on the basis of the initial etching rate, followed by a second etching step after the measurement of the actual radii of curvature of the resulting concavities. During the second etching step, the frequent change of the solution and the regular checking of the dept of structures using a profilometer and/or realizing some test sample has been essential to reaching the target radius of curvature. After reaching the desired etched profile in the fused silica substrate the chromium protective layer was removed by wet etching with the previously described solution.

Before replica moulding, the surface of fused silica molds has been functionalized with an antiadhesive coating, to improve the detachment of mold in the follow step of replica. The functionalisation of silica surface by Self Assembled Monolayer as been made by dipping the master in a 5 mM solution of Dodecyl-trichlorosilane in heptane for a time comprised between 30 minutes and 1 hours. The quality of SAM was not precisely assessed: due to the large size and the shape of the structures, the problem of stamps adhesion is muchless severe than in the case of nanoimprinting of high resolution structures with vertical sidewalls. Just a simple qualitative test done with a drop of water on the flat surface to verify naked-eye that the contact angle is approssimately of 90° or more was perfectly enough to predict the possibility of easy separation from the molded structures. In order to explore the effects of geometrical parameters on the properties of the final light trapping elements, different types of patterns, namely, gratings of $10\mu\text{m}$ wide lines with 200, 250, $400\mu\text{m}$ periods and triangular arrays of dots $8\mu\text{m}$ of diameter with center-to-center distance of 80, $200\mu\text{m}$ were tested as the pattern openings in the chromium layer. Correspondingly, cylindrical lenses with periods of 200, 250, $400\mu\text{m}$ and triangular array of spherical lenses with center-to-center distance of 80 and $200\mu\text{m}$ were obtained after moulding. The radii of curvature were $350\mu\text{m}$ in all cases, due to the fact that the focal length is fixed by the thickness of the glass slides substrates supporting the microlenses. At the beginning, microlenses have been realized in the polymer Ormocomp of the Ormocer family produced and sold by Micro Resist Technology GmbH; this is UV curable material for imprinting, designed for manufacturing microstructures like micro lenses, optical couplers and connectors or prisms. The quality of obtained lenses (surface finish, adsence of defects, trapped air bubbles...)was very high, but first measurements showed a rater poore transmission of this material under 400nm of wavelength with the quite completely absorption. This is the reason for the search of an alternative material, characterised by higher transparency in the short wavelength region, where the polymeric semiconductor shows the

largest responsivity. We choose a different UV curable polymer, the Norland Optical Adhesive 73 (NOA 73), which is an optically clear, liquid adhesive that quickly cures when exposed to near ultraviolet light, in the range of $350 - 380\text{nm}$ where transparency starts to decay.

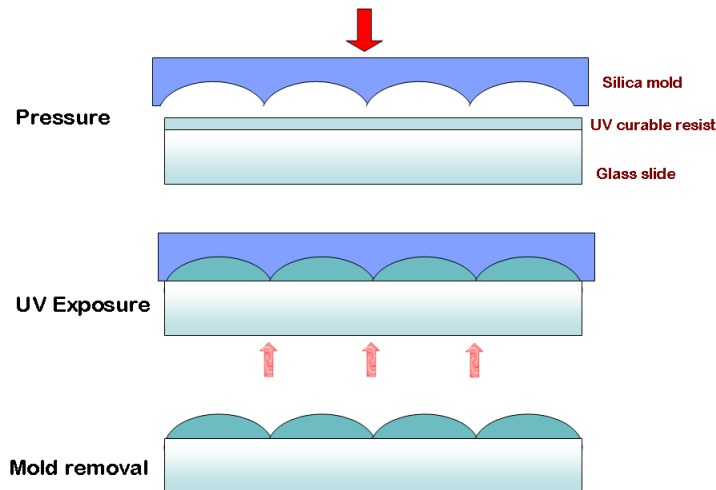


Figure 5.8: Scheme of fabrication of microlenses.

NOA 73 has an adhesion promoter in it that provides maximum adhesion and moisture resistance when used on glass: this characteristic makes this polymer really suitable to our aim. The adhesion promoter begins working after the cure and provides the extra strength after 1 week at room temperature. Generally, the procedure can be accomplished more quickly by warming the optics to 140°C for 2 hours. As substrate for the array of microlenses we used a 20×20 mm microscope 1 mm thick glass slide, after thorough cleaning in hot acetone and IPA. A drop of NOA was placed on the surface of the master and the latter placed gently in contact with the glass slide, avoiding the formation of air bubbles during this step (fig.5.8). An UV mercury lamp with main peaks emission at 350nm was employed to cure the NOA 73; during the exposure the sample and the master were kept together under pressure, in order to obtain the parallelism between the plane of the lenses and that of glass substrate and a thin residual layer at the base of microlenses, in order to keep as low as possible the absorption of incident light (see fig. 5.9 and 5.10).

The pressure was ensured either by putting on top of mold a weight or by inserting the mold and substrate in a specific, home made clamping device. As seen in optical transmission measurements on final optical trapping devices, the reduction of residual layer has been the first improvement in the device. After the bake of sample, to make harder the polymer, the precision of focus depth position with respect of the surface of opposite side of slide was checked. This procedure has been accomplished making use of a microscope with possibility of reflection and transmission light methods.

The procedure consist of observing the position of focus of microlenses and measuring the distance from the surface of slide. If the focus falls still inside the glass, it's possible to go back to the mold and carry on with etching in order to correct (increase) the radius

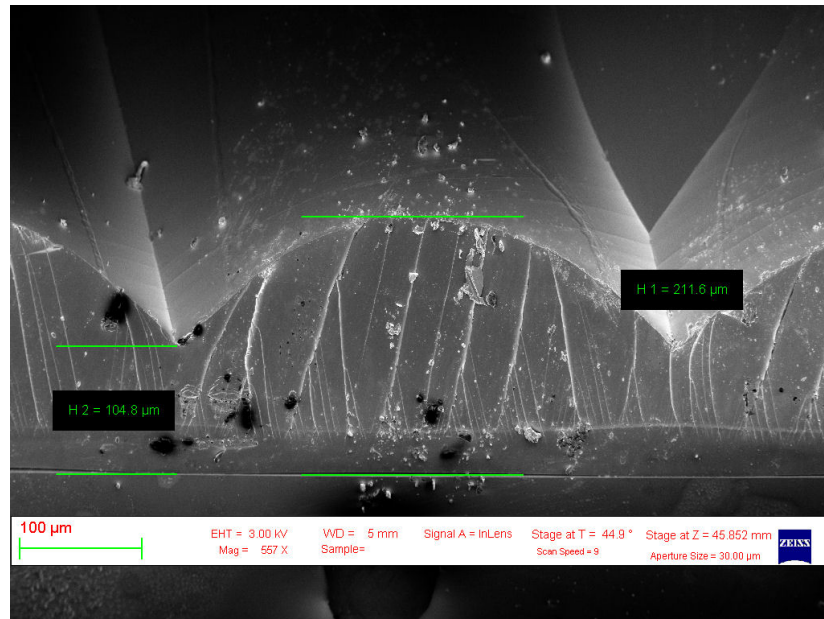


Figure 5.9: SEM picture of lenses fabricated without applying pressure during the exposure.

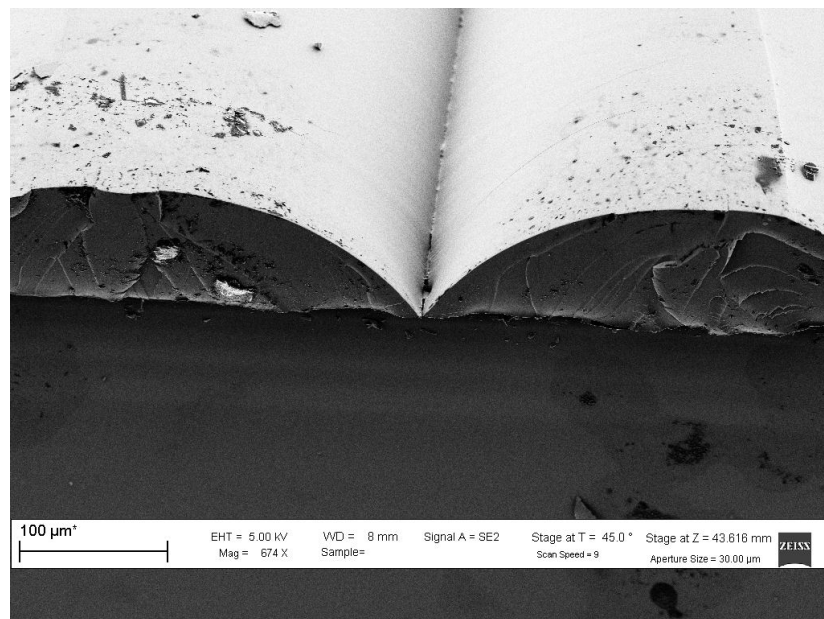


Figure 5.10: SEM picture of lenses fabricated from same the mold applying pressure during the exposure.

of curvature. Using this feedback procedure, the focus can be obtained with an estimated accuracy of $\pm 5 \mu m$. In figures 5.11, 5.12 and 5.13 are show some examples of microlenses.

The fabrication of silver mirror, with holes or slits, is the most interesting and innovative procedure of the process. It would be possible to produce it by a lithographic step, aligning a pattern of dots, or lines, precisely with focus of lenses: this procedure is quite hard, requiring a precise alignment which might become an obstacle in the case of upscaling, if this would have to enter an industrialisation phase. Our idea has been that of carrying out a self aligned

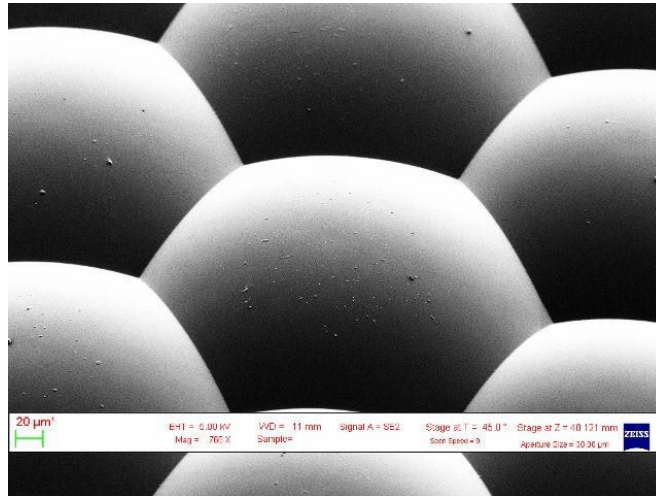


Figure 5.11: SEM picture of spherical microlenses.

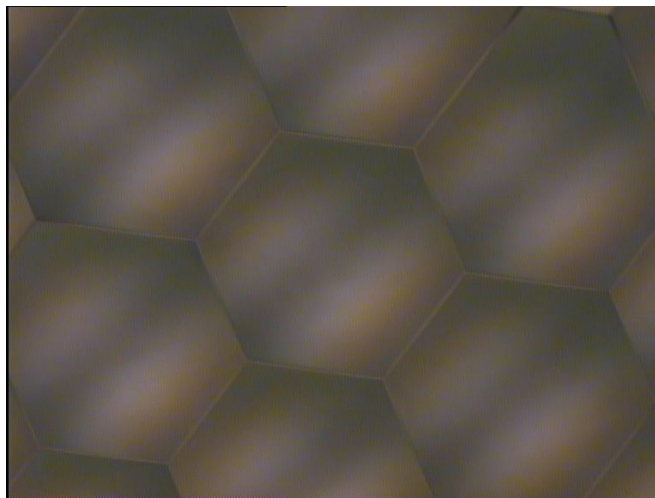


Figure 5.12: Optical microscope of spherical microlenses.

optical lithography making use of concentrated light of microlenses: in this way the alignment between fenditures and light spots of focus is ensured by construction. First attempt has been accomplished exposing a positive resist (SPR 220 3.0 thickness 3 mm) exposed trough a very thin film of silver (30 nm thick) deposited by thermal evaporation: a long exposure, in order to ensure the necessary dose to the resist, gave as result well defined structures in the resist film. By a subsequent step of wet etching the exposed silver is etched producing the deviced apertures in the film. however, some problems have been observed with this procedure of fabrication: first is the quality of etching of silver. We employed a solution of KI and I_2 in water 10:1; unfortunately the quality of the profile of the structures was not satisfactory. Moreover, we needed to exploit a very thin film of silver to permit a sufficient exposure of the resist trough it by incident UV light, although concentrated by microlenses: that means that the light is partially transmitted and partially reflected by the metal layer, and the consequent loss of trapping light efficiency. The alternative solution is based on a lift-off process using a negative photoresist 5.14.

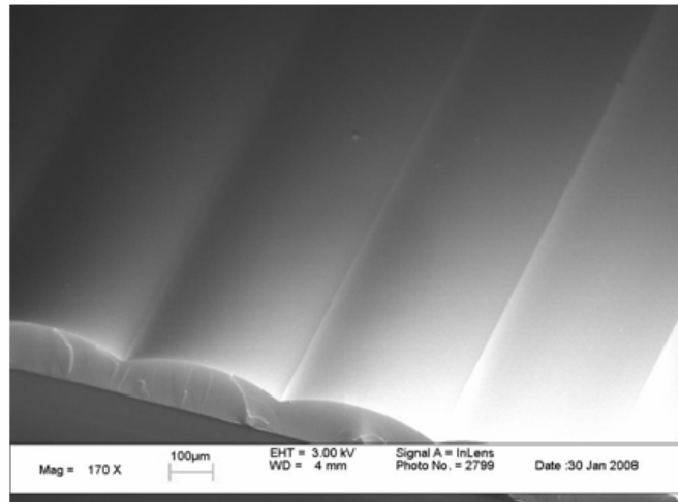


Figure 5.13: SEM picture of cylindrical microlenses.

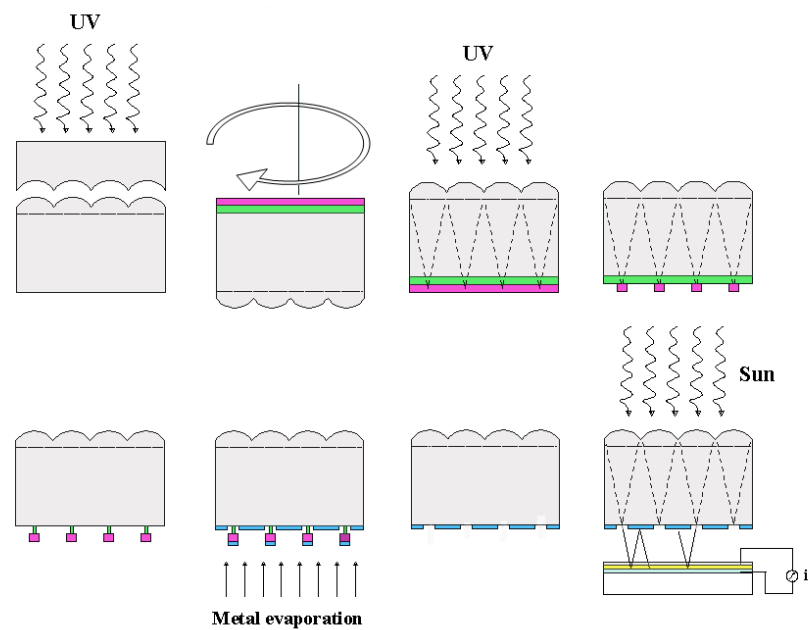


Figure 5.14: Fabrication scheme of light trapping system.

A double layer of LOR 10 B (MicroChem) and negative resist MR-L6005 (Micro Resist Technology GmbH) were deposited on the opposite side of the glass substrate with respect to the lenses. LOR 10-B, a lift-off resist, was required to disconnect the negative resist from the substrate making it possible to produce an undercut for the subsequent metal lift-off process. It has been spun to a thickness of 700 nm and baked at 190° C for 5 minutes. In the baking process the microlenses, previously fabricated on the opposite side, were kept in contact with the surface of the hot-plate, without exhibiting any damage as a consequence of this step. The negative resist was deposited by spin coating (3500 rpm to produce a 7.5µm thick film): 150° C for 5 minutes and 100° for 5 minutes were respectively the pre-bake and post-bake conditions

set for the processing of the negative resist. The exposure of negative resist was accomplished by the same self aligned process previously described: the maskless UV exposure exploits the light focused by microlenses, resulting in a self-aligned structure pattern in the sacrificial resist layers. The observations made during the first attempts highlighted some problems to solve: the quality of the edges of the structures and the insufficient control on the feature size, as show in figures 5.15a and 5.15b.

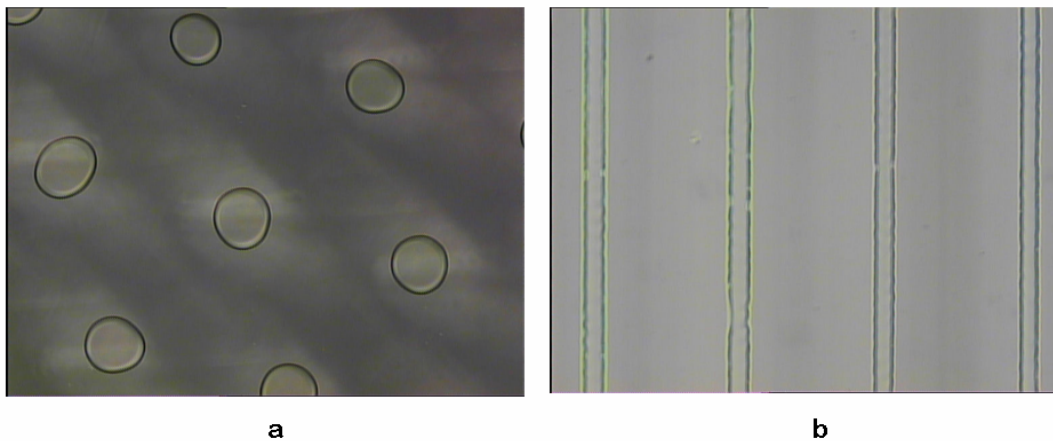


Figure 5.15: Optical micrograph of structures in negative resist produces from exposure through spherical (a) and cylindrical (b) microlenses. The quality of the edges and the control of feature size look insufficient.

Defects in microlenses are the cause of inconsistency on structures, because the light is not homogeneously focused by lenses. Moreover, the light trapping efficiency is strongly correlated to the size of the openings in the mirror. Narrow slits or holes result in a high reflection coefficients, but forward transmission is hampered. Instead, large openings increase the transmission of direct light but the trapping efficiency becomes inadequate. The trade-off can be obtained only by fine control of the size of the openings, that, in this exposure configuration, was not possible. Therefore a solution was conceived to solve simultaneously both problems. The samples were mounted on a rotating stage with the possibility of tilting the rotation axis and the plane of the microlens array with respect to the optical axis of the partially collimated UV source of the mask aligner (Fig. 5.16).

By tilting the rotation axis, the illuminated spots describe a circular path, causing the enlargement of the photoresist exposed area; varying the tilt angle allows to vary continuously the exposed size of dots or lines. Furthermore, the rotation, obtained by an electric motor with 60 rmp rotation speed, allows to reduce the distorting effects of chromatic aberrations, UV source divergence and diffraction, thus improving the line edge roughness of the structures produced in the negative resist.

Unexposed MR-L 6005 was developed in acetone, obtaining the structures on negative resist. An oxygen plasma treatment in ICP (Inductively Coupled Plasma STS) or in RIE (Reactive Ion Etching) equipments was performed to clean the surface from thin layer of cross linked residuals of negative resist MR-L 6005, produced by stray light, reflected or diffused during the exposure. The removal of this thin layer is absolutely mandatory to ensure uniform access

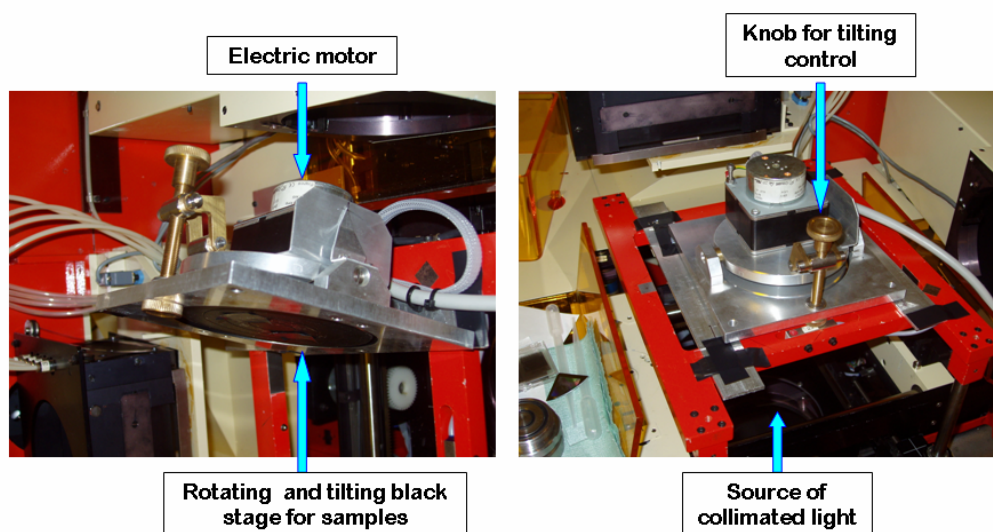


Figure 5.16: The rotating stage with possibility of tilting. In the picture is set on the mask aligner used for the UV-exposure.

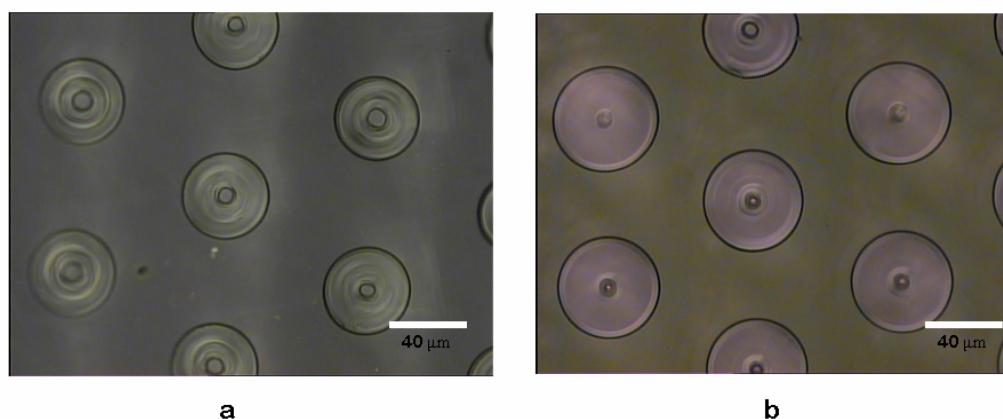


Figure 5.17: Optical micrograph of negative resist structures produced by exposure through microlenses. a) Doughnut like structures were obtained. b) posts exposed at larger tilt angle of the rotation axis with respect the (a). The central region was not sufficiently exposed.

of the MF 319 developer to the LOR layer underneath and for the formation of a well defined undercut. Some examples are shown in figures 5.17a and 5.17b. They show first structures produced in negative resist by exposure through spherical lenses (period $80\mu m$). The diameter of external circle of structures is approximately between 40 and $50\mu m$. The defect is evident: the central area is underexposed. The resulting structure is similar to a doughnut. In figure 5.18a and 5.18b: the collimated light had produced a very well defined structure. Unfortunately, as we will show in the follow, the correspondent slits or holes, achieved after the evaporation of metal, were too small to allow the transmission of a sufficient large fraction of the focused light.

In figure 5.19: negative resist structures. The quality of edges definition is very high but

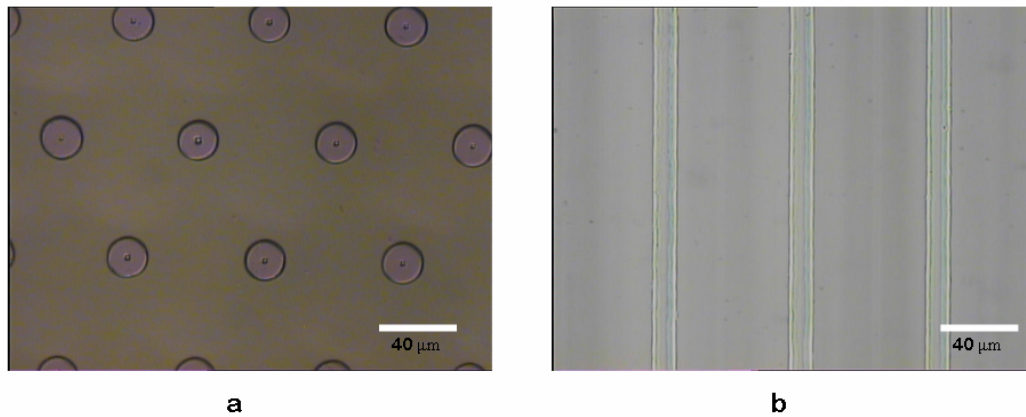


Figure 5.18: Optical micrograph of negative resist structures produced by (a) spherical and (b) cylindrical lenses. The size of the corresponding metal apertures would be too small in the final devices.

the size of dots was too large. In this case the transmission in forward direction (lens first) of the light is satisfactory but the trapping efficiency, related to the transmission in backward direction, is poor.

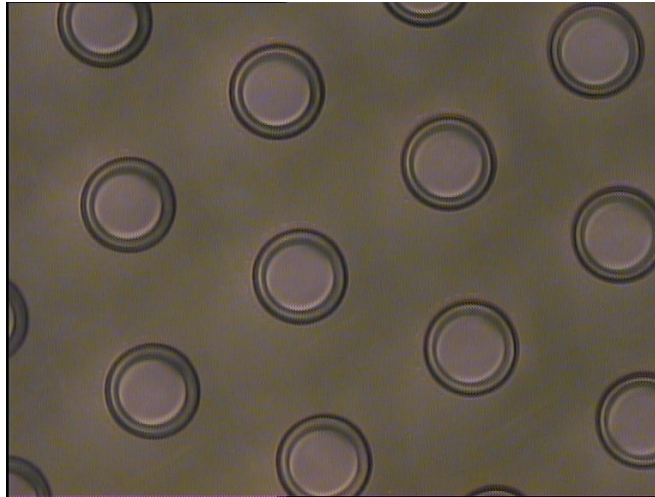


Figure 5.19: Negative resist dots with large size. To notice the very well defined edges.

In figure 5.20, 5.21 and 5.22: optical micrographs of samples with optimized size of the resist structures, corresponding to the openings in the mirror. The roughness of the edge is very limited and the lateral dimensions is very controlled perfectly. In the circular structures, the center area is correctly exposed.

Final structures (i.e. the patterned mirror) were obtained by metal evaporation and lift-off. A metal tri-layer of chromium, silver and gold was deposited by thermal evaporation. The first deposited layer of chromium (5nm) was introduced for improving the adhesion of the sequent film of silver (150nm), whereas gold (5nm) was deposited to prevent the oxidation of silver. After the evaporation, the sacrificial polymer structures and the metal on top were lifted by

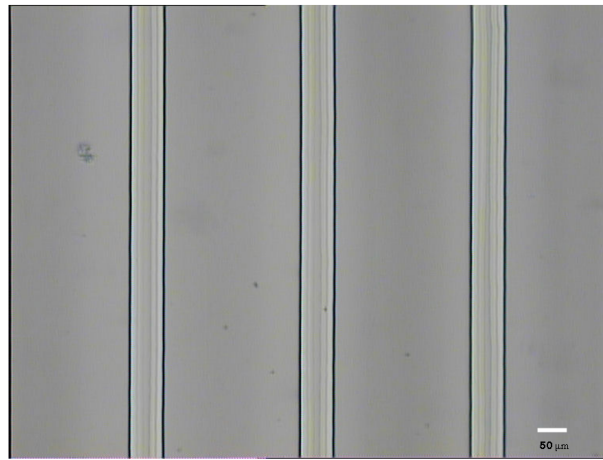


Figure 5.20: Optical micrograph of $200\mu\text{m}$ period lines. The width of lines is on average $40\mu\text{m}$.

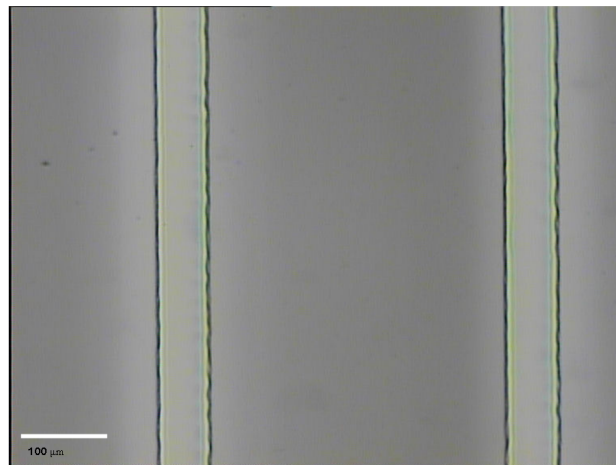


Figure 5.21: Optical micrograph of $400\mu\text{m}$ period lines. The width of lines is on average $50\mu\text{m}$.

developing the bottom LOR resist in MF 319. In this last it was important to stir the developer the develop to prevent the re-depositing of metal structure on the surface of patterned mirror, that was not possible to remove anymore, given the strong adhesion forces. In figure 5.23 two example of optical transmission microscope picture of the backside of the samples comprising the perforated mirrors.

5.2 Characterisation of devices

The characterization of the samples has been carried out in two steps: the preliminary test of quality LTS based on microlenses was that of measuring the transmission and the reflection of incident light in both direction; subsequent tests of the trapping system were made by coupling them to solar cells in order to assess their performances in real working conditions. The first

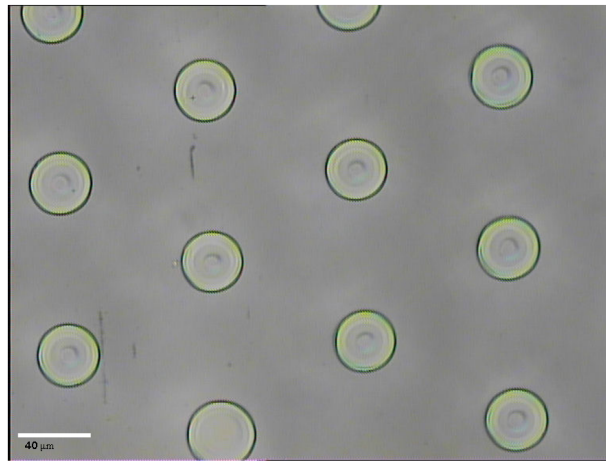


Figure 5.22: Optical micrograph of $80\mu\text{m}$ period dots. The diameter of circles is around $25\mu\text{m}$

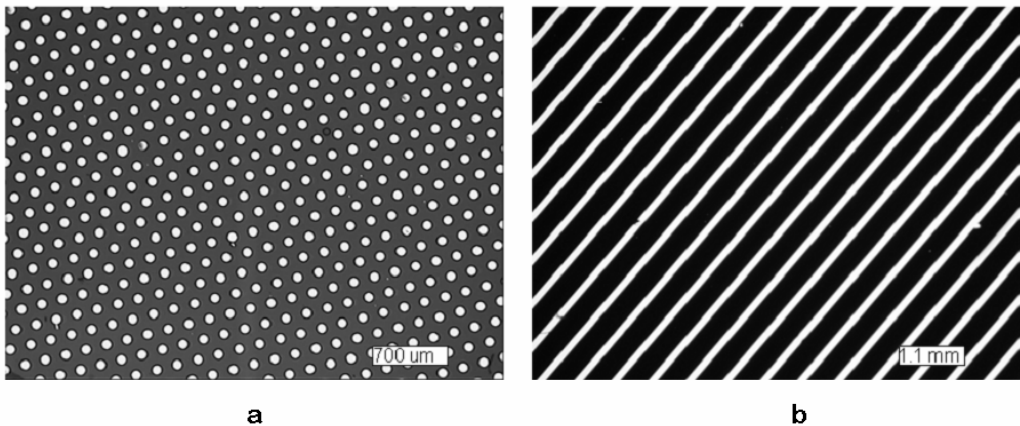


Figure 5.23: Optical transmission microscope picture of the backside of the samples: the backside mirrors for spherical (a) and cylindrical (b) lenses are displayed.

characterisation step was fundamental to understand the possible improvements of devices, in order to maximize the transmission in forward direction and the reflection in the backward direction.

The measurements were performed by placing the light trapping device in front of an integrating sphere (fig.5.24): the transmission in the forward and backward directions has been characterized as a function of wavelength. Integrating sphere, in combination with UV/Vis and UV/Vis/NIR spectrophotometers, provides an ideal solution for accurate and reproducible measurements on transmission of the samples: we concentrated onto the characterization of the transmission in the range of interest of solar cells application (from 300nm to 900nm).

The first samples showed a strong attenuation of transmitted light in front direction in the case of spherical lenses with $80\mu\text{m}$ period (fig.5.25), with good reflection coefficient in the spectral range of interest, whereas, in cylindrical geometry ($400\mu\text{m}$ period), we obtained good front transmission and low reflection in the backward direction by the mirror (fig.5.26).

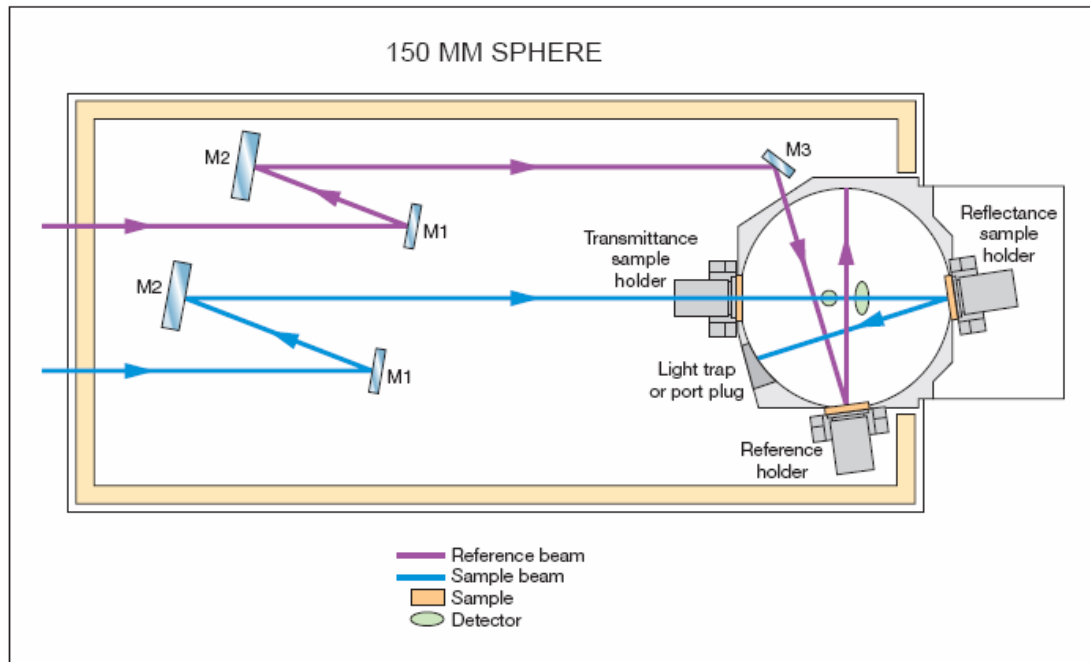


Figure 5.24: The integrating sphere setup. Blue beam is the sample beam and violet beam is reference beam.

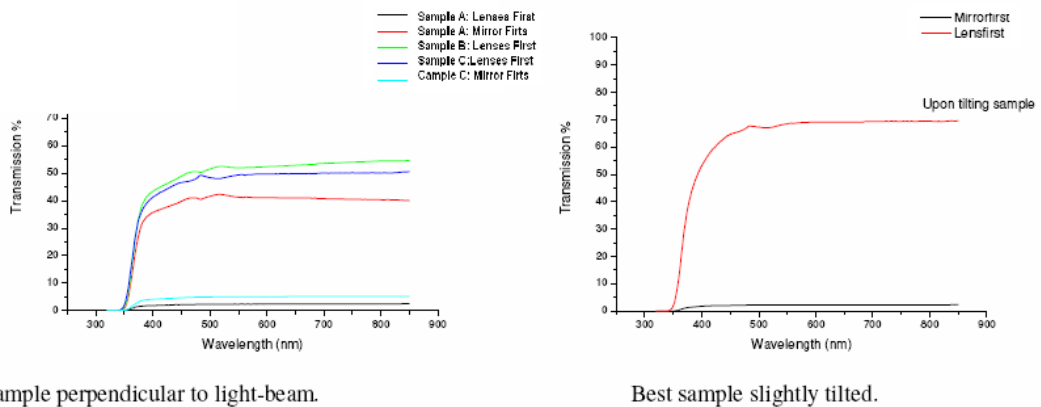


Figure 5.25: Transmission of spherical lenses: it is clear that when illuminated through the lenses a smaller portion is transmitted compared to the cylinder case. A significantly lower backside transmission (illuminated through mirror side) is also confirmed. This is in agreement with the smaller area the holes occupy compared to the stripes. The transmission lies around 50% when illuminated through lenses and around 2 – 5% when illuminated through the holes. When the best sample is tilted slightly to optimize the transmission it is possible to reach a value as high as 69%. The influence of tilting the samples effectively demonstrates how sensitive this configuration is to non perpendicular light.

Cylindrical lenses with $200\mu\text{m}$ of period showed much lower transmission in forward direction: for this reason we have concentrated our attention on improving the devices with large period cylindrical lenses. The forward transmission is rather sensitive to the angle of incident light; a slight misalignment will simply prevent or lower the transmission of light. This might explain the finding that with cylindrical lenses the transmission is much larger than the analogous

system made with spherical lenses. This setback is pronounced for the cells exploiting the 2D hexagonal array of semi spherical lenses, where perpendicular alignment in two directions is very crucial. However, for the 1D semi cylindrical array, it is sufficient to have alignment only in the plane parallel to the axis of the lenses.

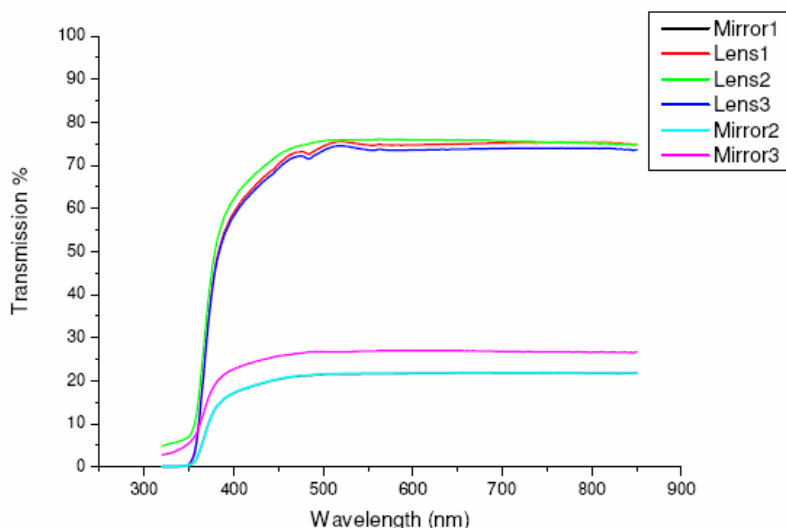


Figure 5.26: Cylindrical lenses transmission with period $400\mu\text{m}$ of period: it displays rather high transmission (75%) over a large spectral range when the lenses are illuminated. When the mirror side is instead illuminated we record a transmission of 20 – 25%. A minor angle dependence of transmission can be observed. As can be seen the transmission is limited below wavelengths of 450nm to reach a zero value at 350nm . This significant limitation for photovoltaic applications is solely attributed to the absorption of the negative photoresist employed in the lenses.

In the case of spherical lenses, the focused light is concentrate on a small spot: the ratio between the reflecting surface and the total area (x_s) is

$$x_s = \frac{2\pi r^2}{\sqrt{3}p^2}$$

Where p is the period of elementary hexagonal cell and r is the radium of holes. When the radium vanish ($r \rightarrow 0$), the ratio $x_s \rightarrow 0$: back reflection is maximum for $x_s \rightarrow 0$ (i.e. the mirror has no holes), whereas the foward transmission is maximum when $r \rightarrow p/2$ and consequently

$$x_s \text{ for } r \rightarrow 0 = \pi/2/\sqrt{3}$$

(i.e.the holes are in contact). We judge better to have a bigger transmission in front direction, to haven't loss in incident radiation. It's important to remember that, since the incident light is focalized, very large holes don't lead significant enhancement in the transmitted light which is concentrated in the middle of the hole, whereas reducing their size, the back reflection is significantly enanced. In the case of cylindrical lenses, the focus is line parallel to the axis of lens; as consequence, the area covered by metal is wider that in the spherical lenses. The fraction of reflective surface is

$$x_c = l/p$$

Where l is the width of the fenditue and p the period. When $l \rightarrow p$ we achieve the maximum transmitted light and the lowest back reflection. Therefore, it is very important to optimize the size of structures to maximize the performances of devices for the highest back-reflection with a high forward transmission. The fine control of lateral dimension of slits and holes has been obtained by the rotating stage previously described. In particular, increasing the tilt angle of the stage with respect to the axis of collimated light, and rotating the sample during the exposure, we obtain the enlargement of exposed area, and, consequently, the increase of lateral size of structures.

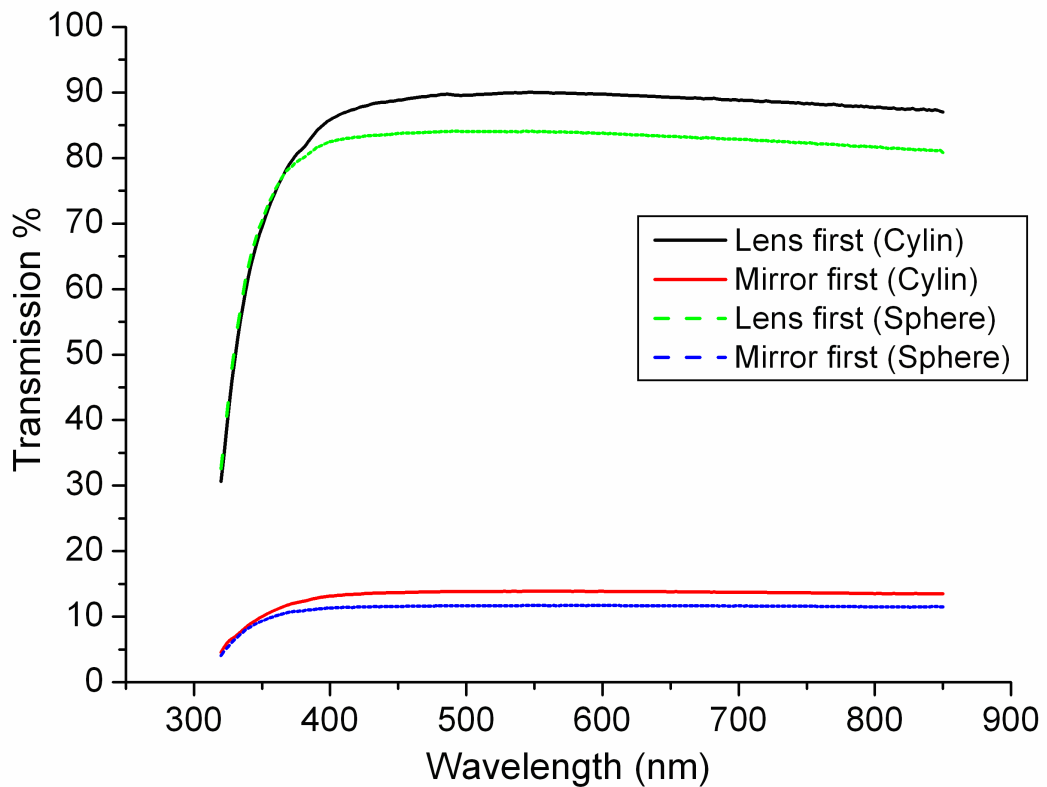


Figure 5.27: Graphic shows the obtained transmission as a function of wavelength for $400\mu m$ cylindrical and $80\mu m$ spherical lenses. In the case of cylindrical lenses, as high as 90% transmission was measured in the forward direction whereas a transmission of $< 15\%$ is measured when the sample is illuminated from the side of the mirror first. The dip in transmission at shorter wavelength is attributed to absorption in the lens material and in the metal, which primarily consists of silver.

In figures 5.27 are shown the measurement of samples of light trapping device with best performances obtained till now: a strong asymmetry between the forward and backward transmission was measured, with transmission close to 90% in a wide spectral range ($\approx 380 - 800 nm$) in the forward direction (first through lenses and then mirror) and $< 15\%$ measured with the sample illuminated from the side of the mirror. We observe that high forward transmission, obtained without the use of antireflection coatings or moth-eye structures, could be

achieved only with the full surface coverage with micro lenses, made possible by the present fabrication process. The dip in transmission at shorter wavelength is attributed to absorption in the lens material (the NOA 73 is not perfectly transparent at short wavelengths). These last results are rather satisfactory due to the strong asymmetry between the transmission coefficients for light impinging on the optical trapping device from the front and the back side. This fact prompted us to try to couple these object with some thin film organic cells where absorption is incomplete and an important fraction of impinging light is reflected. Although, this concept of light trapping system was conceived especially for organic photovoltaics, it can, in principle, be applied any solar cell where some part of the light is reflected instead of being absorbed for improving its performances.

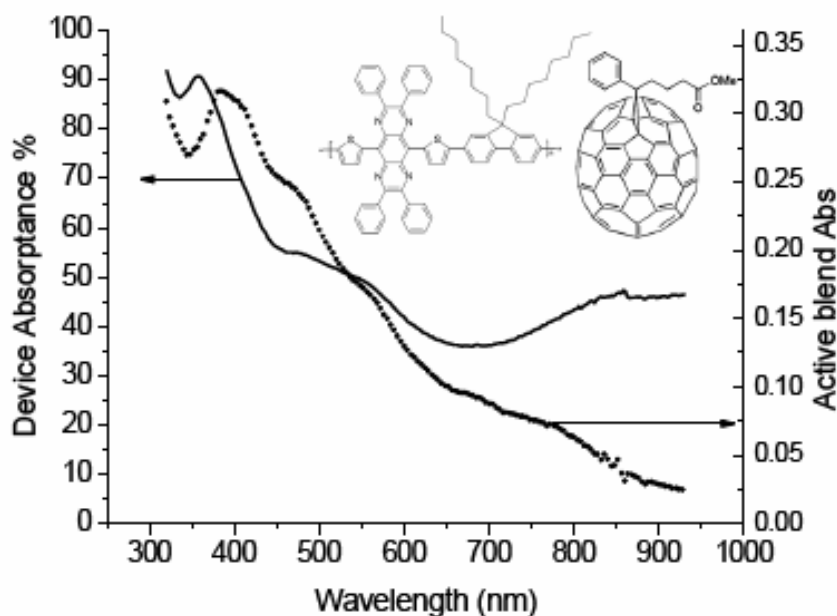


Figure 5.28: Device absorbance as measured from reflectance and blend material absorption as measured from transmission. Inset: chemical structures of the utilized donor (APFO Green 9) and acceptor (PCBM[70]) materials in the blend.

The organic solar cells used specifically in our experiments, were produced in the frame of collaboration with the group of prof. Olle Inganäs of the University of Linköping. They consist of Bulk-Heterojunction cells made with a 1:3 ratio blend of the low band gap alternating polyfluorene APFO Green-9 and the soluble fullerene derivative PCBM[70] whose molecular structures are inset in figure 5.28. Apfo green 9 is a low band gap alternating polyfluorene copolymer; these polymers incorporated fluorine units alternating with groups including electron-withdrawing (A) and electron-donating (D) groups in donor-acceptor-donor (DAD) sequence in order to lower the HOMO-LUMO gaps. For a detailed description of the chemical and electronic properties of this molecule and its application, we refer to [62], [63], [64] and [65]. The active layer in the fabricated device is spin coated from a 7 mg/ml chloroform solution at different speed to deposit different film thickness. The layer thickness is comprised between 30 and 100 nm: the thinnest ones have clearly a limited absorption of light. The thickness of the deposited organic films was determined with a surface profilometer (Sloan Dektak).

The Reflection (R) from a working solar cell with an area of 1.3cm^2 and 30 nm thick active layer was measured and the corresponding device absorptance (1-R) together with the active layer absorption is presented in figure 5.28.

The photoresponsivity (PR) and the External Quantum Efficiency (EQE) from the solar cells have been measured with and without the light trap laminated to the device. When laminating the lenses on top of a photovoltaic cell PDMS was used as an optical spacer. The intention of exploiting PDMS was that it would be possible to delaminate the lenses and put them onto a new cell. The photocurrent action spectra under short circuit conditions were recorded with a Keithley 485 picoammeter as the devices were illuminated with monochromatic light from a halogen lamp. Unfortunately, we mistook the first solar cells, or we explain better, we prepare solar cells with thick active film to test the devices with cylindrical lenses. Thick film, as previously explained, don't suffer from bad absorption and all the impinging light is absorbed in one passing. As shown in fig. 5.29 a pronounced difference in current response is obtained between a thick and a thin active film. The thicker film generates more current in the red part of the spectra compared to the thinner film. Probably this is due to thickness related interference effects or substrate absorption effects.

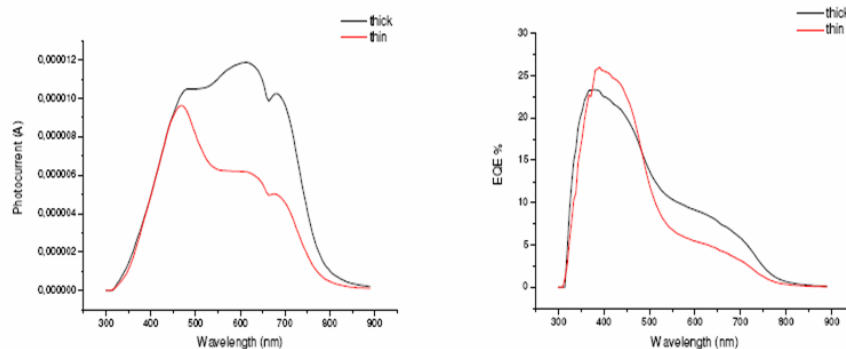


Figure 5.29: Photocurrent (left) and EQE (right) of thick and thin samples without laminated lenses. A pronounced difference in the current response was obtained between the thicker film that generates more current than the thinner film. Also for the EQE the thicker cell performed better than thinner one except in the spectral range 350-470 nm with LTS.

Therefore, no improvements for thick cells is verified since the presence of trap element doesn't raise the absorbed light; it is just the opposite, given that the intensity of impinging light that passing through the LTS is decreased by a factor dependent on the quality of the LTS as show in 5.26. The measured PR and the EQE are shown in fig. 5.30: both PR and EQE are lower then for simple solar cell.

On the contrary, cells with thinner active layer showed some enhancement in the photocurrent and EQE when coupled to LTS. Spherical lenses have been tested coupled to thin film solar cells, showing (see fig.5.31) to improve their performances in a small spectral range.

These initial measurements of improved devices confirm the validity of the method. The enhancement of forward transmission and the back reflection raised further the improvement of the Photocurrent density (fig. 5.32), PR (fig. 5.33) and EQE (fig. 5.34) of tested solar cells: light trapping was shown to work with good results for very thin films and for the trap element

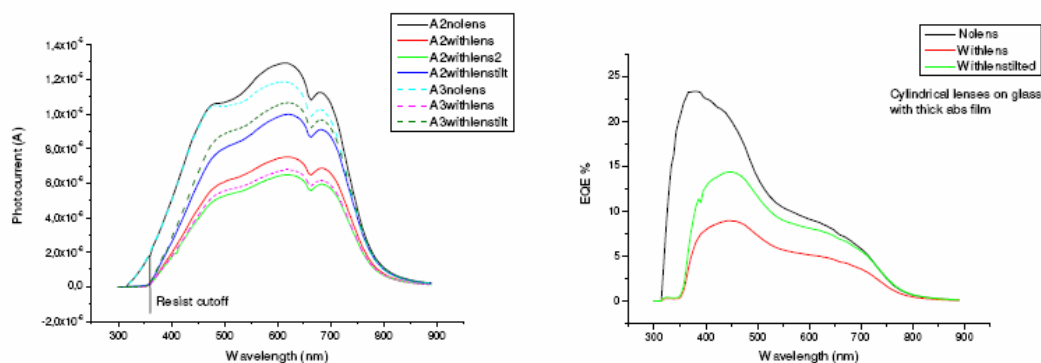


Figure 5.30: Left) Photocurrent from two samples with laminated cylindrical lenses. The photocurrent depends rather strongly from the angle of incidence of the light on LTS. The effect of tilting is strong: the tilt angle was not evaluated. We tilted the sample until obtain the maximum of light transmission in forward direction. Right) EQE for device 3. The cells primarily lose efficiency upon lamination of lenses. Nowhere in the spectrum can an enhancement be seen.

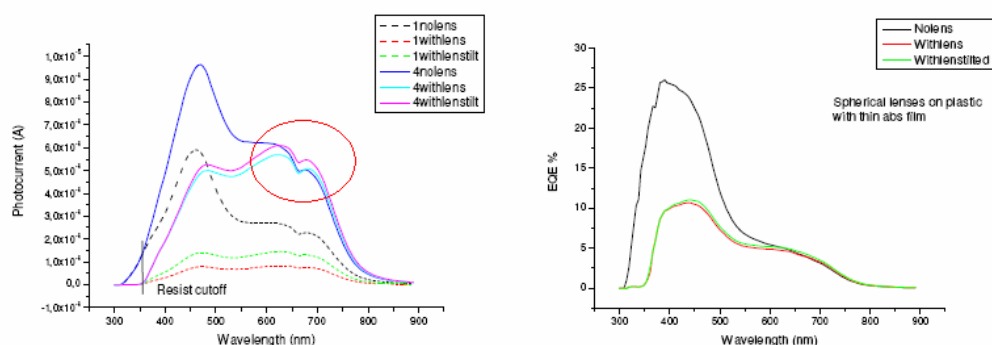


Figure 5.31: Left) Photocurrent from two samples with laminated spherical lenses. A very small improvement can be identified for wavelengths above 620 nm in sample 4 (the area in the red circle). Right) EQE for device 4. The cells primarily lose efficiency upon lamination of lenses and the small photocurrent improvement can hardly be identified in the EQE curve.

with the largest cylindrical microlenses ($400 \mu\text{m}$ period). However, the same observations as previously persisted; the enhancement due to LTS cannot be obtained in the blue part of the spectrum but only for the red. This was attributed to higher absorption in the blue than in the red by the material of which the lenses consist, but also to the fact that in the blue the absorption of the cell is already large even with very thin layers, so that few photons remain to be absorbed in subsequent reflections. Our materials always have a higher extinction coefficient in the blue part compared to the red and accordingly it is harder to improve absorption there. By making the active films very thin, the intersection of enhancement shifts to the blue and a larger part of the spectrum is enhanced by light trapping, but at the expense of a generally lower performing device. Nevertheless light trapping with this method is demonstrated to work. In figure 5.35 we show the enhancement in short circuit current of the same cell/LTS couple: a few percents ($\approx 5\%$) enhancement of efficiency is demonstrated. The photocurrent action spectra under

short circuit conditions were recorded with a Keithley 485 picoammeter as the devices were illuminated with monochromatic light from a halogen lamp.

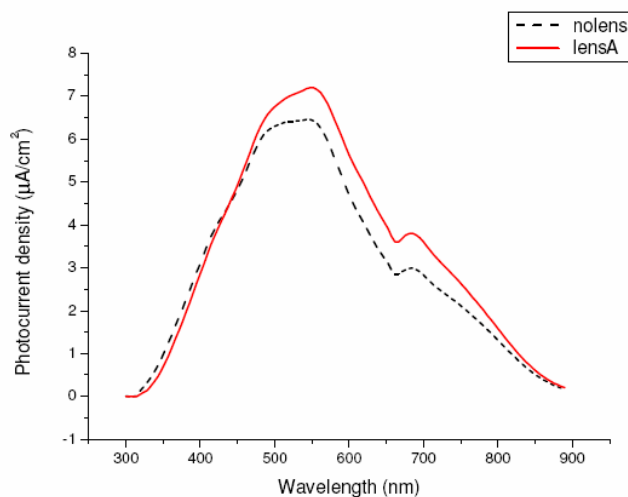


Figure 5.32: Sample with 35 nm active layer and $400\mu\text{m}$ period lenses placed in front. The measured photocurrent is improved from 450 nm and above.

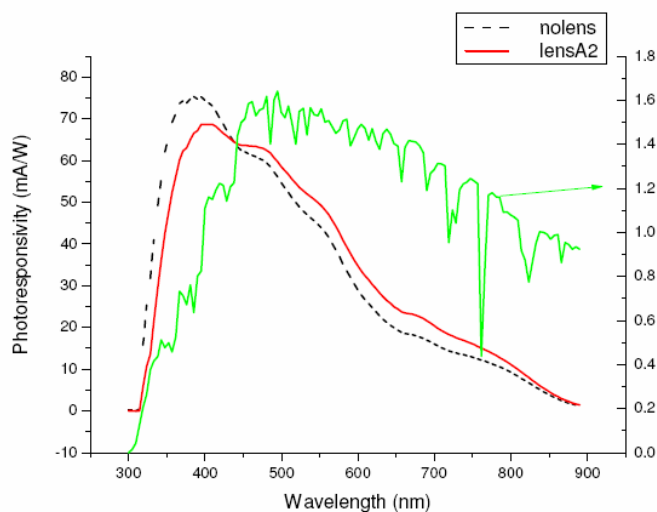


Figure 5.33: Photoresponsivity of same thin sample. Here we pay attention to the intensity of the lamp. Green inset displays solar illumination spectra.

Last tests, made on thin solar cells coupled with samples with best transmission reflection ratio (i.e. fig. 5.36) confirm the enhancement of efficiencies. As can be seen from the PR curve (fig.5.27), the light trap works very effectively over a broad spectral range. For this material and thickness, light trapping is beneficial for all wavelengths longer than 450 nm. This is adequate since the amount of high energy photons from the sun is rather limited. The current/voltage curve under AM 1.5 simulated solar illumination (the photon flux of the AM 1.5 solar illumination spectra is inserted as a comparison.) also demonstrates an increase in short circuit current, as high as 25%, upon the inclusion of the light trap (fig.5.37).

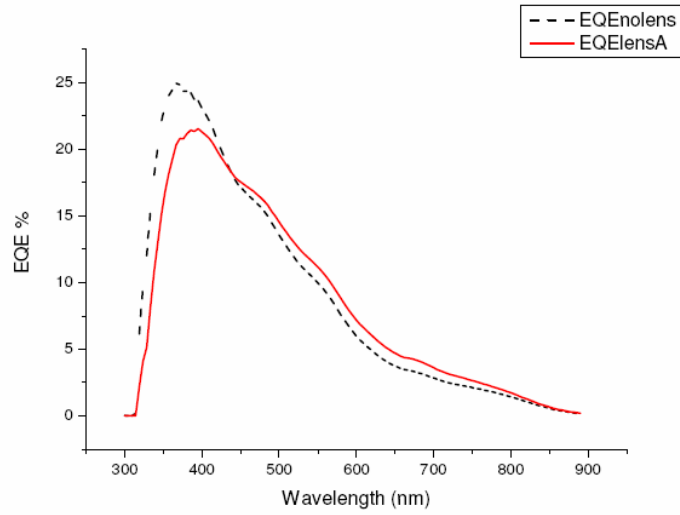


Figure 5.34: External quantum efficiency of same thin sample. Electrons out per photons in.

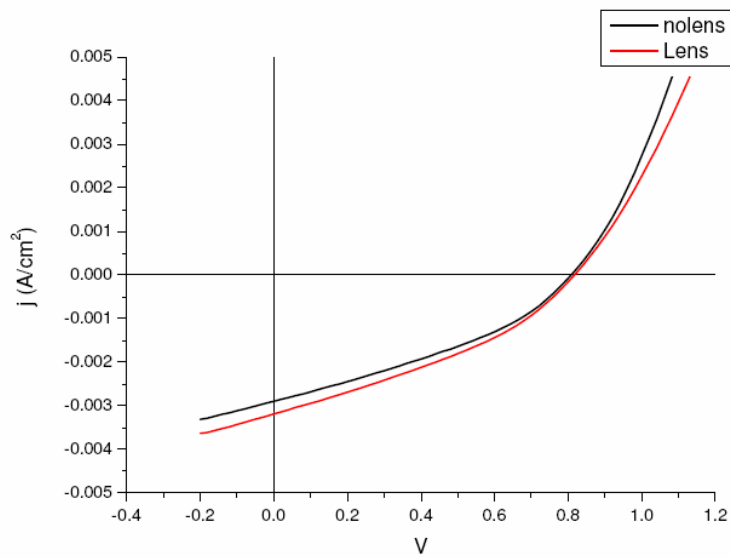


Figure 5.35: An increase in short circuit current of 5% can be confirmed upon the addition of the light trap.

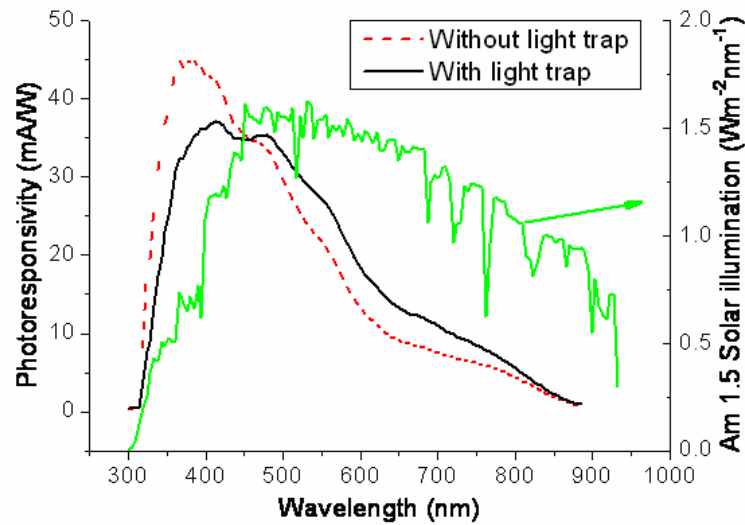


Figure 5.36: Photoresponsivity and solar irradiance graph.

5.3 Modeling of LTS behaviour

For devices with significantly higher absorption, less or no improvement from the light trap can be observed. If solar cell device reflectance (R_S), forward transmission (T_T) and backward reflection (R_T) of LTS is measured, it is possible to make a series expansion of the multiple absorption events in the cell, and compare it to the absorption of a device without a light trapping element and determine when trapping will be beneficial. Figure 5.38a, on the describes how the intensity is decreasing at the different interfaces after transmission and reflection at the

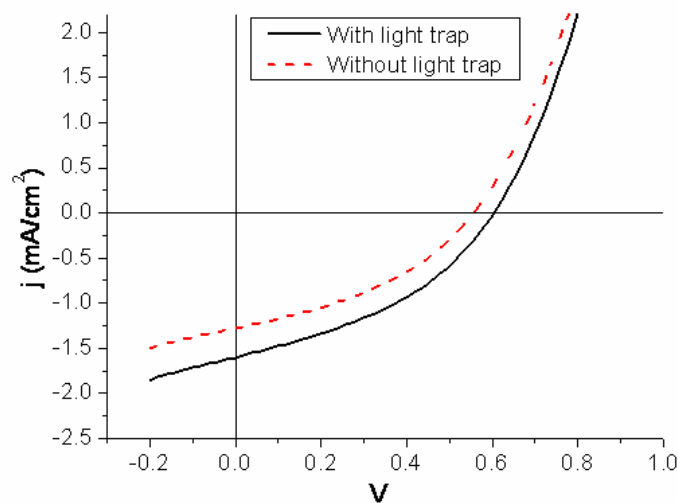


Figure 5.37: JV characteristics from simulated AM 1.5 solar illuminated APFO Green 9/PCBM[70] solar cell with and without the light trapping element. An increase in short circuit current of 25% can be confirmed upon the addition of the light trap.

involved interfaces.

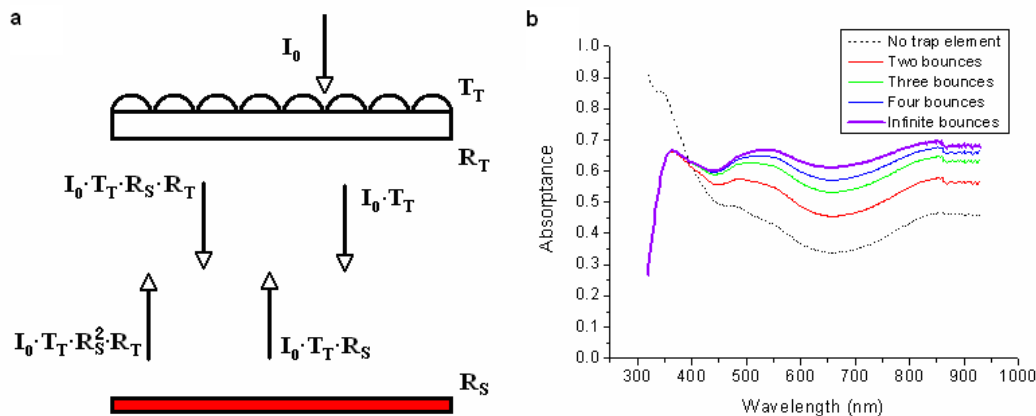


Figure 5.38: a. Schematic of the multiple bounces and the according Fresnel intensity coefficients. b. Calculated total cell absorptance for the APFO Green 9/PCBM[70] system with and without the trap system. For different number of absorption events included, a noticeable improvement above 400 nm can be found.

Light trapping will therefore be beneficial if the following holds:

$$(1 - R_s) \leq T_T(1 - R_s) + T_T R_S R_T(1 - R_s) + T_T R_S^2 R_T^2(1 - R_s) + \dots$$

$$(\text{Absnotrap}) \leq (\text{FirstorderAbs} + \text{secondorderAbs} + \text{thirdorderAbs} \dots)$$

For infinite bounces, the series in the right hand side of the equation will converge to:

$$T_T(1 - R_s) \frac{1}{(1 - R_S R_T)} \quad (5.1)$$

Hence only if

$$R_S(\lambda) > \frac{1 - T_T(\lambda)}{R_T(\lambda)} \quad (5.2)$$

will light trapping be favorable. From equation 5.2 it is clear that for thicker samples with high absorption (i.e. low reflection R_S), the forward transmission and back reflection needs to be very high. In order for the light trapping device to be beneficial for the EQE of the cell. For the 30 nm thin APFO Green 9/PCBM[70] device used, with a rather limited absorption, this is fulfilled for all wavelengths above 400 nm. The absorptance from a cell with no lenses compared to a cell exploiting the light trap is displayed in Figure 5.38b. In the graph different number of reflections is also considered via eqn. 5.2. A strong enhancement of the solar photocurrent is possible when the reflectance from the thin film solar cell is sufficiently high, compared to the trapping efficiency of the light trap. For thin film solar cells where the conflict between optical absorptance versus electrical transport and collection is the rule, this light trap can therefore be an advantage. The possibility to produce light traps over large areas using simple imprint methods further enables the use of these elements also for low cost organic photovoltaics. In principle, for any solar cell where some part of the light is reflected instead of being absorbed, the described light trapping element may improve the photovoltaic performance.

5.4 Conclusions

A novel light trapping system for organic solar cells has been presented and realized. An innovative fabrication process, exploiting a self aligned UV exposure through microlenses, has been developed in order to optimize the device performance. The preliminary measurements confirm that the simple fabrication scheme is potentially up scalable to large systems, at low production cost is suitable for application in photovoltaics; moreover, we have demonstrate the concept was successfully implemented in our device exhibiting performances: we have verified forward transmittance about 90% and backward reflection 75% in our best samples. Different geometries have been adopted and tested to determine the best configuration. The photoresponsivity (PR) for thin solar cells, measured with and without the light trap laminated to the devices, has been characterised. The light trap works effectively over a broad spectral range. For the employed material and thickness, light trapping is beneficial for all wavelengths longer than 450 nm. The current/voltage curve under AM 1.5 simulated solar illumination also demonstrate an increase in short circuit current, as high as 25%, upon the inclusion of the light trap.

Next improvements are concentrated on the choice of better materials for microlenses and substrates. Moreover it will be very interesting to extend the application field of the LTS: the possibility to produce light traps over large areas using simple imprint methods further enables the use of these elements also for any solar cell where some part of the light is reflected instead of being absorbed, the described light trapping element may improve the photovoltaic performance. The micro-lens system has generate a patent. The detailed description and discussion of LTS has been published (22 December 2008 / Vol. 16, No. 26 / OPTICS EXPRESS 21608). The fabrication process, for its innovation, has been accepted as invited at MNE conference 2008 in Athens. The relative manuscript in the Special Issue of Microelectronic Engineering devoted to the MNE08 conference has been accepted.

Chapter 6

Nanostructured solar cells

The second aspect of my PhD project is related to the fabrication of organic solar. In particular the main idea that we conceived and tried to carry out is to improve the efficiency of polymeric solar cells applying our knowledge on nanofabrication based on top down methods. In the follow, first of all, we will explain some concepts, already discussed in the third chapter, but that are really important to understand the motivation of our work.

6.1 Some concepts in organic solar cells

In 1995, Yu and al. have demonstrated a substantial improvement in polymeric solar cells by introducing the Bulk-Heterojunctions [66]: more than 5% of efficiency has been measured in the past [67]. This concept has also been demonstrated in small-molecular organic PVs [68]. BHJ cells are based on the concept of mesoscopic mixing of two materials (acceptor and donor) to generate random nanophase domains. A uniform and extended donor-acceptor distribution at the molecular level allows for maximum charge generation; however, collection of the charges must be ensured as well. These simultaneous requirements contradict with a too fine-scale mixing since each material must provide continuous pathways along which the charges can be readily transported to the electrodes. Bottlenecks and isolated domains can act as charge traps and charge recombination centres; thus, reduced carrier mobility [69] and increased cell series resistance [1] are potential issues in blend heterojunctions photovoltaic devices. Like other semiconducting polymers, Polythiophene has a rigid backbone of conducting conjugated rings, with floppy non-conducting alkyl-side groups to provide solubility. The polymer conduction is highly anisotropic, with one dimensional movement of charge carriers along the chain. As the conductivity of a macroscopic film is only as good as the weakest link in the conduction path, the fundamental problem in achieving high mobility is the efficient transfer of charge from one polymer chain end to another. Even a gap that is a fraction of a nanometre effectively prevents charge transfer. An amorphous polymer conducts poorly because the chains are randomly positioned. Due to the trade-off between efficient dissociation of excitons on one hand and loss-free charge transport on the other, a uniform phase-separation throughout the film may even not be the best-performing configuration. The first step is the molecular design of the polymer. It is energetically favourable for polymer chains to stack in well-organized

two dimensional crystallites, in which the conjugated rings face each other to form a compact lamellar structure, as illustrated in Fig. 6.1.

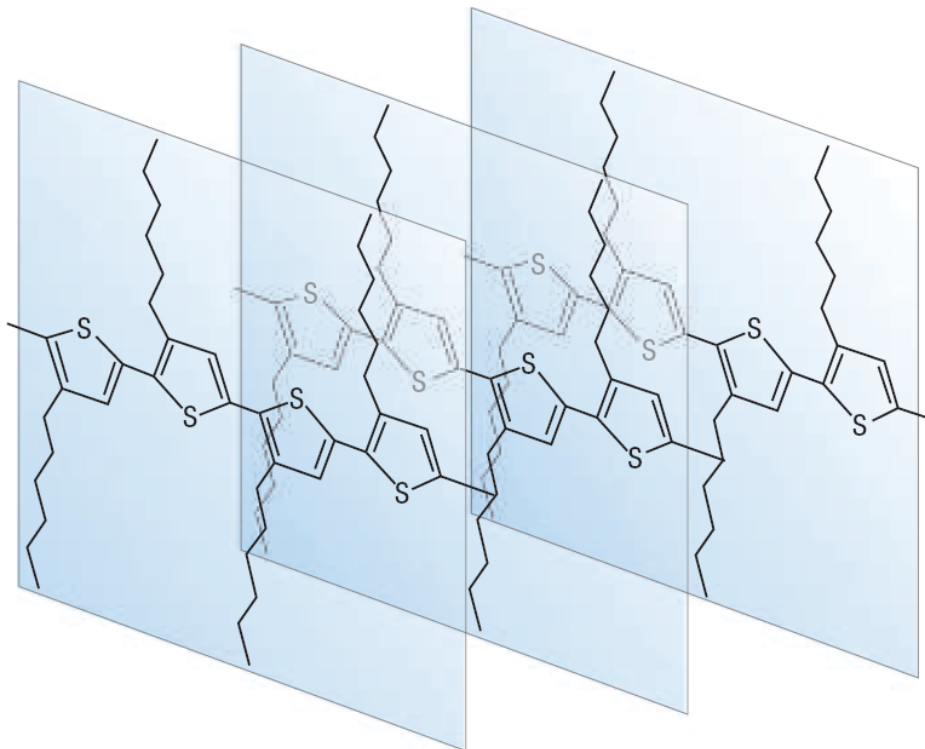


Figure 6.1: Lamellar structure of regio-regular P3HT.

In this way, a two-dimensional conducting region can be created, which improves the probability of charge transfer to the next lamella. To form the ordered lamellae, the polymer chains must be regio-regular, with side chains always attached at the same position on the ring, otherwise the disordering effects prevent the lamellae from forming. Having ordered crystallites is still not enough to give high mobility, as randomly orientated lamellae still have inefficient charge transfer. Conduction in a solar cell is perpendicular to the surface. The organized Polythiophene lamellar structure, that is so favourable for the in-plane conduction, might be expected to be less advantageous for vertical conduction. So it is, Kim et al. [70] find that the mobility is lower by 2-3 orders of magnitude. However, they also show that the structural order associated with regioregularity does improve the efficiency of the solar cells. Evidently the structural order has electronic benefits beyond high in-plane mobility. Indeed, as shown recently [71], the P3HT/PCBM network consists of a hierarchical architecture at different length scales. Low order P3HT and PCBM nanocrystals form the charge-generating heterojunction, while short P3HT crystals connect these amorphous regions with long fibrillar crystals suggested to be responsible for charge transport. This structural order probably explains the outstanding performance of this material combination. In this context, P3HT occupies a central position among semiconductor polymers, exhibiting high carrier mobility when regioregularity promotes organisation of polymer backbone forming sheet-like lamellae. From these considerations, we lead that the best configuration that we can pursue, and that is one of the aims of the research in the organic cells field, is having orderly nanostructures like in figure 6.2.

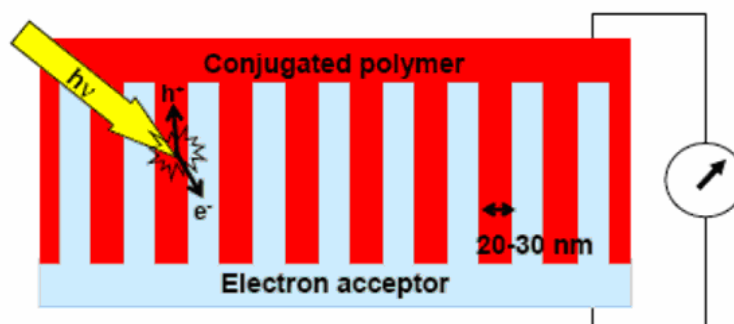


Figure 6.2: Ideal nanostructure for organic solar cell.

The best configuration possible is indeed an interdigitated array of nanostructures with lateral dimension comparable to the diffusion length of exciton. The fabrication of this kind of structure is clearly hard. Some different techniques have been tested: best results have been obtained by growth from vapour-phase deposition [72]. The authors presented this new method to control the positions and orientations of donor and acceptor materials; these are determined during growth by organic vapour-phase deposition (OVPD), eliminating contorted and resistive conducting pathways while maximizing the interface area. The result is a substantial increase in power conversion efficiency compared with the values obtained by 'random' small-molecular-weight BHJ solar cells formed by high-temperature annealing.

6.2 Main idea: nanostructured solar cells

A top down technique, like lithography, has not yet tested to produce a similar structure in organic solar cells. The new approach that we have conceived is to exploit the typical properties of polymers used in organic solar cells to replicate a nanostructured master in the conjugated polymer applying the simplicity and high resolution Nano Imprinting Lithography (NIL) to replicate nanometer scale patterns. The process of fabrication of nanostructured solar cell is schematically represented in fig. 6.3.

It starts with the deposition of PEDOT:PSS on top of ITO transparent electrode: the use of PEDOT:PSS has been illustrated in 3.7. P3HT dissolved in chloroform or dichlorobenzene is then spun to obtain a thin film of Polythiophene (about 100 nm). A brief annealing (between 110 to 140°C) is needed to permit the complete evaporation of solvent. A master with suitable nanostructures can be imprinted in the P3HT film, heating the sample at $t > t_g$ of polymer. After the master release, the sample is transferred in the evaporation chamber where a film of C60 is sublimated on top to completely fill the nanostructures. The evaporation of suitable metallic electrode (Al for example) completes the fabrication process.

Our work started trying to solve the first evident problem: the fabrication of nanostructured master.

In the survey of lithographic methods, there is a few lithographic techniques that permit to obtain the nanoscale resolution consistent with the diffusion length of exciton : we remember

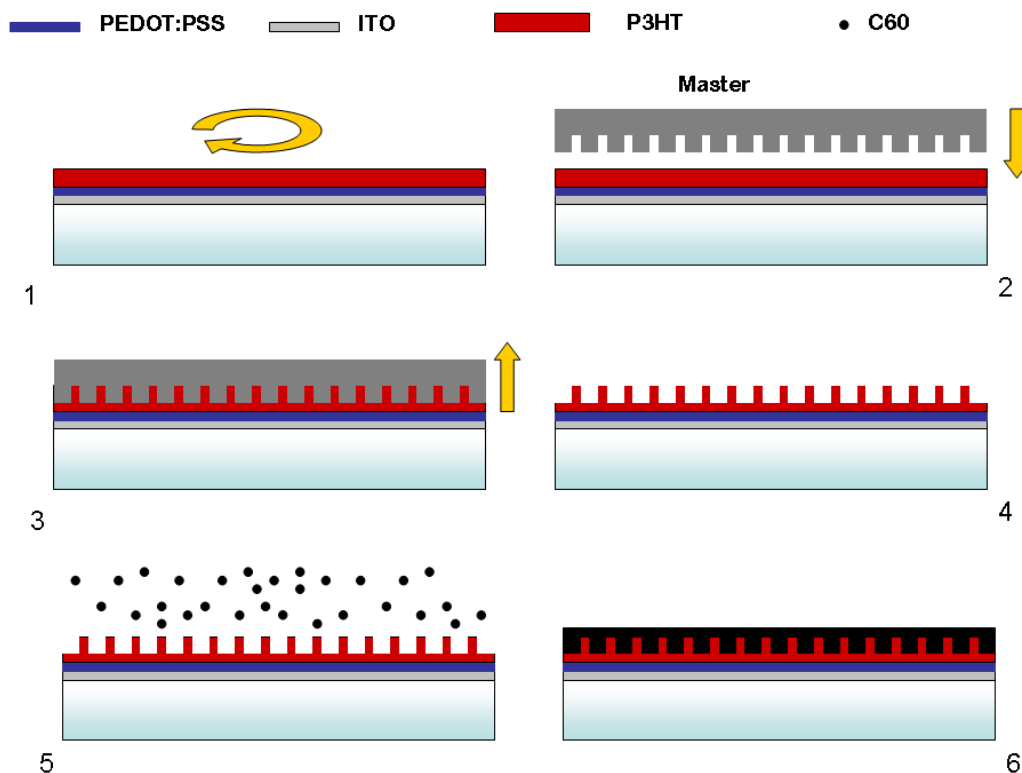


Figure 6.3: Fabrication scheme of nanostructured solar cells: (1) Deposition by spin coating of PEDOT:PSS and P3HT on ITO coating. (2) Imprint of the nanostructured master in the P3HT film by nanoimprinting process at temperature $t > t_g$, with t_g the glass transition temperature of polymer. (3) Master release at $t < t_g$. (4) Transfer of sample in evaporation chamber. (5) Deposition by sublimation of C60 to fill the nanostructures. (6) The final structure of cell.

for example Electron Beam Lithography (EBL), Focus Ion beam Lithography or other alternative and innovative Scanning Probe Lithography, based on the use of a sharp tip in proximity to a sample to pattern nanometer-scale features. Electron beam lithography is one of the most powerful methods for nanostructure forming. It uses high voltage electrons ($1 \text{ kV} - 100 \text{ kV}$) to transfer nanopatterns into an e-beam resist (ex. PMMA) by directly writing. Very high resolution achieved several 10 nm can be obtained by this method; the high resolution makes this method a very important and useful tool in a lot of research applications. The big problem of EBL, particularly in the optic of application in our project, is the slowness and the expense: this is the reason why it is impossible to use EBL to create a pattern sufficiently wide for solar cells.

Focused ion beam (FIB) systems have been produced commercially primarily for large semiconductor manufactures. FIB systems operate in a similar fashion to a scanning electron microscope (SEM) except, rather than a beam of electrons and as the name implies, FIB systems use a finely focused beam of gallium ions that can be operated at low beam currents for imaging or high beam current for site specific sputtering or milling. At low beam currents, very little material is sputtering; modern FIB system can achieve 5 nm imaging resolution. Clearly, FIB has mutual problem to EBL, and its employment has been not possible.

SPL possess high potentially in nanotechnology: it has been demonstrate that using these methods, resolution of few nanometres is possible. They exploit the high resolution of different Scanning Probe Microscope Instruments (like Scanning Tunneling Microscope (STM) or Atomic Force Microscope (AFM)) to modify the sample surface by atomic manipulation, mechanical and termomechanical patterning, local oxidation or electron exposure of resists. Their ability to pattern nanometre-scale features gives these techniques a very attracting method for semi-conductor industry. The limit is throughput capabilities, for the very low coverage rates.

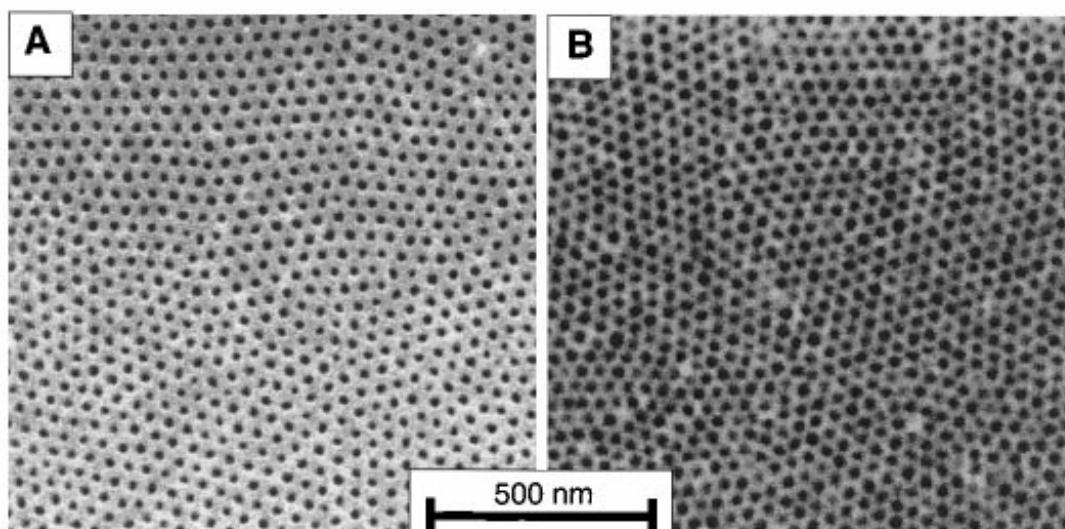


Figure 6.4: SEM micrograph of a partially etched, ozonated monolayer film of spherical microdomains. (B) An SEM micrograph of hexagonally ordered arrays of holes in silicon nitride on a thick silicon wafer. The pattern was transferred from a copolymer film such as that in (A). The darker regions are 20-nm-deep holes in silicon nitride, which has been etched out [2].

It has needed to think up an alternative way to produce a master sufficiently wide (more then 1cm^2) having homogeneously dispersed nanostructures in the range of $5 - 50\text{ nm}$ of lateral size and comparable period. The best method, actually developed, consistent with the size requirements of our application could be the Block Copolymer Lithography [73].

6.2.1 Block Copolymer Lithography

Block copolymers have become of great interest for high-resolution patterning because of their simplicity and high throughput. An alternative approach to achieve miniaturization goals is the so-called 'bottom-up' approach. This uses the uniform nano- and supermolecular structures that result from organized macromolecule packing, the so-called 'self-assembly' process. Block copolymers tend to self-assemble into a variety of well-ordered nanostructures with almost continuously tuneable resolution from several to hundreds of nanometres because of the chemical immiscibility of the covalently linked segmental chains. Through various templating processes with these block copolymer microdomains masks, high-resolution functional nanostructures can be generated 6.4.

The molecular packing, and thus thermodynamically stable microdomains patterns, of

block copolymers in the bulk state are governed by the positive mixing enthalpy and low mixing entropy of component segments. Because of the covalent bonding between the segments, the system can not macroscopically phase separate, and so it minimizes the interfacial energy by adopting well-defined microdomains patterns with constant interfacial curvature and stretched interfacial chain configurations. For the simplest and most extensively studied coil-coil diblock copolymers, the molecular weight, volume fraction of the component, and the degree of segment incompatibility as expressed by the Flory-Huggins parameter [74], that are the three independent parameters used to determine thermostable morphologies [75]. The convergence of top-down/direct-write approaches with bottom-up fabrication may be achieved through design of the block copolymer architecture. By incorporating multiple functionalities into the building blocks, the merits of various types of patterning can be achieved in the same block systems. Bal et al.[76] and Spatz et al. [77] have used direct write e-beam lithography to generate spatial control of poly(styrene-*b*-methyl methacrylate) (PS-*b*-PMMA) and PS-*b*-P2VP microdomains, respectively. Through the incorporation of high resolution poly(4-hydroxystyrene) (PHS) photoresist and poly(α -methylstyrene) (P α MS) in the same diblock architecture, researchers have successfully achieved microdomains spatial control through high-resolution top-down deep ultraviolet lithographic processes [78]. Large-area, uniform, nanometer-sized cylinders in submicron-sized patterns were generated through simple fabrication processes (fig. 6.5).

Unfortunately, the tuning of this method of nanofabrication required an excessive work to be completed at the same time of the project in photovoltaic cells of my PhD.

6.2.2 Self assembled tin nano-islands

A preliminary alternative route (however, the development of Block Copolymer Lithography in our laboratory is planned) has been worked out employing the properties of self assembly in random nano-islands of thin film of tin on silicon surface. A very thin films (less than 5 nm) of Sn has been sublimated on top of a silicon wafers: for the poor wetting of tin on silicon, in order to minimize the interfacial energy, the metal atoms grow generating high density nano-islands with diameters dependent on the thickness of evaporated Sn (fig. 6.6). When vaporized atoms land at the substrate and become adsorbed, they can still migrate on the surface: when a second atom lands in the neighbourhood it can form a doublet with the first atom, which is more stable than a single atom and has more chance to remain stuck. New atoms arrive at the substrate and nucleate to form little atomic islands that coalesce together to form nanoscale islands of increasing sizes. In this way, nanodots with diameter smaller than 50 nm can be obtained.

Moreover, to reduce the size of the tin "dots", we reduced the wettability of silicon surface removing the native oxide always present dipping few second the substrate on a solution of HF (10% *wt* in water). The surface topography was characterised by scanning electron microscopy (Zeiss Supra 40) at 5 KV, to quantify the average nano-feature size, area fraction and surface density from the two-dimensional SEM images. In the graphic 6.7e are summarized the area distributions of dots in function of the theoretical thickness, correspondent to a homogeneous and compact metal film, as measured by a quartz balance.

Representative SEM images of these islands characterising their random pattern, size and size distribution are reported in Fig. 6.7.

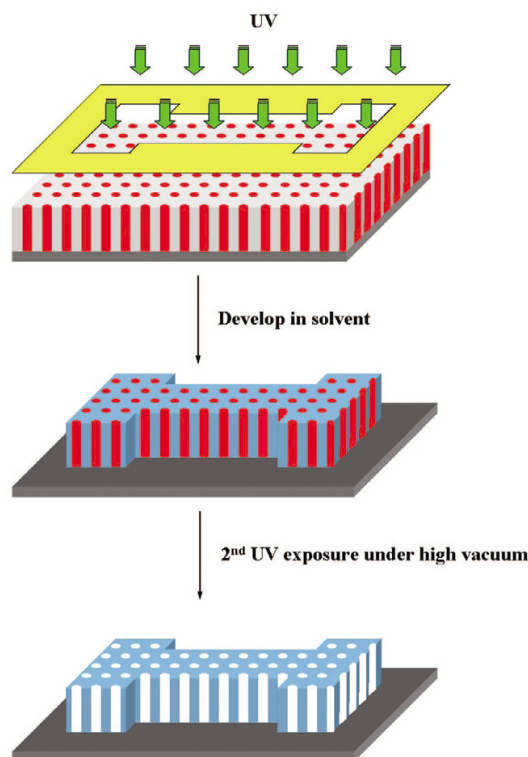


Figure 6.5: Novel patternable block copolymers to achieve spatially controlled nanostructures. (a) An asymmetric P MS-b-PHS copolymer/photoacid generator/crosslinker solution is spin-coated onto a Si substrate and forms vertical P MS cylinders as a result of rapid solvent evaporation. (b) 248 nm stepper exposure and subsequent development forms micropatterns. (c) Strong ultraviolet irradiation under high vacuum removes P MS, thus generating patterned nanochannels.

Nanodots with diameter in the ranging from 5 to 25 nm have been achieved. The inter-island separation distances grows with the increasing of diameter of tin islands: for smallest dots, it's down to 10nm. We transferred the pattern generated onto the underlying silicon using the nano-islands as masks for a dry etching plasma process conducted in Inductively Coupled Plasma (ICP)(fig. 6.6). the parameters of plasma conditions and time of etching have calibrated to obtain structures about 100 nm height: this is the thickness of active layer of solar cells to have the complete absorption of sunlight. In particular, we have employed a very direction process to obtain high aspect ratio structure limiting the under etching and, therefore, the feature size of dots. In figure 6.8 are shown some example of nanostructures achieved after the dry etching process increasing the time of plasma process.

With very small Sn islands, we observed very poor transferred structures: the cause is probably the bad strength of tin mask to the plasma process. From these tests, we have demonstrated that we can finely control the silicon tips shape and dimension, in order to produce the best structure for our aim. After the etching process, we have removed the residual tin present on the sample surface by dipping the samples in Piranha solution ($\text{H}_2\text{SO}_4\text{-H}_2\text{O}_2$ 7:3, at 90°C). This step is needed to permit the functionalisation of surface: the antiadhesion layer is needed to permit the demolding of master after the imprint in the nanoimprinting process. The deposition

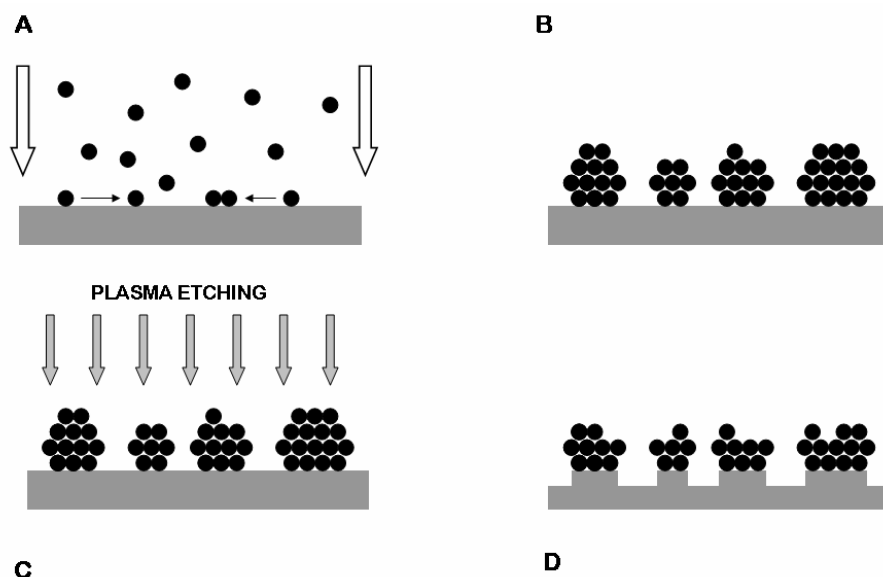


Figure 6.6: Schematic representation of the fabrication process with representation of the phenomenon of nano-droplet formation.

of silanes has been performed from a solution of Octadecyl-Trichloro Silanes (OTS) in Toluene or Eptane.

6.3 Organic solar cell: experimental section

The effective production of nanostructured solar cells was preceded by fabrication of standard bulk-heterojunction solar cells: our first aim was performing a suitable process to fabricate efficient solar cell, helping our self by following the receipts founded in literature, and improving a fine characterization set-up in order to have an effective evaluation of the quality of the produced cells. Moreover, the initial available equipments for the cells preparation were quite limited: we engaged in the improvement and develop of instrumentation set-up. Before my PhD project, in fact, there was no photovoltaic background in the laboratory, and we needed to reach gradually the necessary the know-how. It's not surprising that we met with difficulties to realize devices with acceptable performances and we are still solving some problems. The utility of performing a fabrication process allowing the production of efficient solar cells is also justified to the need of comparing the standard BHL and our nanostructured cells and effectively realize the possible improvement obtained.

The main problem dealing with conjugated polymers (i.e. P3HT), being their general limitation, has been the high sensitivity to the oxygen and humidity present in the air [79]-[80]. The light illumination of P3HT in air will result in the oxidation degradation of polymer and the formation of polar functional groups, thus potentially reducing the conjugation length, the absorption/emission intensities, the size of the crystal domain and the charge-carrier mobility. These effects can lead to the poor performance of P3HT-based optoelectronic devices. For this reason, all fabrication processes are generally done in glove box, under N_2 atmosphere to prevent degradation in organic materials.

Unfortunately, at the moment, it has been possible to perform just the annealing and the metal electrode deposition in a clean atmosphere; but now we are getting ready to complete all fabrication steps (specially, the spin-coating of materials) in glove box. A future step, that require big capital outlay, is to perform a system where complete the fabrication process, never bringing the cells into contact of the air. The fabrication of all the cells referred on this thesis has included a certain number of steps in air: the spin coating of all organic layers, the transfer on evaporator for the deposition of metal electrodes and the characterisation.

Surely, the kind and the quality of the employed materials are strictly linked to the performances of the solar cells: not suitable compounds are clearly limiting. The choice of best materials, as we learned from literature and, above all, from expertise acquired in laboratory, can really make the difference. In the follow we want show the evolution and carried improving of the produced cells: in particular we will previously give a general description of the fabrication process and then we will describe in detail the met problems and the relative solutions we found.

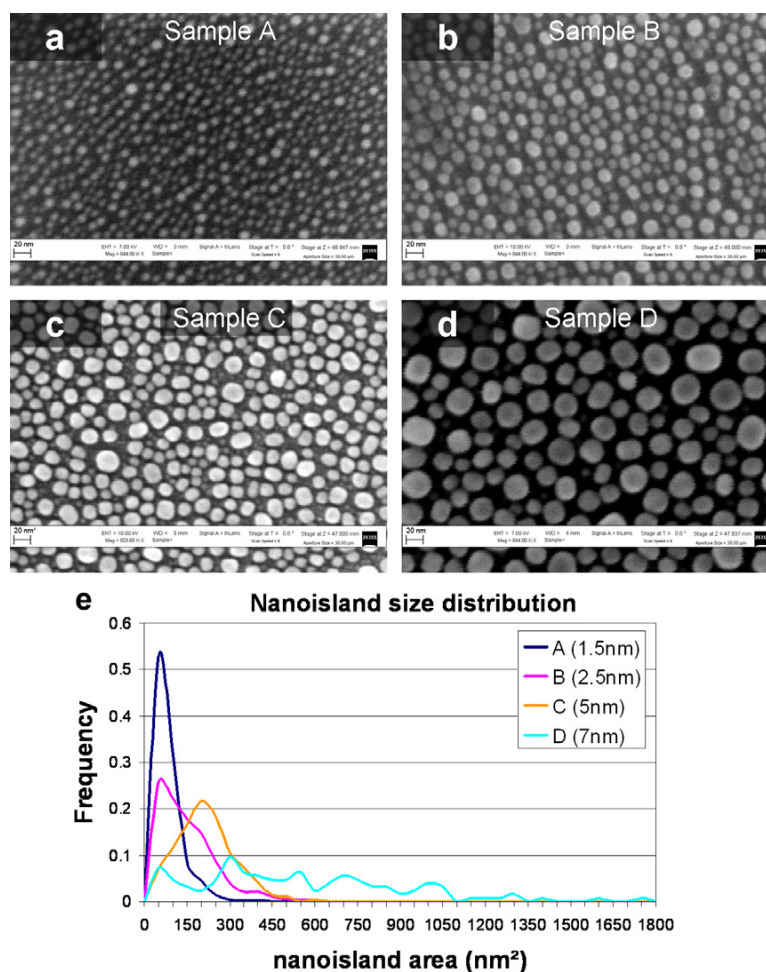


Figure 6.7: Representative SEM micrographs depicting biomimetic samples A, B, C and D realised by incremental tin deposition of thickness 1.5, 2.5, 5 and 7 nm, respectively.

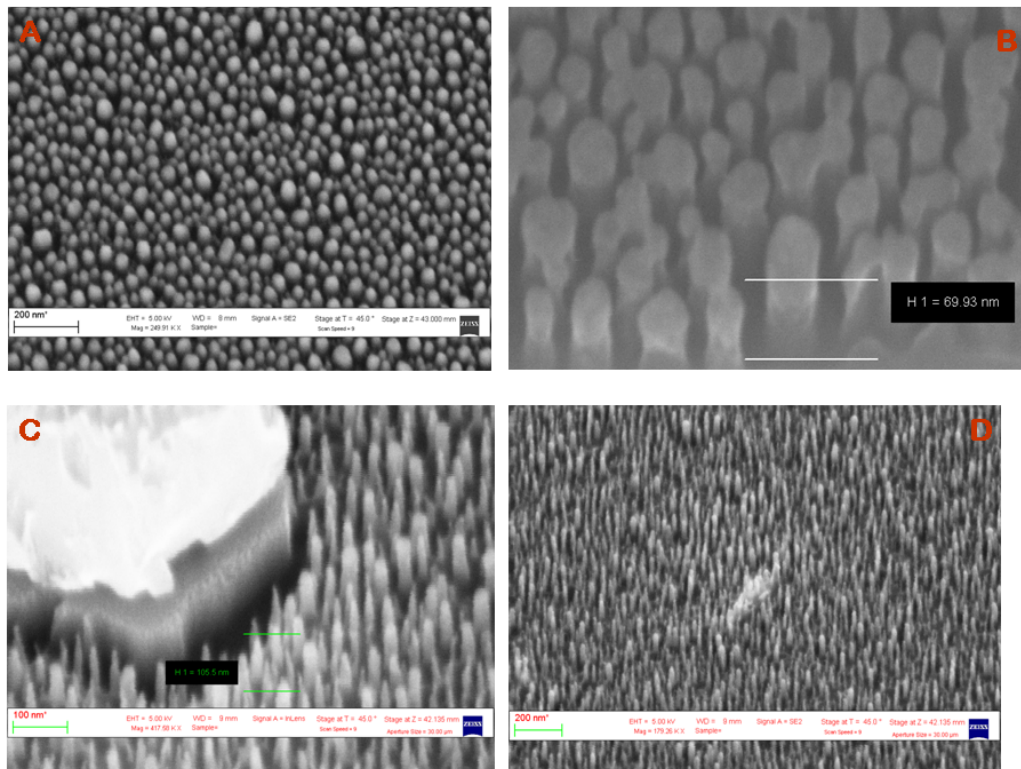


Figure 6.8: Silicon nanostructures fabricated by dry etching in ICP using the small tin island as mask. Increasing the etching time, we observe the decrease of the diameter of structure, the increase of their height and a change in the aspect: for prolonged etching, the structures look more sharpened, where, for brief processes, they remain a round tip, probably due to the presence of tin mask. A) Etching time: 3 sec. B) Etching time: 6 sec. C) Etching time: 9 sec. D) Etching time: 12 sec.

6.3.1 Cells fabrication

The fabrication process of solar cells is relatively simple and can be schematically illustrated as in Fig.6.9.

All the solar cells were fabricated on indium-tin-oxide (ITO) on glass substrates with an active area of $6,36 \text{ mm}^2$. The active area is determined by the size of the metal electrode: just the charges generated in the blend covered by the metal are collected for their short diffusion length in these materials. The first step is the patterning of ITO electrode to have a final configuration of solar cell as shown on the left of Fig.6.10. The requirement of patterning the ITO is needed to prevent the risk of shorts when the cell is contacted: in fact, for their softness, when we contact the Aluminum electrode, the organic material could be pierced by the sharpened points of the probes arriving to touch the ITO electrode. In this way, all probability of generate shorts are avoided.

The patterning has been achieved by simple proximity UV-lithography: we use the pattern generated by exposure of S1813 positive resist as mask for the wet etching of ITO. The employed solution consists on 1 % of HCl 37% in water: a dip of 30 minutes is needed to remove completely the conductive film in the exposed areas. The samples were then accurately washed

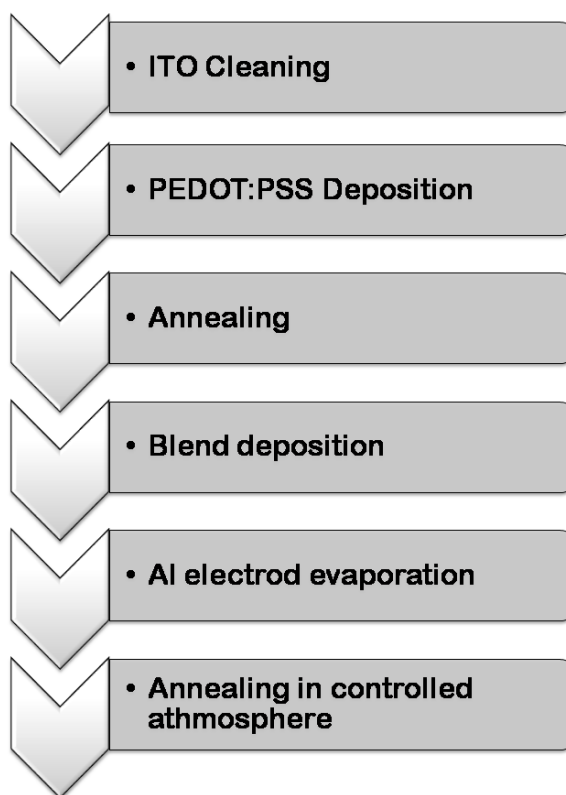


Figure 6.9: The scheme of the fabrication process of solar cells investigated in this thesis.

to remove the residual resist mask and any kind of dirt from surface. This step is really important to permits the deposition of a fine PEDOT:PSS film. The imperfect cleanness of the surface implies the dewetting of water based solution: in these conditions, when we want deposit a film by spin coating, the solution slip out of the sample surface and the produced film is disuniform or thinner than we expect. The cleaning has been done by sequentially washing the samples with deionized water, propan-2-ol, acetone in ultrasound bath; a final treatment with oxygen plasma is needed to obtain really cleaned .

A thin layer (from 30 to 100nm thick) of PEDOT/PSS was spun on top of the ITO surface. A baking at 120°C for 1 h is needed to remove the water present in the film, that could be very harmful for the organics that will be spun on top. We observed that a prolonged bake doesn't damage the PEDOT film, reducing instead the quantity of water present in the film and, therefore, improving the quality of the cell. P3HT/PCB blend (1:1 wt/wt ratio) were prepared: P3HT regiorandom was first dissolved in 1,2 - dichlorobenzene (DCB) to make 17 mg/ml solution, followed by blending with PCBM in 50 wt %. The blend was placed in ultrasound bath at 50°C for 2h and then stirred for more then 10 h at 40°C in the glove box. The active layer was obtained by spin-coating: numerous tests have been performed, modulating the film thickness. Best performances are achieved spinning at 600 r.p.m. for 150 s using the lowest acceleration. The thickness of film was between 150 and 230 nm, as measured with a profilometer: these values of thickness permits to absorbe the most of incident radiation

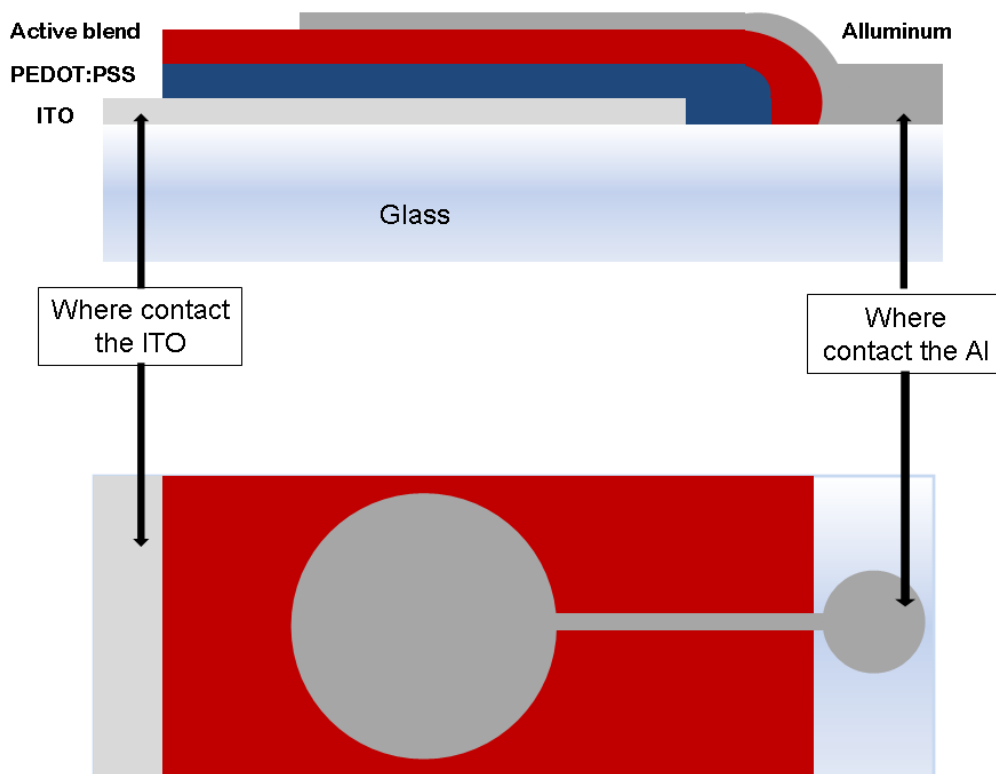


Figure 6.10: Schematic representation of polymeric solar cells.

maintaining fine conductivity of active film, manifesting in higher collected current. In some cases, before cathode deposition, the films were thermally annealed at $110 - 140^{\circ}\text{C}$ for 30 minutes on hot plate in glove box. The samples were then transferred in evaporator to deposit the Al electrode by thermal sublimation; the pressure in the chamber before the evaporation was measured $< 10^{-6}\text{ torr}$. The evaporated film thickness was evaluated with a quartz balance; the average thickness was 100 nm. An example of realized cell is shown in fig. 6.11.

The samples were then transferred in glove box for a last annealing at 140°C 1 h; this step has a central role to promote the crystallinity of P3HT. Moreover, the annealed films show a higher roughness compared to the untreated. Li and al. [81] found from the morphology study a relation between the devices performance and the surface roughness of the films: the higher roughness of the film will give higher efficiency device. The possible reason for this might be the increased contact area between the polymer film and the metal cathode for the films with higher surface roughness. The increased surface roughness might also enhance internal reflection and improve light collection, which would also increase device PCE.

6.3.2 Materials and processing

ITO

The morphologic and electric properties of the ITO coating are strictly linked to the performances of the solar cells. Numerous studies have been done about this transparent conductor



Figure 6.11: A P3HT:PCBM cell after the deposition of Al electrode and the annealing carried in glove box.

[82]-[83]-[84]-[85]. The sputtering process, that is the most used for the ITO deposition, can easily generate needle-shaped structures that are one of causes of shorts in devices; these structures can cross the thin organic film constituting the active layer until the opposite electrode. Moreover, the amorphous and/or polycrystalline phase is strongly correlated with I-V characteristics influencing the conductivity and the transmittance [86]-[87]. Whatever the deposition method care has to be taken to grow particular crystalline orientation to obtain the desired film properties. Commercial ITO cover glass has strong differences between different manufacturer and not all are suited for OSC application: the high resistivity, for example, reveal it self in the strong fall of the extracted current. High quality coatings are very expensive, for the intrinsic cost of employed material (Indium in particular) and for the care in the deposition process. A first stock purchased from Sigma-Aldrich demonstrated quite low features for photovoltaic thin polymer cells: high resistance (reported surface resistivity of $15 - 25 \Omega/sq$) and poor film morphology produced low current and frequent short circuit in the made cells. Evident improvement has been achieved employing ITO coated glass slide from Hitachi (courteously supplied by CRP of Amaro, 6.5), demonstrated by the strong reduction of short circuits. However, we planned to develop a sputtering process of ITO in order to have the possibility of produce our self the transparent electrode.

PEDOT:PSS

Second bottleneck was the PEDOT-PSS conductive film. PEDOT is built from ethylenedioxythiophene (EDOT) monomers. It is insoluble in many common solvents and unstable in its neutral state, as it oxidizes rapidly in air. PSS is added to improve its processability, and these results in an aqueous dispersion of PEDOT:PSS, where PEDOT is its oxidized state; each phenyl ring of the PSS monomer has one acidic $-SO_3H$ (sulfonate) group, (Figure 3.13). The degree of polymerization of PEDOT is limited and it is assumed that PEDOT is a collection of oligomers with lengths up to ≈ 20 repeating units. The role of PSS, which has a much

higher molecular weight, is to act as the counter ion and to keep the PEDOT chain segments dispersed in the aqueous medium. Different aqueous dispersions of PEDOT:PSS are commercially available. With this material, thin, highly transparent and conductive surface coatings can be prepared by spin-casting or dip-coating on almost any hydrophilic surface. Depending on solid content, doping concentration, particle size and additives, films with different properties can be made. The composition of solution, and in particular the ration between PEDOT and PSS, defines the conductivity of material. Strong differences exist between compounds of different producer: specialized companies produce specific products for various applications. In particular, for OSC application, as for OLED, is recommended a PEDOT:PSS with high conductivity, that reduces the R_S and then generating higher J_{SC} .

Composition	
PEDOT content	0.5 wt.
PSS content	0.8 wt.
concentration	1.3 wt dispersion in H2O
Properties	
band gap	1.6 eV
conductivity	1 S/cm
density	1 g/mL at 25 °C(lit.)

Table 6.1: Sigma Aldrich Pedot:Pss specifications

We bought the PEDOT from Sigma Aldrich: in table 6.1 are resumed the main properties of purchased solution. With overall measurements on thin PEDOT:PSS films carried out by 4 point probe methods, we verified high sheet resistance. Some improvements in film properties has been achieved modifying the solution introducing a small quantity of glycerol as explained in literature [88]-[89]-[90]: the conductivity of PEDOT:PSS, in fact, can be dramatically increased without any loss in its optical transparency giving a better hole transport a small amount of a polyalcohol such as glycerol and sorbitol. The increased conductivity is accompanied by a remarkable increase in environmental stability after thermal annealing, which we attribute to a denser packing of the PEDOT:PSS material.

In fig.6.12a is shown the comparison of some kind of solution of PEDOT:PSS (named Clevios) of company H.C. Starck, one of most important producer. In fig 6.12b is highlighted the difference in resistivity in function of PEDOT:PSS ratio. We bought the Clevios P Al 4083, but not test are still available; we are hopeful to obtain strong enhancements by the use of this compound.

The correct annealing process is indeed important to remove the water used as solvent that could be a problem for the following deposition of active materials, without exceedingly altering the conductivity of the material. Some different recipe for the treatments post deposition are present in literature [91]-[92], and for this reason some different tests have been performed. No evident differences have been verified: we believe that a prolonged annealing at temperature over 120° is recommended in order to remove all the water, or better, the most possible water present in the film after the deposition from solution. It would be recommended lead the annealing process in inert atmosphere or in vacuum to promote the extraction of water.

Also the P3HT have been purchased from Sigma Aldrich: the elevate cost of this compound

a

	Application	PEDOT : PSS (by weight)	Solvent	Resistivity [Ohm cm]	Viscosity at 700 s ⁻¹ [mPas]	pH	Solid Content [%]	Work Function [eV]
CLEVIOS™ P AI 4083	Buffer layer (low ohmic)	1 : 6	Water	500 – 5 000	5 – 12	~ 1.7	1.3 – 1.7	5.0 – 5.2
CLEVIOS™ P JET	Buffer layer (by Ink-Jet deposition)	1 : 6	Water	500 – 5 000	5 – 11	~ 1.7	1.2 – 1.4	5.0 – 5.2
CLEVIOS™ P CH 8000	Buffer layer (high ohmic)	1 : 20	Water	100 000 – 300 000	9 – 20	~ 1.5	2.5 – 3.0	5.0 – 5.2
CLEVIOS™ HIL1 *	Buffer layer (low ohmic)	Composition not disclosed	Water-Alcohol	10 – 100	5 – 15	~ 2.2	1.2 – 1.6	5.4 – 5.9
CLEVIOS™ HIL 1.3 *	Buffer layer (low ohmic)		Water-Alcohol	1 000 – 10 000	3 – 12	~ 1.6	2.8 – 3.2	5.4 – 5.9
CLEVIOS™ HIL 1.5 *	Buffer layer (high ohmic)		Water-Alcohol	100 000 – 1 000 000	3 – 12	~ 1.6	3.2 – 3.6	5.4 – 5.9

* Material will only be distributed under signed NDA

b

	moderate conductivity	high conductivity	PEDOT : PSS ratio	Viscosity at 100 s ⁻¹ [mPas]	Solid Content [%]
CLEVIOS™ P			1 : 2.5	60 – 100	1.2 – 1.4
CLEVIOS™ PH			1 : 2.5	Max 25	1.2 – 1.4
CLEVIOS™ P AG			1 : 2.5	50 – 90	1.1 – 1.3
CLEVIOS™ P HC V4			1 : 2.5	100 – 250	1.1 – 1.4
CLEVIOS™ PH 500			1 : 2.5	8 – 25	1.0 – 1.3
CLEVIOS™ PH 510			1 : 2.5	20 – 100	1.5 – 1.9
CLEVIOS™ P HS			1 : 2.5	not specified	2.6 – 3.2
CLEVIOS™ S HT			1 : 2.5	3-5 dPas	not specified
CLEVIOS™ S V3			1 : 2.5	15 – 200 dPas	not specified
CLEVIOS™ F CPP 105 DM			1 : 2.5	30 – 60	1.0 – 1.4
CLEVIOS™ F E			1 : 2.5	40 – 80	2.2 – 2.6
CLEVIOS™ F PVA			1 : 2.5	150 – 200	3.8 – 4.3

After addition of 5% Dimethylsulfoxid

Figure 6.12: Different PEDOT:PSS solution from H.C.Starck.

we forced to choose materials with not suitable properties. In particular, the low purity grade and much more the use of a regio-random polymer was a the most limiting factor of low efficiency verified from characterisation: as previously shown, in 6.1, the regioregularity improves the organization two dimensional crystallites, in which the conjugated rings face each other to form a compact lamellar structure, promoting the probability of charge transfer. Moreover, it has been demonstrated [93] that at room temperature hole mobility of regioregular P3HT is estimated to be one order of magnitude larger than that of the random one. The effect of disorder in polymer packaging has been higher than we expected, resulting a very low generated current determined by the low EQE and the high R_{Sh} . Consequently, poor PCE has been measured for devices fabricated with this conjugated polymer.

About PCBM, we can suppose that also this compound is one of causes of low efficiency of fabricated devices. The purity of compound (assay of 99.5%) could be identified the major problem. We evidenced any improvement when we used a higher purity (99,9%) sold later: probably, it was impossible noticing these low enhancements when measuring so low generated current.

6.4 Cells characterisation

In the follow we will present the details of characterisation of fabricated cells. The entire test have been done in air: N_2 atmosphere would be preferable to avoid the deterioration of solar cells. At the moment we can't realize a system with this peculiarity: all the characterisation setup would be realized in glove box. However, we kept the cells in a dedicate box under N_2

flux until the measurement and we took out just for the needed time. Anyway the life of devices is still very short and it has be possible verifying the deterioration in the cells performances when we lead multiple subsequent measurements.

The general characterisation procedure can be schematically described as follow:

- the measurement of Spectral Irradiance of the incident light in function of wavelength using Acton SpectraPro SP-2300i spectrographs with monochromators and a calibrated diode as reference.
- the measurement of generated current versus wavelength with the same instrumentation.
- the determination of EQE from previous two measurements and 4.3.
- the draws of I-V curve of solar cell under ABET 2000 SunSimulator calibrated light.
- the calculation of FF from 4.1 and the PCE from 4.6.

The first cellshas been made using P3HT regiorandom, high resistant PEDOT:PSS and PCBM 99, 5%.

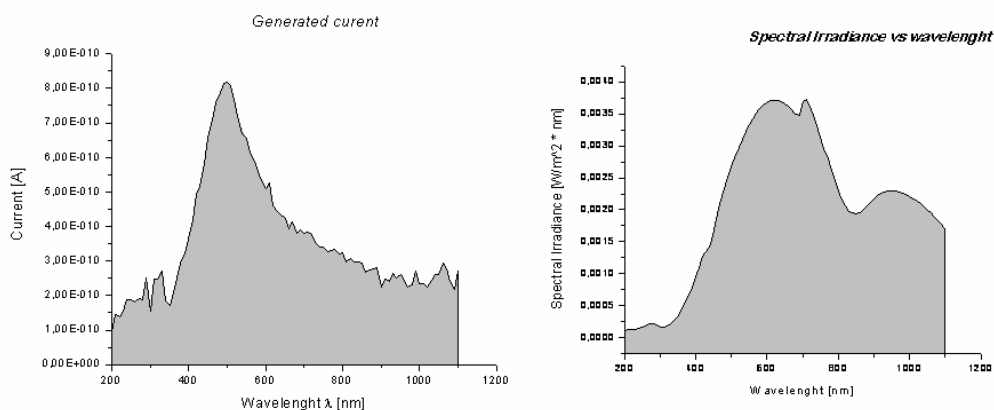


Figure 6.13: On the left, the current/wavelength response of one of solar cell: maximum value 0.827 nA at 490 nm . On the right the Spectral Irradiance measurement.

In the most of cases, measurements shown that fabricated cells were in short circuit: we ascribed the causes to the impurities present in the PEDOT:PSS and blend solutions, as well as the ITO electrode. When these particles (generally dust or unsolved compound) have size comparable with the thickness of layers, since we work with very thin film, they can easily generate short circuits contacting the PEDOT or ITO film to metal electrode. Moreover, the use of very diluted blend solution and consequently the deposition of too thin films (from 30 to 60 nm), emphasize these phenomena causing short circuits with consequent decreasing of collect charges. The second effect of using thin active layers is the incapacity of the cells to exploit the most of incident radiation.

On the left of fig. 6.13, is shown the generated current curve versus the wavelength of incident light referred to a sample that was not in short circuits; as previously said, the generated

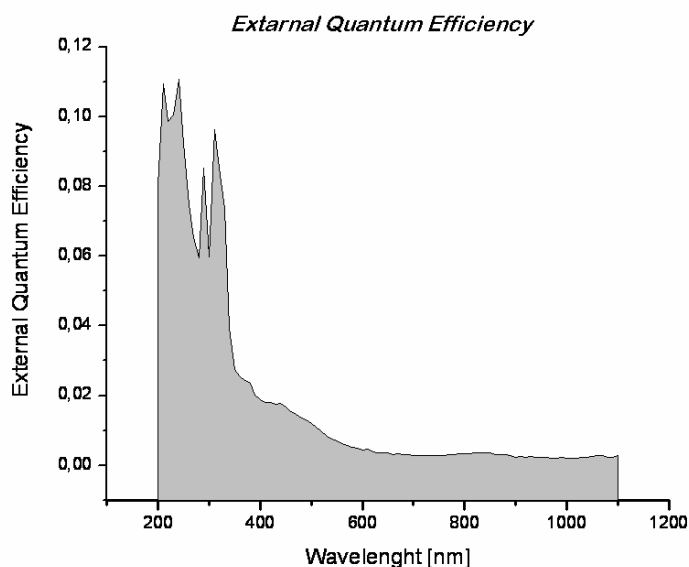


Figure 6.14: The calculated EQE vs wavelength: the maximum EQE at small wavelengths probably derives from an incorrect Spectral Irradiance measurement.

current is very low, we measured a max of $8 \times 10^{-10} A$. We report also the Spectral Irradiance measure on the right of 6.13. The resulting EQE (normalized to 1) is equally low (fig. 6.14): the causes are ascribed to the bad conduction of P3HT, probably rising also from the incorrect parameters of P3HT/PCBM annealing ($110^{\circ}C$ for 30 minutes) after the Al electrode evaporation.

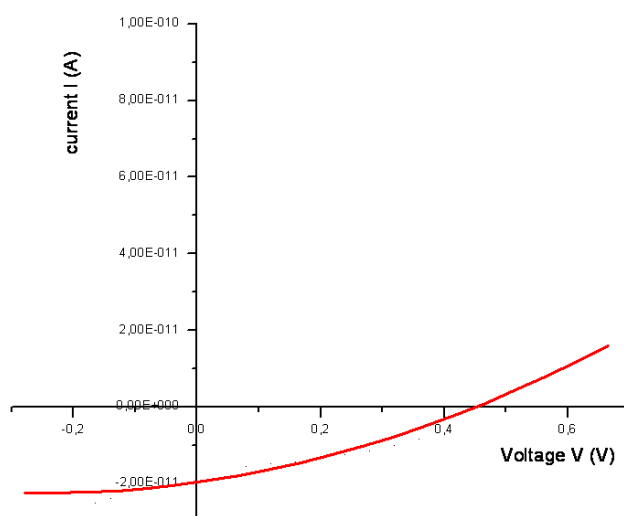


Figure 6.15: I-V curve of a cell realized using regiorandom P3HT, high resistant PEDOT:PSS and PCBM 99, 5%. The I-V curve shows a V_{OC} of 427 mV, a lower value with respect the V_{OC} founded in literature (≈ 700 mV).

The measure of I-V curve (fig. 6.15 show a quite low open circuit voltage ($V_{OC} = 0.49V$) and short circuit current ($J_{SC} \cong 2 * 10^{-11}$): the reason of a very low short circuit current could be explained with the deterioration in the cells performances for exposure to the air and for the use of a light source not proper for this test (we not had yet the sun simulator) having a spectral range centred on IR wavelengths). The resulting PCE has been estimated below 0.001%.

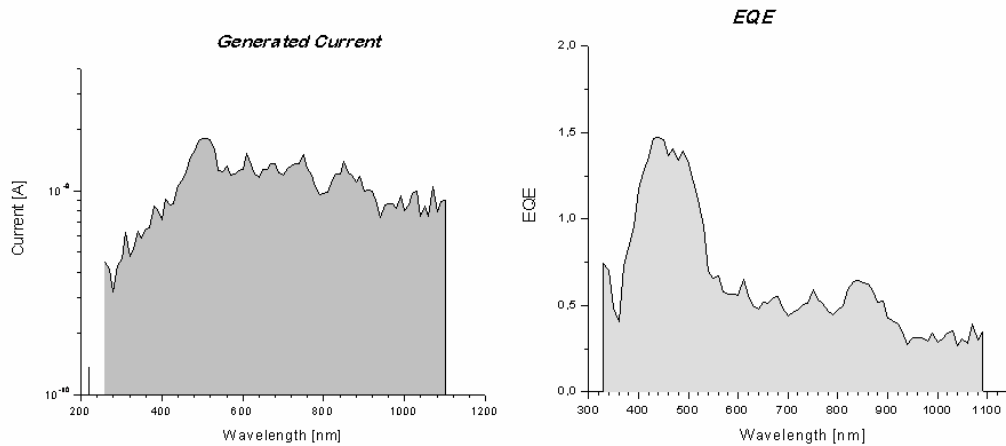


Figure 6.16: On the left, the current/wavelength response: on the right the calculated EQE: not effect of the diode calibration are noticed. The wavelength range correspondent to the maximum values of EQE according to that found in literature.

Some improvements have been obtained modifying the film thickness and annealing parameters: we increased to 150 nm the active layer thickness (the measurement is quite imprecise because, using a profilometer to take it, a damage of film surface has been observed) and the baking temperature was raised to $140^{\circ}C$ for 1h. The current and, consequently the EQE, have been increased as shown in fig. 6.16. The maximum measured current was $1.8 * 10^{-9} A$ (2 order higher than previously) at 500 nm of wavelength. The EQE reaches the maximum value at the same wavelength. The increasing in current and EQE indicate first the rise in absorbed light by the active film, and then the better charge collection at the electrodes, probably due to the better conductivity of PEDOT:PSS film: in fact, we supposed that the electric properties of blend film was not changed because strictly dependent on the material rather than the deposition and annealing processes, as highlighted also in I-V curve 6.17.

The highest improvement of solar cells performances has been obtained by changing the compounds of blend. First we bought new PCBM (99.9% of purity, from Solenne); second we used a purified P3HT regioregular, supplied from a researcher (Alessandro Fraleoni) with who we start to collaborate. The changes are evident in generated current 6.18, EQE 6.19 and in the I-V curves 6.20: the graphics are referred to one of the fabricated samples. In general we noticed the drastic fall of cells in short circuit and the increase of V_{OC} that reaches the values present in literature. In the example, the generated current is $2.1 * 10^{-8} A$, two order higher than first produced cells. The Correspondent EQE is 0.25 (value normalized to 1). These values are still lower than best P3HT-PCBM cells, but quite comparable.

From I-V curves we calculated Fill Factor and PCE: all data are reported in the box in fig-

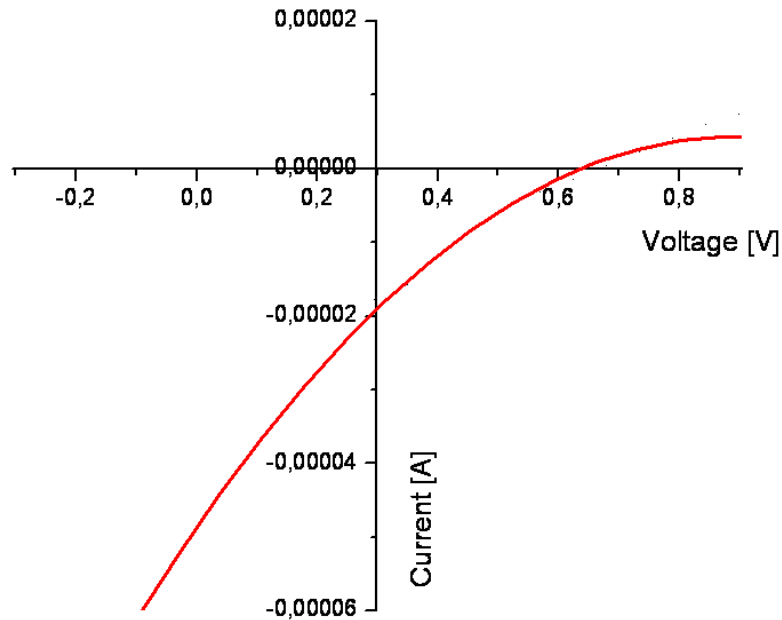


Figure 6.17: I-V curve of a cell realized using regiorandom improved annealing process and thicker active film. The V_{OC} was 637 mV, much higher than before; also the J_{SC} has been increased (20 nA), that is still a low value. The effect of poor electric properties of P3HT is evident.

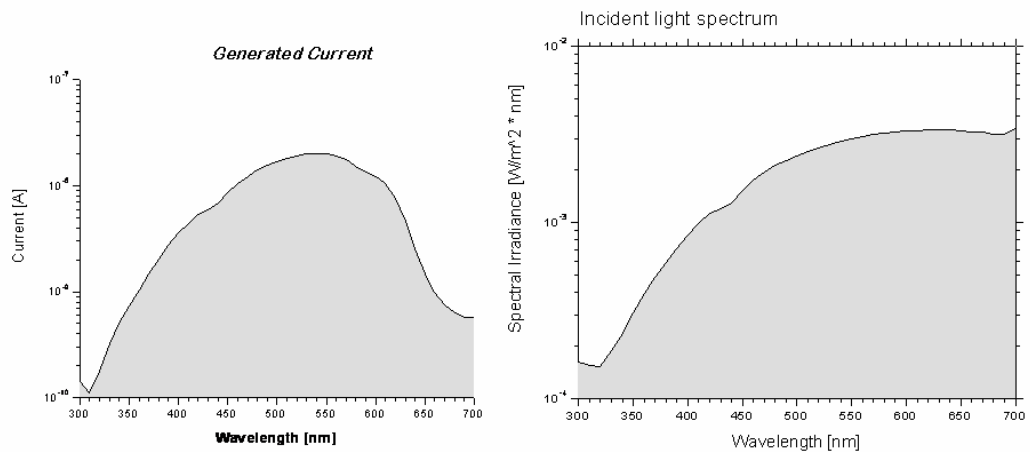


Figure 6.18: On the left, the current/wavelength response of one of our best P3HT/PCBM cells. On the right the Spectral Irradiance measurement.

ure 6.20. As explained in the 4th chapter, the trend of the curve we indicate that the cells have a behaviour dominated by the high series resistance R_S and shunt resistance R_{Sh} : this is evi-

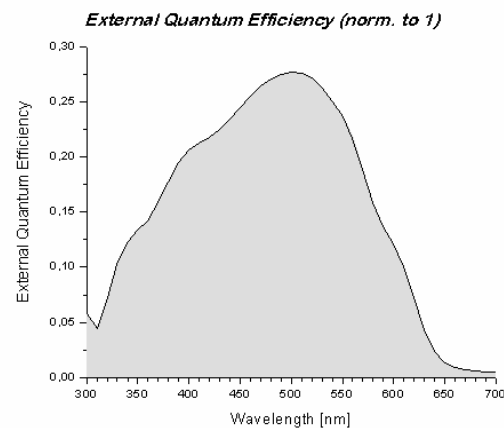


Figure 6.19: The calculated EQE in function of wavelength.

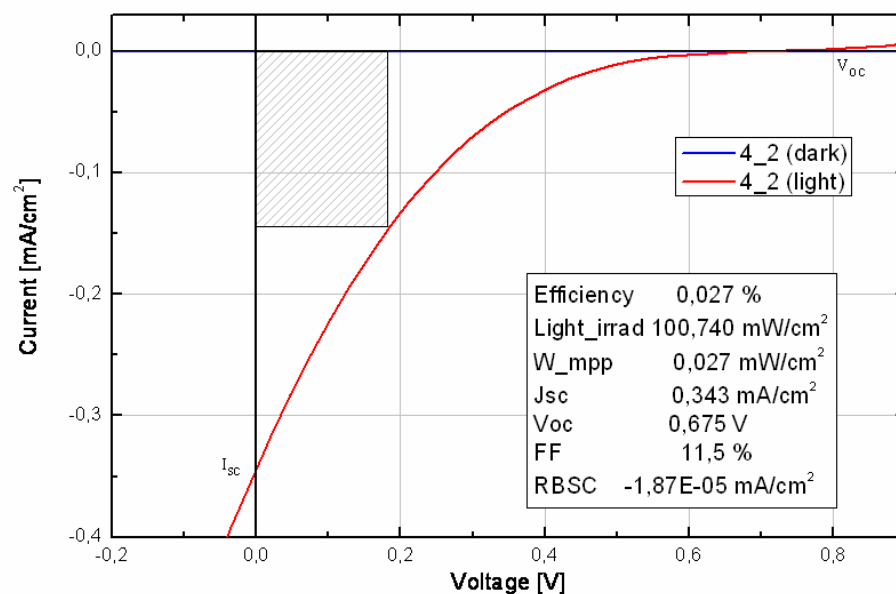


Figure 6.20: The I-V curve under AM 1.5 illumination.

denced by the reduced FF and J_{SC} values. The high R_S probably derives from the PEDOT:PSS electric properties: a better polymer would be suitable to improve the cells efficiency. Instead, the R_{Sh} is determined by the electric properties of active blend: since we used high quality materials, we are inclined to believe that the fabrication process and particularly, the annealing parameters have to be performed.

We can conclude that there are a few of changes that can be done to further improve the quality of our cells and that can be summarized as follow:

- reducing the resistance of PEDOT:PSS improving the deposition and the annealing processes and using a more suitable product, specifically designed for solar cells application

(like Clevios, from H.C.Starck). Moreover, it would be very important leading the annealing process in controlled atmosphere or, better, in vacuum.

- Improving the deposition and annealing process of the active blend: in particular, we are modifying our glove box to allow the complete deposition in oxygen and water free atmosphere. Moreover, we are studying and realizing a system to extend the lifetime of fabricated cells by encapsulation between two glass slides. In this way, we want prolong the cells working time to at least one week (now is less than one day).
- Inserting a sub a nanometric thick film of LiF by sublimation (see 3.7).
- Developing an ITO deposition process with our sputtering: the commercial ITO coating on glass are too expensive and, frequently, have poor quality. The possibility of realizing home made coating of ITO, we will permit to use different substrates (like plastics), explore new cells configuration and, we hope, to have better transparent electrodes.

6.5 Small molecules evaporated solar cells

At the same time of the previous work, we start collaboration with the Centro Ricerche Plastotiche (CRP), a society located in Amaro (UD) born with the collaboration between CRF (Centro Ricerche Fiat) and Agemont. The main idea was to apply the dues of CRP in OLED technology and the facilities present in their laboratories to produce multilayer OSC based on small molecule by sublimation. The realization of these kinds of cells would be very useful for our research in organic photovoltaic: in general, the knowledge and the possibility to exploit different techniques of fabrication of solar cells is really important for a group as our group that is investing in this research theme. Moreover, it offer a chance for application and improvement in the project explained until now. First because the deposition by evaporation is a fundamental step in the realization of nanostructured solar cell as showed in this chapter; indeed, after the nanoimprinting process, the nanostructures have to be filled by an evaporation step with the second semiconductor (the acceptor one, like C60, if we use P3HT for example) to realize the needed heterojunction promoting the exciton scission (see fig.6.3). Second, to be applied in the second generation of LTS showed in the fourth chapter: the main idea is to insert a further cell in the made device. The opportunities of our light trapping system, deriving from its throughput, combined with the processing versatility of organic solar cells, permits to conceive and generate different configuration scheme; an idea could be fabricating an evaporated organic solar cell between microlenses and the metallic film with aperture, to collect the diffused sunlight that would be lost. Just the collimated light can be concentrated and pass trough the small aperture; all the remaining light is lost because reflected by the metallic film. Fabricating an additional cell, all the light is utilized. Obviously, as intuitive from the fabrication process illustrated in chapter 4, it is easier realize this cell by evaporation than from solution method.

6.5.1 Fabrication of evaporated solar cells

The solar cells fabricated in collaboration with CRP are pretty similar to the polymeric ones realized in our laboratories. The main differences are related to the organic semiconductor

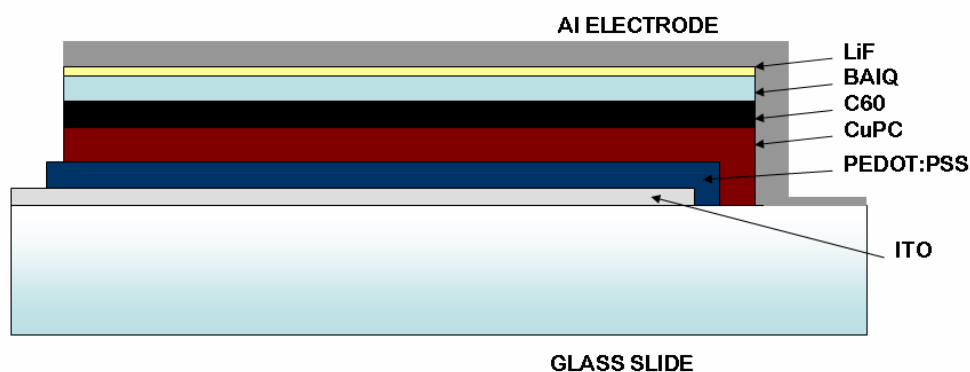


Figure 6.21: The general scheme of a cell fabricated by evaporation.

employed, but it is also important evidencing some details that have made these cells more performing. In figure 6.21 is showed the general structure and the schematic sequence of cells and in fig.6.22 how it looks: every sample contains 2 cell with same characteristics.

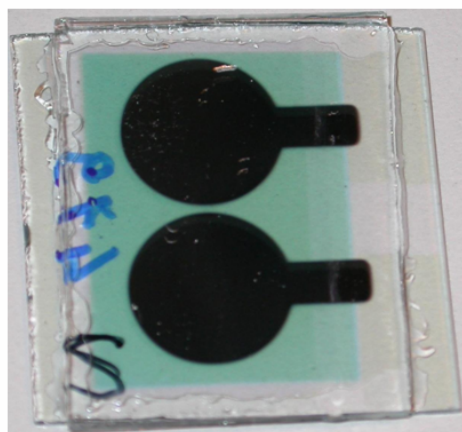


Figure 6.22: Two cells fabricated at CRP of Amaro.

As we can see from figure, the cell is constituted by the classical transparent electrode of ITO on a glass slide substrate and a previous film (thickness between 200 and 500 nm) of PEDOT:PSS deposited from solution as showed for the *P3HT/PCBM* cells. The active layer is constituted of a multilayer of CuPC (see fig. 6.23) and C60. Between the active layer and the metal electrode (Aluminum or Silver) have been deposited two films of Aluminium (III) bis(2-methyl-8-quinolinato)-4-phenylphenolate (BAIq)(see fig. 6.23) and LiF. The role of Lithium Fluoride has been explained previously; BAIq works like exciton blocking layer (HBL) and its application derives from the OLED technology in the CRP.

The electroluminescence (EL) PCE and the degradation of OLED predominantly comes from the hole injection into electron transport layer (ETL). BAIq cations are formed when holes are injected into ETL and, since they are apt to react with water and oxygen, it leads to formation of fluorescence quenchers. Moreover, the mobility of holes in the hole transport

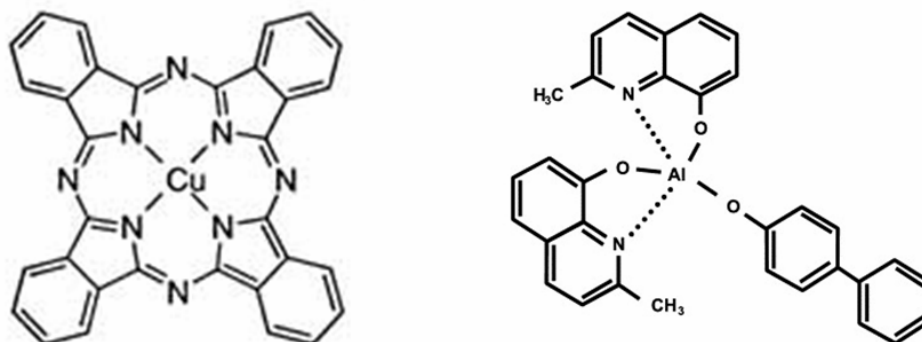


Figure 6.23: The CuPC and BALq molecules.

layer (HTL) is greater than that of electrons in the ETL by some scale orders. Therefore, by reducing the mobility of holes in HTL or promoting electrons to inject into ETL can improve the balance of carriers in OLED. The modified electrode with HBL may be applied to improve the efficiency of OLED: increasing the work function of anode by inserting the HTL between anode and EML can balance carriers. Also the use of hole or electron blocking layer in organic solar cells, typically in BHJ solar cells, is well known. One problem with BHJ solar cells is that both the donor polymer and the acceptor molecule are touching both electrodes. This means that electrons in the PCBM may be formed at an interface very close to the ITO anode, which typically collects the holes. Any electrons transferred to the ITO would essentially recombine with holes and reduce the working voltage of the device. Thus the Voc, would also be reduced. Introducing, for example, an electron blocking layer (EBL) between the active layer blend and the ITO anode, we prevent that electrons, travelling in the PCBM, reach the ITO, forcing the electrons to flow in the correct direction for collection at the cathode. The contrary is valid for hole blocking layer. As we can intuit from the previous explanation, the use of this kind of molecule is not very useful for the cell showed in fig. 6.21 because the two semiconductor are surely not in contact with the opposite electrode. Therefore, the use of BALq would be interesting just when we are in presence of a single co-evaporated layer. This will be one of following tests that we have programmed. Some different solar cells have been made varying the fabrication parameters like: the thickness of every single layers, the temperature during the processes of deposition and of annealing, the employed materials and the sequence of layers. In table are listed the characteristics of the produced cells (not all made cells are listed, we excluded that ones with the worst performances).

6.5.2 Characterisation of evaporated solar cells

The cells have been characterized using the system shown in the 4th chapter and already used for the characterisation of polymeric solar cells. The most interesting results that we obtained until now from the characterisation of cells regard the dependency of extractable current in function of the annealing temperature after the deposition.

In figure 6.24, on the left, are shown the scheme of one of the fabricated cells and, on

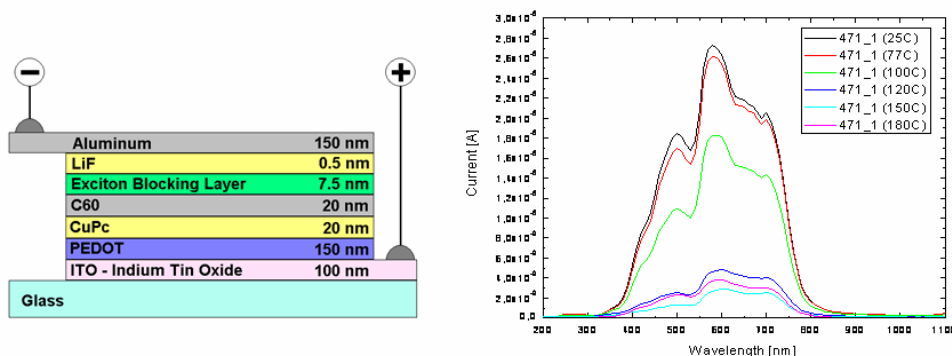


Figure 6.24: left) scheme of cell: the layer and the respective thickness are highlighted. right) the current vs wavelength curve of the cell in function of the baking temperature: the generated current decrease with the increasing of temperature annealing.

the right, the current vs wavelength curve of the cell in function of the baking temperature (the baking time was 30min for each temperature). As we can see, in a similar configuration of organic layers, the increasing of annealing temperature gives as effect the decreasing in collected current. We deduce that the annealing is harmful for the cell efficiency.

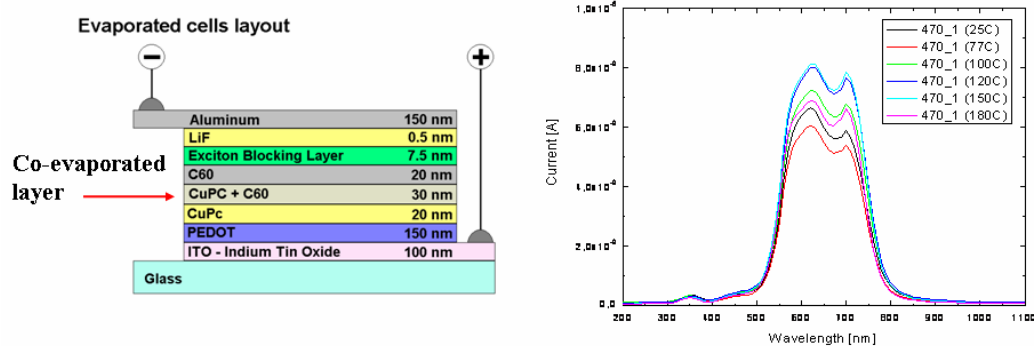


Figure 6.25: left) scheme of cell: the layer and the respective thickness. right) the current vs wavelength curve of the cell in function of the baking temperature: the generated current increase with the increasing of temperature annealing.

Different behaviour when the cell has a layer sequence like that in figure 6.25(left) where a co-evaporated interlayer (between the C60 and the CuPC). As visible in the fig. 6.25(right), the curve current/wavelength, increasing the temperature of annealing, the collected current equally increases until a temperature between 120 and 150°C, and then decreases. We can suppose that the annealing permits to fullerene and CuPC to arrange in a better configuration with higher conduction. The presence of this interlayer is quite beneficial for the cells performances: in fact the cell with similar configuration of layers has demonstrated the best performances for J_{sc} and V_{oc} . In figure 6.26 are shown the I-V curves of the cell in dark and under illumination with sun simulator. The final PCE was 0.02%, two orders higher than other cells of which

is reported one sample of the I-V curves (figure 6.27). In all cases, the curves highlight the influence of series resistance, as previously discussed for the P3HT/PCBM cells.

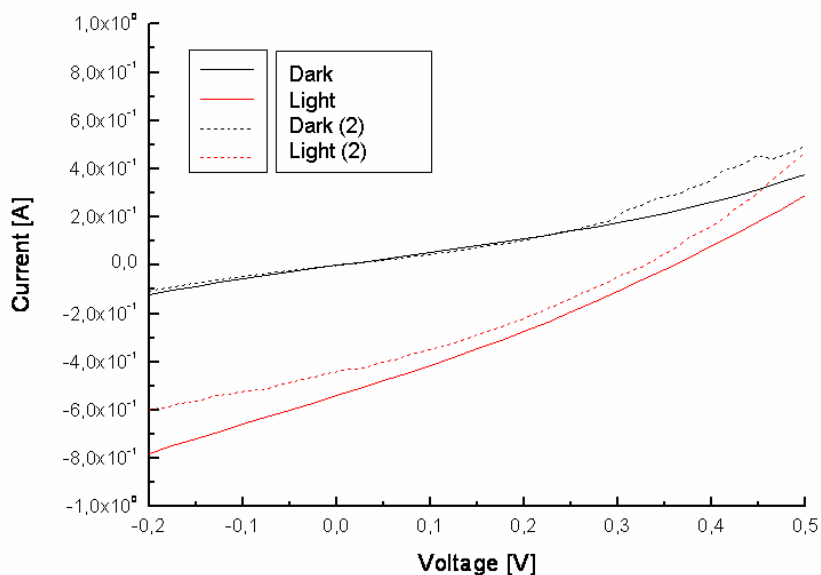


Figure 6.26: I-V curve of the best evaporated cell.

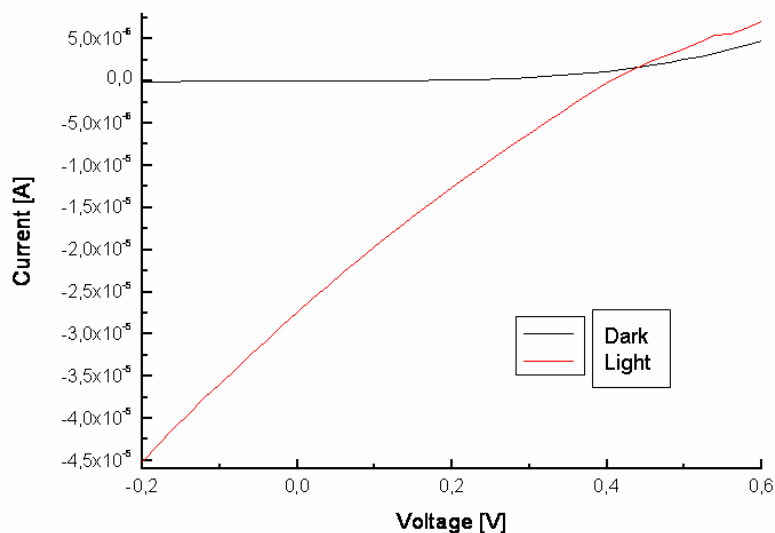


Figure 6.27: I-V curve of a cell with lower PCE.

6.6 Conclusions

The main aim of realization of an interdigitated system in the active layer of nanostructures has not been completed. At the present time, the master for nanoimprinting has been obtained:

feature size of nanopillars are consistent with the exciton diffusion length (5-10 nm). A fabrication process of standard BHJ solar cells have been performed: the performances of realized solar cells are not yet comparable with that present in literature. However, we can estimate that in few time we will be able to produce more performing devices. The best obtained efficiency is 0.027%. A characterization set up has been improved, and the laboratory equipment for the fabrication of solar cell is quite performed. Moreover, in collaboration with the Centro Ricerche Plastotiche of Amaro, we start to realize and test different organic solar cells based on small molecules (CuPC) and fullerenes. The cells, produced at the CRP laboratories, was fabricated by sublimation of this materials: many different cell configurations have been tested, and a preliminary study on the dependency of efficiency from annealing process has been done. The best cells showed a better efficiency (0.1%) than the polymeric ones realized in our laboratory, but many improvements are needed.

Conclusions

The organic photovoltaic technology based on conjugated polymers was the central theme of this thesis. In particular, we have developed two new solutions in order to increase the performances of solar cells, in particular trying to improve their efficiency. The first one is based on the use of nanofabrication methods to modify the structure of solar cells exploiting the group's knowledge on nanofabrication and the facility present in the laboratory. One aim of this project was the realization of an ordinate interdigitated system of nanostructure domains of donor and acceptor type materials with feature size in the order of the exciton diffusion length (5-10 nm). In fact we believe that nanostructured active layer would allow a major efficiency of exciton splitting into free charge carrier and a more direct path towards electrodes of the latter. Our objective was to obtain this using a top down technique, like nanoimprinting lithography, that would be rather easily and cost-effectively transferable to the industry. We pursue two main objectives: the realization of efficient bulk-heterojunction solar cells and the production of the NIL master with feature size consistent with the requirement previously illustrated. The start of research on organic photovoltaic field in a laboratory in which this theme was absent before has required the development of all aspects related to the fabrication and the characterization of solar cells. In particular, the setting up of fabrication schemes and process has absorbed time and resources for the absence of a foregoing background. During these three years, we acquired that background setting up a characterization station for external quantum efficiency and power conversion efficiency. Nevertheless, the results obtained are not completely satisfactory, because the measured efficiency in our devices is still lower than the values presented in literature. But the competences and the capabilities that now we have, will allow to reach hopefully better results. At the present time, the best performances of fabricated bulk-heterojunction solar cells that we realized are two order lower than the best efficiency reported in literature (5%). Our cells reach the 0,03% of efficiency, but we have to highlight the fact that, at the moment, we can not complete all the fabrication steps in inert atmosphere. The consequence is that the materials employed in the solar cell, the conjugated polymers in particular, degrades reducing the effective performances. For this reason, the develop of the nanostructured cells has not been completed: however, at the same time, the other major aspect related to the project, the NIL stamp, has been developed. The structures size has required conceiving a method of fabrication different from the standard lithographic techniques. The solution we found was the self assembly properties of thin tin film that in the early stage of deposition grow in nanodots. By the evaporation of nano-metric layers on top of the silicon wafer surface, we were able to generate random patterns on large area, with island size comprised between 5 and 40 nm. The set up of a dedicated dry etching process in ICP completed the fabrication of the

master: the tin nanodots were used as mask in order to be replicated in the silicon bulk and obtain the suitable nanopillar. Soon we will be able to complete the nanofabrication process, imprinting the fabricated stamps in conjugated polymers. Moreover, in collaboration with the Centro Ricerche Plastotiche of Amaro we have started to work and test a different kind of organic solar cells based on small molecules (CuPC) and fullerenes. The cells, produced at the CRP laboratories, were fabricated by sublimation of these materials: many different cell configurations have been tested, and a preliminary study on the dependency of efficiency from annealing process has been done. The best cells showed a better efficiency (0.1%) than the polymeric ones realized in our laboratory, but other improvements are needed. The second main line of research was devoted to the realization of a novel light trapping device based on a micro-optic system. We have elaborated a concept that would solve efficiently the problem of incomplete absorbing of light for cells with reduced active layer thickness by making use of a new type of light trapping elements. The simple fabrication scheme, based on a self aligned UV exposure process, suggests its potential up scalability to large systems, at low production cost. Moreover, the scattering and light trapping features are separated from the active layer in order to avoid the possibility of electrical defects. The trap element is transparent to collimated light in one direction and highly reflective in the opposite direction to both collimated and directionally random light. As light bounces back and forth between the reflective metal surface of the cell electrode and the back surface of the trap element, multiple transits through the active layer will occur, thus increasing the probability of photon absorption. The concept of the proposed device is that the light focused by an array of microlenses and passing through small apertures is introduced into a cavity delimited by the reflective back-electrode of the cell and the mirror of the trapping system. The characterisation of device has been done in the collaboration of group of Olle Inganäs from Biomolecular and Organic electronics Center of Organic Electronics of Linköpings Universitet, in Sweden. A strong asymmetry between the forward and backward transmission was confirmed, with transmission up to 90% in the forward direction (first through lenses and then mirror) and less than 15% measured with the sample illuminated from the side of the mirror. The optical characterisation of transmission has been followed by the testing of device coupling with a solar cell. The current/voltage curve under AM 1.5 simulated solar illumination also demonstrate an increase in short circuit current, as high as 25% in relative, upon the inclusion of the light trap. The micro-lens system has been patented. Moreover, two articles, one on innovative fabrication process and the other one for the result of test have been submitted. A poster on the micro-fabrication of system has been accepted as invited at the MNE conference in Athens.

Bibliography

- [1] P. Peumans, V. Bulović, and S. R. Forrest. Efficient photon harvesting at high optical intensities in ultrathin organic double-heterostructure photovoltaic diodes. *Applied Physics Letters*, 76(19):2650–2652, 2000.
- [2] Miri Park, Christopher Harrison, Paul M. Chaikin, Richard A. Register, and Douglas H. Adamson. Block copolymer lithography: Periodic arrays of 1011 holes in 1square centimeter. *Science*, 276(5317):1401–1404, 1997.
- [3] A Rohatgi. Road to cost-effective crystalline silicon photovoltaics. *Photovoltaic Energy Conversion, 2003. Proceedings of 3rd World Conference on*, 1:A29– A34, 2003.
- [4] M. Wolf. *Proceedings of the 14th IEEE Photovoltaic Specialists Conference, San Diego*, page 674, 1980.
- [5] E.S. Vera J.J. Loferski M. Spitzer, J. Shewchun. *Proceedings of the 14th IEEE Photovoltaic Specialists Conference, San Diego*, page 372, 1980.
- [6] H.F. Sterling R.C. Chittick, J.H. Alexander. *J. Electrochem. Soc.*, 116:77, 1969.
- [7] Xuanzhi Wu. High-efficiency polycrystalline cdte thin-film solar cells. *Solar Energy*, 77(6):803 – 814, 2004. Thin Film PV.
- [8] J. AbuShama F. Hasoon D. L. Young B. Egaas R. Noufi Miguel A. Contreras, K. Ramanathan. Diode characteristics in state-of-the-art zno/cds/cu(in1-xgax)se2 solar cells. *Prog. Photovolt. Res. Appl.*, 13:209, 2005.
- [9] Brian O’Regan & Michael Grätzel. A low-cost, high-efficiency solar cell based on dye-sensitized colloidal tio2 films. *Nature*, 353:737, 1991.
- [10] masayoshi Suzuki, Sato H, A. Atsushi, and S. Naemura. Organic light emitting materials based on liquid crystals. *Journal of photopolymers science and technology*, 16:323–328, 2003.
- [11] Kyoko Kogo, Tadashi Goda, Masahiro Funahashi, and Jun ichi Hanna. Polarized light emission from a calamitic liquid crystalline semiconductor doped with dyes. *Applied Physics Letters*, 73(11):1595–1597, 1998.

- [12] Lukas Schmidt-Mende; Mark Watson; Klaus Muumlillen; Richard H. Friend. Organic thin film photovoltaic devices from discotic materials. *Journal Molecular Crystals and Liquid Crystals*, 396:73–90, 2003.
- [13] A. Lux G. Rozenberg S.C. Moratti K. Petritsch, R.H. Friend and A.B. Holmes. Liquid crystalline phthalocyanines in organic solar cells. *Synthetic Metals*, 102:1776–1777, 1999.
- [14] Fichou D. Nunzi J.-M. Pfeffer N. Charra, F. Picosecond photoinduced dichroism in solutions of thiophene oligomers. *Chemical physics letters*, 192:566–570, 1992.
- [15] Brazovskii S. Bishop A.R. Kirova, N. The model for optical properties of ppp-type polymers. *Synthetic Metals*, 101:271–272, 1999.
- [16] A. Moliton. Electrical and optical properties of polymers. *Actualite Chimique*, 319:24–32, 2008.
- [17] J. G. Fripiat J. L. Brédas, B. Thémans and J. M. André. Highly conducting polypara-phenylene, polypyrrole, and polythiophene chains: An ab initio study of the geometry and electronic-structure modifications upon doping. *Phys. Rev. B*, 29:6761–6773, 1984.
- [18] B. Scott S. E. Gledhill and B. A. Gregg. Organic and nano-structured composite photovoltaics: An overview. *Journal of Materials Research*, 20 (12):3167–3179, 2005.
- [19] William Barford, Robert J. Bursill, and Richard W. Smith. Theoretical and computational studies of excitons in conjugated polymers. *Phys. Rev. B*, 66(11):115205, Sep 2002.
- [20] Norihiko Takeda, Sadayuki Asaoka, and John R. Miller. Nature and energies of electrons and holes in a conjugated polymer, polyfluorene. *Journal of the American Chemical Society*, 128(50):16073–16082, 2006.
- [21] H. Bässler, V. I. Arkhipov, E. V. Emelianova, A. Gerhard, A. Hayer, C. Im, and J. Rissler. Excitons in [pi]-conjugated polymers. *Synthetic Metals*, 135-136:377 – 382, 2003. Proceedings of the International Conference on Science and Technology of Synthetic Metals.
- [22] J. Frenkel. Some remarks on the theory of the photoelectric effect. *Phys. Rev.*, 38(2):309–320, Jul 1931.
- [23] N. F. Mott. Conduction in polar crystals. ii. the conduction band and ultra-violet absorption of alkali-halide crystals. *Transactions of the Faraday Society*, 34:500–506, 1938.
- [24] J. J. M. Halls N. T. Harrison A. B. Holmes A. Koehler A. Lux S. C. Moratti K. Pichler N. Tessler K. Towns R. H. Friend, G. J. Denton and H. F. Wittmann. Electronic excitations in luminescent conjugated polymers. *Solid State Communications*, 102:249–258, 1997.
- [25] J. J. M. Halls N. T. Harrison A. B. Holmes A. Koehler A. Lux S. C. Moratti K. Pichler N. Tessler R. H. Friend, G. J. Denton and K. Towns. Electronic processes of conjugated polymers in semiconductor device structures. *Synth.Met.*, 84:463–470, 1997.

- [26] Partee J. Shinar, J. On the nature of trapped polarons in p-conjugated polymers. *Synthetic Metals*, 84 (1-3):525–528, 1997.
- [27] J. Grüner M. G. Harrison and G. C. W. Spencer. Analysis of the photocurrent action spectra of meh-ppv polymer photodiodes. *Physical review B*, 55:7831–7849, 1997.
- [28] R. B. M. Koehorst T. J. Schaafsma E. E. van Faassen H. R. Kerp, H. Donker. Exciton transport in organic dye layers for photovoltaic applications. *Chemical Physics Letters*, 298:302, 1997.
- [29] Thomas Stubinger and Wolfgang Brutting. Exciton diffusion and optical interference in organic donor–acceptor photovoltaic cells. *Journal of Applied Physics*, 90(7):3632–3641, 2001.
- [30] B. Kraabel, Jan C. Hummelen, D. Vacar, D. Moses, N. S. Sariciftci, A. J. Heeger, and F. Wudl. Subpicosecond photoinduced electron transfer from conjugated polymers to functionalized fullerenes. *The Journal of Chemical Physics*, 104(11):4267–4273, 1996.
- [31] Niyazi Serdar Sariciftci and Alan J. Heeger. Role of buckminsterfullerene, c[₆₀], in organic polymeric photoelectric devices. *Fullerenes and Photonics II*, 2530(1):76–86, 1995.
- [32] G. Zerza, C. J. Brabec, G. Cerullo, S. De Silvestri, and N. S. Sariciftci. Ultrafast charge transfer in conjugated polymer-fullerene composites. *Synthetic Metals*, 119(1-3):637 – 638, 2001.
- [33] B. de Boer L. J. A. Koster P. W. M. Blom V. D. Mihailetschi, H. X. Xie. Charge transport and photocurrent generation in poly(3-hexylthiophene): Methanofullerene bulk-heterojunction solar cells. *Advanced Functional Materials*, 16:699–708, 2006.
- [34] J. G. Muller, J. M. Lupton, J. Feldmann, U. Lemmer, M. C. Scharber, N. S. Sariciftci, C. J. Brabec, and U. Scherf. Ultrafast dynamics of charge carrier photogeneration and geminate recombination in conjugated polymer:fullerene solar cells. *Phys. Rev. B*, 72(19):195208, Nov 2005.
- [35] Masahiro Hiramoto, Hiroshi Fujiwara, and Masaaki Yokoyama. Three-layered organic solar cell with a photoactive interlayer of codeposited pigments. *Applied Physics Letters*, 58(10):1062–1064, 1991.
- [36] L. Schmidt-Mende, A. Fechtenkotter, K. Mullen, E. Moons, R. H. Friend, and J. D. MacKenzie. Self-Organized Discotic Liquid Crystals for High-Efficiency Organic Photovoltaics. *Science*, 293(5532):1119–1122, 2001.
- [37] G. Yu, K. Pakbaz, and A. J. Heeger. Semiconducting polymer diodes: Large size, low cost photodetectors with excellent visible-ultraviolet sensitivity. *Applied Physics Letters*, 64(25):3422–3424, 1994.

- [38] Pavel Schilinsky, Christoph Waldauf, and Christoph J. Brabec. Recombination and loss analysis in polythiophene based bulk heterojunction photodetectors. *Applied Physics Letters*, 81(20):3885–3887, 2002.
- [39] W. Geens, T. Aernouts, J. Poortmans, and G. Hadziioannou. Organic co-evaporated films of a ppv-pentamer and c60: model systems for donor/acceptor polymer blends. *Thin Solid Films*, 403-404:438 – 443, 2002. Proceedings of Symposium P on Thin Film Materials for Photovoltaics.
- [40] G. Yu and A. J. Heeger. Charge separation and photovoltaic conversion in polymer composites with internal donor/acceptor heterojunctions. *Journal of Applied Physics*, 78(7):4510–4515, 1995.
- [41] Walsh C.A. Greenham N.C. Marseglla E.A. Friend R.H. Moratti S.C. Holmes A.B. Halls, J.J.M. Efficient photodiodes from interpenetrating polymer networks. *Nature*, 376:498–500, 1995.
- [42] F. Wudl. *Acc. Chem. Res.*, 25:157161, 1992.
- [43] Allen Miller and Elihu Abrahams. Impurity conduction at low concentrations. *Phys. Rev.*, 120(3):745–755, Nov 1960.
- [44] R. A. Marcus. Nonadiabatic processes involving quantum-like and classical-like coordinates with applications to nonadiabatic electron transfers. *The Journal of Chemical Physics*, 81(10):4494–4500, 1984.
- [45] M. Fahlman and W.R. Salaneck. Surfaces and interfaces in polymer-based electronics. *Surface Science*, 500(1-3):904 – 922, 2002.
- [46] Mingirulli N. Zimmermann B. Ziegler T. Kern R. Niggemann M. Hinsch A. Gombert A. Glatthaar, M. Impedance spectroscopy on organic bulk-heterojunction solar cells. *Physica Status Solidi (A) Applications and Materials*, 202:R125–R127, 2005.
- [47] Petritsch K. Arias A.C. Lux A. Andersson M.R. Friend R.H. Granstrom, M. Laminated fabrication of polymeric photovoltaic diodes. *Nature*, 395:257–260, 1998.
- [48] Sugiyama K. Ito E. Seki K. Ishii, H. Energy level alignment and interfacial electronic structures at organic-metal and organic-organic interfaces. *Advanced Materials*, 11:605–625, 1999.
- [49] Th. Kugler, W. R. Salaneck, H. Rost, and A. B. Holmes. Polymer band alignment at the interface with indium tin oxide: consequences for light emitting devices. *Chemical Physics Letters*, 310(5-6):391 – 396, 1999.
- [50] C. J. Brabec, A. Cravino, D. Meissner, N. S. Sariciftci, M. T. Rispens, L. Sanchez, J. C. Hummelen, and T. Fromherz. The influence of materials work function on the open circuit voltage of plastic solar cells. *Thin Solid Films*, 403-404:368 – 372, 2002. Proceedings of Symposium P on Thin Film Materials for Photovoltaics.

- [51] Klaus Petritsch. *Organic Solar Cell Architectures*. PhD Thesis, 2000.
- [52] Cravino A. Meissner D. Serdar Sariciftci N. Fromherz T. Rispens M.T. Sanchez L. Hummelen J.C. Brabec, C.J. Origin of the open circuit voltage of plastic solar cells. *Advanced Funtional Materials*, 11 (5):374–380, 2001.
- [53] Adolf Goetzberger. Optical confinement in thin si-solar cells by diffuse back reflectors. *Conference Record of the IEEE Photovoltaic Specialists Conference*, pages 867–870, 1981.
- [54] Wang A. Green M.A. Ferrazza F. Zhao, J. 19.8monocrystalline silicon solar cells. *APPLIED PHYSICS LETTERS*, 73, NUMBER 14:1991–1993, 1998.
- [55] J. Springer, B. Rech, W. Reetz, J. Müller, and M. Vanecek. Light trapping and optical losses in microcrystalline silicon pin solar cells deposited on surface-textured glass/zno substrates. *Solar Energy Materials and Solar Cells*, 85(1):1 – 11, 2005.
- [56] M. Niggemann, M. Glatthaar, A. Gombert, A. Hinsch, and V. Wittwer. Diffraction gratings and buried nano-electrodes–architectures for organic solar cells. *Thin Solid Films*, 451-452:619 – 623, 2004. Proceedings of Symposium D on Thin Film and Nano-Structured Materials for Photovoltaics, of the E-MRS 2003 Spring Conference.
- [57] M. Niggemann, M. Glatthaar, P. Lewer, C. Müller, J. Wagner, and A. Gombert. Functional microprism substrate for organic solar cells. *Thin Solid Films*, 511-512:628 – 633, 2006. EMSR 2005 - Proceedings of Symposium F on Thin Film and Nanostructured Materials for Photovoltaics - EMRS 2005- Symposium F.
- [58] R. Barry Johnson and Gary A. Jacobsen. Advances in lenticular lens arrays for visual display. *Current Developments in Lens Design and Optical Engineering VI*, 5874(1):587406, 2005.
- [59] Kristofer Tvingstedt, Viktor Andersson, Fengling Zhang, and Olle Inganäs. Folded reflective tandem polymer solar cell doubles efficiency. *Applied Physics Letters*, 91(12):123514, 2007.
- [60] Inganaas O. Granlund T. Nyberg T. Svensson M. Andersson M.R. Hummelen J.C. Roman, L.S. Trapping light in polymer photodiodes with soft embossed gratings. *Advanced Materials*, 12:189–195, 2000.
- [61] Carpentiero A. Ferrari E. Cojoc D. Fabrizio E.D. Tormen, M. Novel fabrication method for three-dimensional nanostructuring: An application to micro-optics. *Nanotechnology*, 18 (38):art. no. 385301, 2007.
- [62] K. Colladet, M. Nicolas, L. Goris, L. Lutsen, and D. Vanderzande. Low-band gap polymers for photovoltaic applications. *Thin Solid Films*, 451-452:7 – 11, 2004. Proceedings of Symposium D on Thin Film and Nano-Structured Materials for Photovoltaics, of the E-MRS 2003 Spring Conference.

- [63] Wendimagegn Mammo, Shimelis Admassie, Abay Gadisa, Fengling Zhang, Olle Inganäs, and Mats R. Andersson. New low band gap alternating polyfluorene copolymer-based photovoltaic cells. *Solar Energy Materials and Solar Cells*, 91(11):1010 – 1018, 2007. Low Band Gap Polymer Materials for Organic Solar Cells.
- [64] Gang Zeng, Soo-Jin Chua, and Wei Huang. Influence of donor and acceptor substituents on the electronic characteristics of poly(fluorene-phenylene). *Thin Solid Films*, 417(1-2):194 – 197, 2002.
- [65] Xiangjun Wang, Erik Perzon, Juan Luis Delgado, Pilar de la Cruz, Fengling Zhang, Fernando Langa, Mats Andersson, and Olle Inganäs. Infrared photocurrent spectral response from plastic solar cell with low-band-gap polyfluorene and fullerene derivative. *Applied Physics Letters*, 85(21):5081–5083, 2004.
- [66] Gao J. Hummelen J.C. Wudl F. Heeger A.J. Yu, G. Polymer photovoltaic cells: Enhanced efficiencies via a network of internal donor-acceptor heterojunctions. *Science*, 270:1789–1791, 1995.
- [67] Marisol Reyes-Reyes, Kyungkon Kim, and David L. Carroll. High-efficiency photovoltaic devices based on annealed poly(3-hexylthiophene) and 1-(3-methoxycarbonyl)propyl-1-phenyl-(6,6)c[₆₁] blends. *Applied Physics Letters*, 87(8):083506, 2005.
- [68] Uchida S. Forrest S.R. Peumans, P. Efficient bulk heterojunction photovoltaic cells using small-molecular-weight organic thin films. *Nature*, 425:158–162, 2003.
- [69] S. Uchida S. R. Forrest J. Xue, B. P. Rand. A hybrid planar-mixed molecular heterojunction photovoltaic cell. *Advanced Materials*, 17:66, 2005.
- [70] Sachetan M. Tuladhar Stelios A. Choulis Jenny Nelson James R. Durrant Donal D. C. Bradley Mark Giles Iain McCulloch Chang-Sik Ha Youngkyoo Kim, Steffan Cook and Moonhor Ree. A strong regioregularity effect in self-organizing conjugated polymer films and high-efficiency polythiophene:fullerene solar cells. *nature materials*, 3:197–203, 2005.
- [71] Xiaoni Yang, Joachim Loos, Sjoerd C. Veenstra, Wiljan J. H. Verhees, Martijn M. Wienk, Jan M. Kroon, Matthias A. J. Michels, and Rene A. J. Janssen. Nanoscale morphology of high-performance polymer solar cells. *Nano Letters*, 5(4):579–583, 2005.
- [72] Max Shtein & Stephen R. Forrest Fan Yang. Controlled growth of a molecular bulk heterojunction photovoltaic cell. *Nature Materials*, 4:37–41, 2004.
- [73] Mingqi Li and Christopher K. Ober. Block copolymer patterns and templates. *Materials Today*, 9(9):30 – 39, 2006.
- [74] Paul J. Flory. Thermodynamics of high polymer solutions. *The Journal of Chemical Physics*, 9(8):660–660, 1941.
- [75] M. W. Matsen and F. S. Bates. Unifying weak- and strong-segregation block copolymer theories. *Macromolecules*, 29(4):1091–1098, 1996.

- [76] M. Bal, A. Ursache, M. T. Tuominen, J. T. Goldbach, and T. P. Russell. Nanofabrication of integrated magnetoelectronic devices using patterned self-assembled copolymer templates. *Applied Physics Letters*, 81(18):3479–3481, 2002.
- [77] S. Mößner F.-M. Kamm A. Plettl P. Ziemann M. Möller J.P. Spatz, V.Z.-H. Chan. A combined top-down/bottom-up approach to the microscopic localization of metallic nanodots. *Advanced Materials*, 14:1827 – 1832, 2002.
- [78] Mingqi Li, Katsuji Douki, Ken Goto, Xuefa Li, Christopher Coenjarts, Detlef M. Smilgies, and Christopher K. Ober. Spatially controlled fabrication of nanoporous block copolymers. *Chemistry of Materials*, 16(20):3800–3808, 2004.
- [79] Mohamed S. A. Abdou and Steven Holdcroft. Mechanisms of photodegradation of poly(3-alkylthiophenes) in solution. *Macromolecules*, 26(11):2954–2962, 1993.
- [80] Yi-Ming Chang, Wei-Fang Su, and Leeyih Wang. Influence of photo-induced degradation on the optoelectronic properties of regioregular poly(3-hexylthiophene). *Solar Energy Materials and Solar Cells*, 92(7):761 – 765, 2008. Degradation and Stability of Polymer and Organic Solar Cells.
- [81] Gang Li, Vishal Shrotriya, Yan Yao, and Yang Yang. Investigation of annealing effects and film thickness dependence of polymer solar cells based on poly(3-hexylthiophene). *Journal of Applied Physics*, 98(4):043704, 2005.
- [82] Davood Raoufi, Ahmad Kiasatpour, Hamid Reza Fallah, and Amir Sayid Hassan Rozatian. Surface characterization and microstructure of ito thin films at different annealing temperatures. *Applied Surface Science*, 253(23):9085 – 9090, 2007.
- [83] Davood Raoufi. Morphological characterization of ito thin films surfaces. *Applied Surface Science*, 255(6):3682 – 3686, 2009.
- [84] D Vaufrey, M Ben Khalifa, J Tardy, C Ghica, M G Blanchin, C Sandu, and J A Roger. Ito-on-top organic light-emitting devices: a correlated study of opto-electronic and structural characteristics. *Semiconductor Science and Technology*, 18(4):253–260, 2003.
- [85] T. F. Stoica, V. S. Teodorescu, M. G. Blanchin, T. A. Stoica, M. Gartner, M. Losurdo, and M. Zaharescu. Morphology, structure and optical properties of sol-gel ito thin films. *Materials Science and Engineering B*, 101(1-3):222 – 226, 2003. EMRS 2002 Symposium S: Micro- and Nano-structured Semiconductors.
- [86] G. Kavei and A. Mohammadi Gheidari. The effects of surface roughness and nanostructure on the properties of indium tin oxide (ito) designated for novel optoelectronic devices fabrication. *Journal of Materials Processing Technology*, 208(1-3):514 – 519, 2008.
- [87] E. Terzini, P. Thilakan, and C. Minarini. Properties of ito thin films deposited by rf magnetron sputtering at elevated substrate temperature. *Materials Science and Engineering B*, 77(1):110 – 114, 2000.

- [88] L. Stolz Roman M. Svensson O. Inganäs T. Granlund, T. Nyberg. Patterning of polymer light-emitting diodes with soft lithography. *Advanced Materials*, 12:268–273, 2000.
- [89] S. L. Lai, M. Y. Chan, M. K. Fung, C. S. Lee, and S. T. Lee. Concentration effect of glycerol on the conductivity of pedot film and the device performance. *Materials Science and Engineering B*, 104(1-2):26 – 30, 2003.
- [90] W. H. Kim, A. J. Mäkinen, N. Nikolov, R. Shashidhar, H. Kim, and Z. H. Kafafi. Molecular organic light-emitting diodes using highly conducting polymers as anodes. *Applied Physics Letters*, 80(20):3844–3846, 2002.
- [91] J. Huang, P. F. Miller, J. C. de Mello, A. J. de Mello, and D. D. C. Bradley. Influence of thermal treatment on the conductivity and morphology of pedot/pss films. *Synthetic Metals*, 139(3):569 – 572, 2003. Proceedings of the Fifth International Topical Conference on Optical Probes of Conjugated Polymers and Organic and Inorganic Nanostructures.
- [92] Youngkyoo Kim, Amy M. Ballantyne, Jenny Nelson, and Donal D.C. Bradley. Effects of thickness and thermal annealing of the pedot:pss layer on the performance of polymer solar cells. *Organic Electronics*, 10(1):205 – 209, 2009.
- [93] Takashima W. Nagamatsu S. Endo T. Rikukawa M. Kaneto K. Pandey, S.S. Regioregularity vs regiorandomness: Effect on photocarrier transport in poly(3-hexylthiophene). *Japanese Journal of Applied Physics, Part 2: Letters*, 39 (2 A):L94–L97, 2000.

Curriculum vitae

February 27, 1978 Born in Treviso, Italy.

November 24, 2004 Laurea degree in Material Science.

2009 PhD in Material Science.

Publications

Superhydrophobic surfaces fabricated by nanoimprint lithography

Alessandro Pozzato, Simone Dal Zilio, Giovanni Fois, Diego Vendramin, Giampaolo Mistura, Michele Belotti, Yong Chen and Marco Natali
2006 Microelectronic Engineering 83 (4-9 SPEC. ISS.), pp. 884-888

Water slip and friction at a solid surface

L. Brigo, M. Natali, M. Pierno, F. Mammano, C. Sada, G. Fois, A. Pozzato, S. Dal Zilio, M. Tormen and G. Mistura.
2008 Journal of Physics Condensed Matter 20 (35), art. no. 354016

Trapping light with micro lenses in thin film organic photovoltaic cells

Tvingstedt, K., Dal Zilio, S., Inghanas, O., Tormen, M.
2008 Optics Express 16 (26), pp. 21608-21615

Fabrication of substrates with extended nanostructured surface areas for wetting studies

Alessandro Pozzato, Simone Dal Zilio, Giampaolo Mistura, Nicola Bruschi and Massimo Tormen
2008 Microelectronic Engineering (SPEC. ISS.), in press.

Evaluation of nano-scale surface topography as a tool in directing differentiation of embryonic stem cell derived neural precursors

Gerald James Bakeine, Jelena Ban, Gianluca Greci, Alessandro Pozzato, Simone Dal Zilio, Mauro Prasciolu, Luca Businaro, Massimo Tormen, Maria Elisabetta Ruaro
2008 Microelectronic Engineering (SPEC. ISS.), in press.

Design and fabrication of large area nano-structured substrates for use in pancreatic beta-cell engineering

Gerald James Bakeine, Alessia Bertolotti, Cristina Zennaro, Gianluca Greci, Alessandro Pozzato, Simone Dal Zilio, Mauro Prasciolu, Luca Businaro, Mario Alessiani, Rosy Nano, Paolo Dionigi.

2008 Microelectronic Engineering (SPEC. ISS.), in press.

Posters

September 16 - 19, 2008, MNE 2008 conference Athens (Greece). Invited poster titled: **Self aligned micro-lenses system for light trapping in organic solar cells**

September 16 - 19, 2008, MNE 2008 conference Athens (Greece). Poster titled: **Studies of wetting behavior on nanostructured surface**

September 16 - 19, 2008, MNE 2008 conference Athens (Greece). Poster titled: **Design and fabrication of large area nano-structured substrates for use in pancreatic beta-cell engineering**

September 16 - 19, 2008, MNE 2008 conference Athens (Greece). Poster titled: **Evaluation of nano-scale surface topography as a tool in directing differentiation of embryonic stem cell derived neural precursors**

Schools

II scuola sui materiali molecolari per fotonica ed elettronica

Arbatax (Italy) - June 18 - 21, 2006.

PANAMA summer school (NaPa Project)

Toulouse (France) - July 3 -14, 2006.

Corso in self assembled materials organizzato dall'università Bicocca di Milano (European Doctorate in Physics and Chemistry of Advanced Materials)

Milan (Italy) - September 22-25, 2006.

NordForsk summer school: Polymer micro- and nano-fabrication

Parkhotell Palmse (Estonia) - August 31 to September 6, 2007.

ISOPHOS 2007 International School on Organic Photovoltaics

Ventotene Island (Italy) - September 23-27, 2007.

Acknowledgments

Innanzitutto qualche ringraziamento serio e dovuto, ma non per questo meno sentito. Per primo il mio tutor, o si potrebbe chiamarlo capo, **Massimo Tormen** che, nonostante abbia centinaia di cose da fare nel tempo in cui ce ne starebbero dieci, ha sempre trovato il tempo di aiutarmi e ben consigliarmi. Poi il professore **Alberto Carnera**, mio supervisore, che ringrazio per avermi accettato come suo dottorando. E il professor **Gaetano Granozzi**, per la sua disponibilità e la sua comprensione nei mille problemi che la mia disorganizzazione ha causato.

Giampaolo Mistura, un supervisore aggiunto, ma indispensabile. E' grazie a lui che la mia carriera ha imboccato questa strada ricca di soddisfazioni e ripagate fatiche nel mondo della ricerca.

E ora i ringraziamenti informali. Il primo pensiero va al mio **Coccolino**, che proprio in questo momento sento pianzere di là in camera. Per fortuna c'è **Giada**. A cui va (non solo per questo di certo) l'altro mio primo pensiero. Sono proprio felice della nostra giovane famiglia. Che ritengo il mio migliore risultato, senza nulla togliere al lavoro fin qui svolto. Ma il sorriso di un bimbo così bello mentre è in braccio alla mamma vale più di un milione di "Nature".

Poi un pensiero va alla mia famiglia: **Giorgia**, zia joja, che si fa in quattro per me, e mi fa sentire sempre orgoglioso di lei. Nonché babysitter impeccabile. **Papa'**, che mi aiuta sempre quando serve. E zia **Marghe**, dopo la quale ora devo aggiungere **Eleonora** e **Isabella**, le mie nipotine (i maschi li facciamo noi!). E ovviamente al genero, lo zio **Gabriele**.

Un grazie ai miei nonni, **Franca** e **Aldo**, che sento sempre vicini, nei miei pensieri e nel mio cuore.

Un sincero ringraziamento ai **suoceri**, soprattutto per essere dei nonni super appassionati. E poi dico la verità: a me la mia suocera me piaci, checché si dica con la suocera non si va d'accordo. E a **Fabio**, che presto si accorgerà com'è davvero il mondo della ricerca.

A tutto il gruppo **Lilit**, in cui mi sento davvero a casa: il mio ingegnere/consigliere tecnico di fiducia Gianluca, Mauro, Enrico, Enrico, Silvia, Carpenter, il mio dirimpettaio di scrivania Giovanni, Gabriele, Laura, James, Benedetta (anche se non è più Lilit) i capi Filippo, Luca, Dan, Marco. Tutti insomma.

E il gruppo **Lafsi**, di cui mi sento ancora membro, pur non facendone più parte.

Un pensiero a tutti gli amici che nonostante la distanza sono sempre vicini: **Marco**, **Fede**, **Fabio** e famiglia, **Davide**... e tutti gli altri.

E infine voglio ringraziare in maniera particolare **Alessandro**: la nostra avventura insieme continua inesorabile. Devo ammettere che la speranza che ci siano ancora molti anni da passare insieme è grande, non solo perché è un validissimo collega e ottimo amico, ma ora anche perché gli ho affidato la grande responsabilità di essere il padrino del bimbo più importante (e bello)

che c'è.

Ovviamente un grande pensiero e ringraziamento va a mia mamma. Grazie.

